Thirty Meter Telescope Detailed Science Case: 2007

TMT Science Advisory Committee

TMT Detailed Science Case: 2007

TMT Document Number: TMT.PSC.TEC.07.003.REL01
Public release 1: 22 October 2007

TMT Observatory Corporation
2632 E. Washington Blvd.
Pasadena, CA 91107
http://www.tmt.org

Editors

David Silva (AURA, Thirty Meter Telescope)
Paul Hickson (U. of British Columbia)
Charles Steidel (Caltech)
Michael Bolte (U. of California at Santa Cruz, U. of California Observatories/Lick Observatory)

TMT Science Advisory Committee (October 2007)

Elizabeth Barton (U. of California at Irvine)
Michael Bolte (U. of California at Santa Cruz, U. of California Observatories/Lick Observatory)
Ray Carlberg (U. of Toronto)
Judy Cohen (Caltech)
Tim Davidge (NRC/Herzberg Institute of Astrophysics)
Richard Ellis (Caltech)
Andrea Ghez (U. of California at Los Angeles)
Puragra Guhathakurta (U. of California at Santa Cruz, U. of California Observatories/Lick Observatory)
Paul Hickson (University of British Columbia)
Michael Hudson (University of Waterloo)
Shri Kulkarni (Caltech)
Charles Steidel (Caltech), SAC Chairperson
Charles Telesco (U. of Florida)

Preface

Since the revolution in physics at the dawn of the 20th century, the history of astronomy has been one of exploration guided by the twin beacons of physical insight and technology. Physical insight has guided the questions we ask and the answers we derive from our observational data. Technology has extended our grasp to the very dawn of time.

Those of us alive today are extraordinarily lucky to have the answers to some of the deepest questions about the universe around us. We have arrived at a moment when we can see the imprint of the Big Bang everywhere we look: from the smallest ripples in the cosmic microwave background to the filaments of galaxies stretching across the sky of the present day universe to the very water in our bodies.

But our journey of exploration is not over, not all has been revealed.

Our universe appears to be dominated by mysterious quantities we have named dark energy and dark matter – we can observe their effect but we do not understand what they are or why they exist. The discovery of planetary systems around other stars has revealed that the structure and composition of our solar system may be the exception, not the rule – our ideas about planetary formation and the origin of life have to be completely revised. Beacons of extraordinary brightness shine out across the Universe – what are they and how can they be used to study the intervening universe? Galaxies in the local universe show signs of a violent and turbulent past – what will we see when we actual observe their predecessors in the high redshift universe? We have a good idea of when the first stars formed – can we capture and analyze their light?

We choose to improve our understanding, to seek answers to these questions, not merely to satisfy idle curiosity but for the benefit of all humankind. The steady improvement in our understanding of the physical universe has driven the development of our technological civilization to heights that were simply unimaginable even 100 years ago. We stand on the edge of another breakthrough of unimaginable impact in our understanding of the physical universe – and astronomy will play a key role in taking us over that threshold.

And so we propose to build TMT – the Thirty Meter Telescope – an exploration vehicle that takes advantage of the latest technology. To do this, we bring together the experience and knowledge of a broad, international community. Over the last 15 years, this community has been at the forefront of ground-based astronomical research and technology, having built and operated four 8 – 10m telescopes and participating in many of the most important scientific breakthroughs over this period. Our goal is to build a facility that will be exceptionally powerful in its own right while being capable of working in synergy with other planned facilities (such as the James Webb Space Telescope and the Atacama Large Millimeter Array) to address the key questions of 2015 as well as the new questions that will arise during following 30 years.

In the rest of this document, we present key science topics we believe TMT will start to address in the middle of the next decade. For each topic, a brief introduction is provided, followed by some example observational programs. These examples are not exhaustive in scope but serve to illustrate where TMT will provide breakthrough capabilities and/or illustrate especially demanding technical requirements. We do not pretend that these observations will lead to the only exciting results – our experience tells us that those results will come during explorations we cannot imagine today. But our experience tells us also that what we can imagine today can be used to make sure we will build the right vehicle for the explorations of tomorrow.

Building TMT and starting a new voyage of exploration will not come easily – technologically, scientifically, or financially. But as President John Kennedy said on a bright sunny day in Houston, we choose to do these things "…not because they are easy, but because they are hard, because that goal will serve to organize and measure the best of our energies and skills, because that challenge is one that we are willing to accept, one we are unwilling to postpone, and one which we intend to win".

David Silva
Pasadena, California, USA
April 2006

Table of Contents

Figures

Tables

1 Introduction

This is the Detailed Science Case for the Thirty Meter Telescope project. It is a public document created and managed by the TMT Science Advisory Committee. It will be updated as needed during the design, development, and implementation phases of the TMT project.

1.1 Purpose

The Detailed Science Case (DSC) is the highest-level statement of the Thirty Meter Telescope (TMT) science case. It provides examples of the kinds of exciting, groundbreaking science that will be enabled by a 30m telescope. Wherever possible, synergies with other major upcoming facilities (e.g. the James Webb Space Telescope and the Atacama Large Millimeter Array) are discussed. As appropriate, performance numbers (often conservative) are provided (e.g. sensitivities, integration times, spatial resolutions).

The DSC is not a requirements document. The Science-based Requirements Document (SRD) is the highest-level requirements document for TMT.

1.2 Scope

This document is intended to provide a high-level overview of the TMT science case for the following audiences:

- Private and public funding agencies
- Our North American and international scientific colleagues
- Various astronomy strategic working groups (e.g. the NSF/AURA GSMT Science Working Group, the NAS/NRC Decadal Survey committee)

1.3 Applicable Documents

Applicable documents contain information that shall be applied in the current document. Examples are higher-level requirements documents, standards, rules and regulations.

This high-level document has no applicable documents within the TMT Project.

1.4 Reference Documents

Reference documents contain information complementing, explaining, detailing, or otherwise supporting the information included in the current document.

Documents can be found in the TMT Document Control Center (DCC) using their document number in the following URL:

http://project.tmt.org:8080/docushare/dsweb/Get/Document-XXXX

	Name	TMT Number	DCC Number
RD01	Science-based Requirements Document	TMT.PSC.DRD.05.001	319
RD02	Detailed Science Case v9	TMT.PSC.PRE.05.081	4831
RD03	Extracted Instrument Feasibility Studies Science Cases and Operational Concepts: March 2006	TMT.PSC.COR.06.007	5625

1.5 Change Record

Version	Date	Remarks
Release 1	18 Oct 2007	First public release.

1.6 Abbreviations and Acronyms

ACS	Advanced Camera for Surveys (HST)
AGB	Asymptotic Giant Branch
AGN	Active Galactic Nucleus
ALMA	Atacama Large Millimter Array
AO	Adaptive Optics
AU	Astronomical Unit
AURA	Association of Universities for Research in Astronomy
BLR	Broad Line Region
CIRCE	Canarias InfraRed Camera Experiment
CIT	California Institute of Technology
CMB	Cosmic Microwave Background
CMD	Color-Magnitude Diagram
CoDR	Conceptual Design Review
CRIRES	Cryogenic Infrared Echelle Spectrometer (VLT)
DAZLE	Dark Ages *z* Lyman-Alpha Explorer (VLT)
DCC	Document Control Center
DEIMOS	Deep Imaging Multi-object Spectrograph (Keck)
DLA	Damped Lyman-α Absorber
DSC	Detailed Science Case
EGP	Extrasolar Giant Planet
ELT	Extremely Large Telescope
ESO	European Southern Observatory
FDR	Final Design Review
F2TF	FLAMINGOS 2 Tuneable Filter
FLAMINGOS	Florida Multi-object Imaging Near-IR Grism Spectrometer
FTE	Full-Time Equivalent
GO	General Observer
GSMT	Giant Segmented Mirror Telescope
GTO	Guaranteed Time Observation
GPI	Gemini Planet Imager
GRB	Gamma Ray Burst
HIA	Herzberg Institute of Astrophysics
HIRES	High Resolution Echelle Spectrometer (Keck)
HRD	Herzprung-Russel Diagram
HROS	High-Resolution Optical Spectrometer
HST	Hubble Space Telescope
IFU	Integral Field Unit
IGM	Inter-Galactic Medium
IMF	Initial Mass Function
IoA	Institute of Astronomy
IQ	Image Quality
IR	Infrared
IRIS	InfraRed Imaging Spectrometer
IRMOS	InfraRed Multi-Object Spectrometer

IRMS	InfraRed Multislit Spectrometer
IRTF	Infrared Telescope Facility
ISM	Inter-Stellar Medium
ISO	Infrared Space Observatory
IT	Information Technology
JPL	Jet Propulsion Laboratory
JWST	James Webb Space Telescope
KBO	Kuiper-Belt Object
LMC	Large Magellanic Cloud
MIRES	MidInfraRed Echelle Spectrometer
MCAO	Multi-Conjugate Adaptive Optics
MIRES	Mid-Infrared Echelle Spectrometer
MOAO	Multi-Object Adaptive Optics
MOSFIRE	Multi-Object Spectrometer for Infra-Red Exploration (Keck)
NAS	National Academy of Science
NASA	National Aeronautics and Space Administration
NIO	New Initiatives Office
NIRES	NearInfraRed Echelle Spectrometer
NIRSPEC	Near Infrared (echelle) Spectrograph (Keck)
NFIRAOS	Narrow Field Infrared Adaptive Optics System
NOAO	National Optical Astronomy Observatory
NRC	NAS National Research Council (USA) or National Research Council of Canada
NSF	National Science Foundation
PDR	Preliminary Design Review
PFI	Planet Formation Instrument
PSF	Point Spread Function
PSR	Pre-Shipment Review
PRVS	Precision Radial Velocity Spectrograph
PWV	Precipitable Water Vapor
QC	Quality Control
RGB	Red Giant Branch
RM	Rossiter-McLaughlin
RV	Radial Velocity
SAC	Science Advisory Committee
SDSS	Sloan Digital Sky Survey
SEGUE	Sloan Extension for Galactic Understanding and Exploration
SFRD	Star Formation Rate Diagram
SINFONI	Spectrograph for Integral Field Observations in Near-Infrared (VLT)
SKA	Square-Kilometer Array
SMBH	SuperMassive Black Hole
SNR	Signal-to-Noise Ratio
SPHERE	Spectro-Polarimetric High-contrast Exoplanet Research (VLT)
STIS	Space Telescope Imaging Spectrometer (HST)
STScI	Space Telescope Science Institute
SW	Software
TBC	To Be Confirmed
TBD	To Be Determined
TEXES	Texas Echelon Cross Echelle Spectrograph
TMT	Thirty Meter Telescope
TRGB	Tip of the Red Giant Branch
UBC	University of British Columbia
UC	University of California

UCB	University of California at Berkeley
UCI	University of California at Irvine
UCLA	University of California at Los Angeles
UCSC	University of California at Santa Cruz
UCO	University of California Observatories
UFHIA	University of Florida, Herzberg Institute of Astrophysics
UKIDSS	United Kingdom Infrared Deep Sky Survey
URL	Universal Resource Locator
UV	UltraViolet
UVES	Ultraviolet and Visible Echelle Spectrograph (VLT)
VIMOS	Visible MultiObject Spectrograph (VLT)
VLT	Very Large Telescope
VO	Virtual Observatory
WFOS	Wide-Field Optical Spectrometer
WIRC	Wide-Field Infrared Camera
WMAP	Wilkinson Microwave Anisotropy Probe
YSO	Young Stellar Object

1.7 Acknowledgements

Many scientists from across the TMT collaboration contributed to this document.

Special thanks to Mike Bolte (UCO/Lick) – Version 9 editor.

We thank the authors of the analogous science case documents for our predecessor projects (in alphabetical order): CELT, GSMT, and VLOT.

The following people directly contributed input or review comments to various versions of the TMT Detailed Science Case:

Aaron Barth (UCI)
Betsy Barton (UCI)
James Bullock (UCI)
Judy Cohen (CIT)
Pat Côte (NRC/HIA)
Jay Elias (NOAO/NIO)
Richard Ellis (CIT)
Paul Hickson (UBC)
Mike Hudson (Waterloo)
Andrea Ghez (UCLA)
Raja Guhathakurta (Lick)
James Graham (UCB)
Lynne Hillenbrand (CIT)
Joan Najita (NOAO)
Knut Olsen (NOAO)
David Silva (TMT)
Chuck Steidel (CIT)
Charlie Telesco (U. of Florida)

We also thank the authors of the February 2006 TMT instrument feasibility studies, especially the leaders of the various science teams:

Bob Abraham (UToronto, WFOS-HIA)

John Carr (Naval Research Laboratory, MIRES)
Tim Davidge (NRC/HIA, IRIS)
Richard Ellis (CIT, IRMOS-CIT)
Cynthia Froning (CASA, HROS-CASA)
James Graham (UC Berkeley, PFI)
Rafael Guzman (UFlorida, IRMOS-UFHIA)
John Rayner (IRTF, NIRES)
Connie Rockosi (UCSC, HROS-UCSC)
Eugene Serabyn (JPL, PFI)
Steve Vogt (UCSC, HROS-UCSC)

The TMT Project gratefully acknowledges the support of the TMT partner institutions: the Association of Canadian Universities for Research in Astronomy (ACURA), the California Institute of Technology and the University of California. The TMT Project is also supported by the Canada Foundation for Innovation, the Gordon and Betty Moore Foundation, the National Optical Astronomy Observatory (operated by the Association of Universities for Research in Astronomy under cooperative agreement with the National Science Foundation), the National Science Foundation, the Ontario Ministry of Research and Innovation, the British Columbia Knowledge Development Fund, and the National Research Council of Canada.

2 Overview

The Thirty Meter Telescope (TMT) is a 30 m ground based telescope with a collecting area of 650 m^2. It will observe through the atmospheric windows from 0.31 to 28 μm. Advanced adaptive optics capabilities will allow highly sensitive, diffraction-limited observations beyond 1 μm over most of the sky. A 20 arcmin in diameter field-of-view facilitates the deployment of wide-field, multi-object spectrographs. These capabilities will enable groundbreaking advances in a wide range of scientific areas, from the most distant reaches of the Universe to our own Solar System. We can look ahead and imagine what the key scientific questions might be in the coming decades, and use those insights to guide more detailed observatory design and implementation. However, powerful new facilities have often opened up unimagined areas of research and made important but unanticipated discoveries. We expect the situation with TMT will be no different and hence look forward to a rich and diverse mix of both expected and unexpected scientific results.

2.1 The big picture

Decades of advances with ground and space-based facilities have provided a clear and convincing picture of the overall history of our Universe. We now know that observable Universe began some 13.6 billion years ago when a small region of empty space became unstable and began to expand, rapidly increasing in size by some twenty or thirty orders of magnitude. This period of expansion, called inflation, lasted but a tiny fraction of a second, yet it resulted in the production of all matter and energy in our Universe. When inflation ended an exceedingly hot mixture of elementary particles of all varieties pervaded space. At the same time, tiny 'quantum' fluctuations in the distribution of this energy were stretched to macroscopic scales by inflation. These fluctuations formed the seeds for the galaxies and clusters of galaxies that we see today.

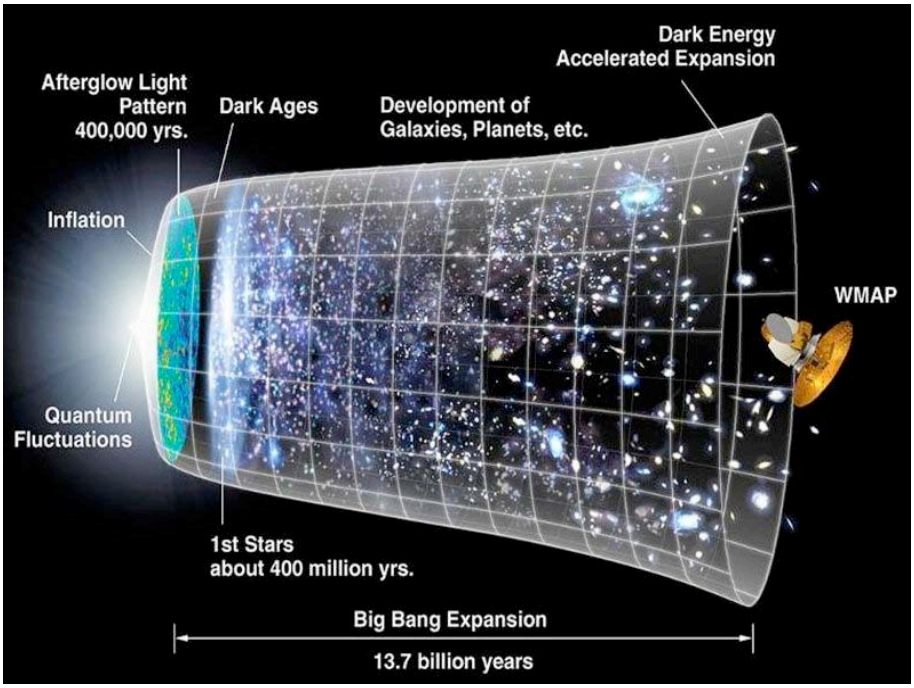

Figure 2-1. Schematic history of the Universe (Credit: NASA/WMAP Science Team)

Following inflation, the Universe continued to expand, but at a slower rate. This expansion resulted in cooling of the plasma allowing the elementary particles to combine to form the familiar protons, neutrons, electrons, photons, neutrinos and ultimately hydrogen and helium nuclei. Also present were large

quantities of what we now refer to as dark matter and dark energy. During this expansion, the gravitational attraction of the small energy fluctuations resulted in the growth of dark matter density fluctuations.

Some 400,000 years after inflation, the nuclei and electrons combined to form neutral atoms and the Universe became transparent to the photons left over from the Big Bang. Today we see those photons as the cosmic microwave background. Once freed from the drag produced by interactions with those Big Bang photons, the neutral gas began to fall into the denser pockets of dark matter. In a complex process of gravitational accretion and radiative cooling, the first stars formed. The intense radiation produced by this first generation of massive stars heated the surrounding gas, creating bubbles of ionized gas. Initially, the light from these first stars was trapped in these bubbles but as more and more of the surrounding gas was re-ionized, this first light began to propagate throughout the Universe.

As star formation continued and dark matter halos merged due to gravitational attraction, the first galaxies were formed. These first galaxies – relatively small collections of stars, gas, and dust caught within the gravitational potential of dark matter halos – merged to form larger more massive galaxies. The end products of this process (known as hierarchical structure formation) surround us today – from the most massive clusters of galaxies, to our home galaxy the Milky Way, and down to its dwarf galaxy neighbors.

Within many galaxies, star formation continues as clouds of gas cool and contract. Dense clouds of molecular gas form stellar nurseries that harbor newly-forming stars. These nascent stars are surrounded by disks of gas and dust within which planets develop. We now know that many, perhaps most, stars have planetary systems and have begun to explore the closest examples. We can presently detect only the largest planets, similar to those in the outer Solar System but suspect that smaller Earth-like planets are also present. Some of these systems should have conditions favorable for the development of life.

2.2 The big questions

TMT will allow astronomers to explore virtually every aspect of this picture, from inflation to exoplanets. The resolution and sensitivity provided by its large aperture and AO systems, combined with a flexible and powerful suite of instruments, will enable us to address many of the most fundamental questions of the coming decades.

What is the nature and composition of the Universe?

Ordinary matter can generally be detected directly, from the light emitted by stars, from radiation emitted by hot gas in galaxies and clusters, and by absorption of light from background luminous sources. We can infer the presence of dark matter from its gravitational attraction, which affects the motion of galaxies and the propagation of light. In contrast, the gravitational effect of dark energy is repulsive, manifested by an increase in the rate of expansion of the Universe. A census of these components reveals the surprising result that normal matter accounts for only a small fraction of the composition of the Universe– the rest is dominated by dark energy and dark matter.

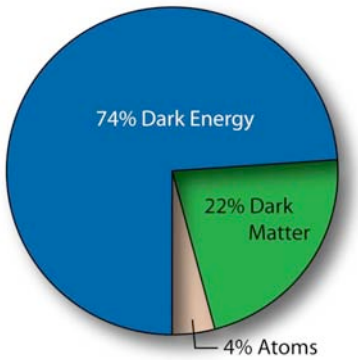

Figure 2-2. Composition of the Universe (Credit: NASA/WMAP Science Team)

When did the first galaxies form and how did they evolve?
By looking into space to greater and greater distances, we are able, thanks to the finite speed of light, to see further and further back into the past. To see the very first stars and galaxies we must look over enormous distances, some 13 billion light years. So far these objects remain beyond the reach of present telescopes. At lesser distances, moving forward in time, we see galaxies interacting dynamically and forming stars. But it is not yet clear how this produces the diversity of galaxy types that are seen today.

What is the relationship between black holes and galaxies?
There is now overwhelming evidence that black holes exist, and that black holes with as much as a billion times the mass of the Sun occupy the centers of galaxies. But, we don't know when or how these supermassive black holes formed, or how they fit into the overall picture of galaxy formation and evolution.

How do stars and planets form?
Stars form within molecular clouds, by a combination of complex physical processes. What determines when these clouds form stars? What determines the masses of these stars? What fraction has planetary systems? There are many questions that we are just beginning to explore.

What is the nature of extra-solar planets?
The exoplanets that have so far been detected are gas giants like Jupiter and Neptune. They were found because their large mass noticeably perturbs the motion of the host star. Surprisingly, many are found very close to their host star. As the higher temperatures there would prevent such planets from forming, it seems that they must have migrated inward, after forming at greater distances. We believe that smaller terrestrial planets exist, but these cannot be detected with present telescopes. Are such planets common? Can they survive the disruption that would result from migration of the massive planets? Do they have atmospheres like Earth?

Is there life elsewhere in the Universe?
If terrestrial planets exist, are conditions conducive to the development of life? Each star has a habitable zone, where a planet would have a surface temperature similar to that of Earth. If, as expected, exoplanetary systems have populations of small icy bodies like comets, it is possible that water and organic molecules could have been delivered to such planets by impacts. If life then develops, it might be detected by signatures of biological activity in planetary atmospheres.

2.3 The required tools

To answer these questions, and many others, advances in technology are needed. The most progress will come from combined studies at many different wavelengths using ground and space-based facilities. Several major new telescopes will begin operation in the next decade. These include the James Webb Space Telescope (JWST) and the Atacama Large Millimeter Array (ALMA). Soon to follow will be the Square Kilometer Array (SKA). By providing powerful new capabilities at infrared, microwave and radio wavelengths, these facilities will open new frontiers.

Yet they will not alone be sufficient. Much as the resolution of the Hubble Space Telescope was complemented by the greater light gathering power of the Keck 10-meter telescopes, these new facilities will need a complementary large-aperture ground-based telescope that can provide high spatial and spectral resolution observations in the optical and infrared. In fact, a revolution in technical capability now makes ground-based telescopes even more effective. Adaptive optics (AO) systems allow the largest optical-infrared telescopes on Earth to achieve higher resolution than telescopes in space, which necessarily have smaller apertures. By compensating atmospheric turbulence, AO allows telescopes to reach the diffraction limit, in which the angular resolution achieved is proportional to the diameter of the telescope aperture.

A useful figure of merit for telescope performance is the time required to achieve a given signal-to-noise ratio for a particular science program or object. The reciprocal of this time is a measure of the sensitivity or productivity of the telescope. Because larger telescopes collect more light, their sensitivity typically increases in proportion to the square of the aperture diameter. In the important case of observations of faint point-like objects, the smaller angular size results in less contamination by background or foreground light from the sky, Solar System and galaxy, so the sensitivity increases in proportion to the fourth power of the diameter. This is an enormous factor, making a thirty-meter telescope a hundred times more sensitive than a ten-meter telescope.

To take advantage of these huge gains in light collection and spatial resolution, TMT must be equipped with a suite of powerful science instruments. The TMT Science Advisory Committee (SAC) has developed recommendations for the instruments and their performance requirements based on a careful consideration of the science programs, as well as the range of capabilities essential for pursuing science areas that are currently unforeseen. The capabilities of these instruments are summarized briefly in the next sub-sections. TMT expects to develop and deploy all of these instruments (or similar) within the first decade of science operations. All instruments will be mounted and kept operationally ready at all times (except of course periods of scheduled maintenance or upgrades). It will be possible to switch from one instrument to another in less than 10 minutes (including target acquisition).

2.3.1 Early light suite

At first light, TMT plans to deploy a laser guide star supported, multi-conjugate adaptive optics (MCAO) system called **NFIRAOS** (Narrow Field Infrared Adaptive Optics System, pronounced “nefarious”). NFIRAOS will provide diffraction-limited resolution (λ/D = 0.008 arcsec and 0.015 arcsec at 1.2 and 2.2 μm, respectively) and high Strehl ratios (> 30% and > 70% at 1.2 μm and 2.2 μm, respectively) over a 30 arcsec science field-of-view. Sky coverage is expected to be 50% at the galactic poles. It will be possible to mount up to three (3) instruments on NFIRAOS.

One of these instruments will be **IRIS (Infrared Imaging Spectrometer),** a combined high-resolution imager and an integral-field unit (IFU) spectrometer. The imaging mode will provide a 10 x 10 arcsec field with 0.004 arcsec/pixel sampling (coarser plate scales will also be available). Both broadband and narrowband filters will be available. The IFU will provide spectral resolving power R = 4000 over the entire J, H, and K bands (one band at a time). At this resolving power, almost all bright telluric emission lines can be identified and removed. For small wavelength coverage ($\Delta\lambda/\lambda \leq 0.05$), 128 x 128 spatial pixels covering 2 x 2 arcsec will be available. IRIS is a scientific descendant of such instruments as OSIRIS on Keck and SINFONI on the VLT.

NFIRAOS will also feed another instrument: **IRMS (Infrared Multi-slit Spectrometer)**. Over a 2.3 x 2.3 arcmin field, IRMS will provide 46 movable, continuously variable width cryogenic slits, each 2.4 arcsec long. These can be combined into a smaller number of longer slits. The two-pixel resolving power is R = 4660. The entire Y, J, H, and K bands can be covered (one at a time) in one grating setting. In imaging mode, IRMS covers the entire NFIRAOS field-of-regard with 0.06 arcsec sampling. As currently planned, IRMS is a near-clone of the Keck instrument MOSFIRE (scheduled for delivery in mid-2009). IRMS leverages the MCAO capabilities of NFIRAOS to early-light exploration of faint objects in the near-IR.

The third early-light instrument is **WFOS (Wide-Field Optical Spectrometer).** Using separate masks in two barrels, it will be possible to observe up to 1500 objects over a 40.5 arcmin^2 field. Spectral resolving powers of 300 – 7500 will be possible. The total available spectral range will be 0.31 to 1.1 μm. WFOS builds on the heritage of such instruments as DEIMOS on Keck.

2.3.2 The rest of the first decade

The rest of the envisioned instrument suite for the first decade includes (in alphabetical order):

HROS (High-Resolution Optical Spectrometer): a single-object, seeing-limited, high-resolution (R = 50 000 for 1 arcsec slit) optical-UV echelle spectrograph in the heritage of HIRES at Keck and UVES at the VLT.

IRMOS (Infrared Multiobject Spectrometer): designed to use multi-object adaptive optics (MOAO) techniques over a 5 arcmin field of regard to feed up to 20 deployable IFUs.

MIRES (Mid-Infrared Echelle Spectrometer): is a diffraction-limited, high-resolution (5000 < R < 100 000) spectrometer and imager operating at 8 – 18 μm. It will employ a separate AO system optimized for the mid-infrared.

NIRES (Near-Infrared Echelle Spectrometer): fed by NFIRAOS, NIRES is a diffraction-limited high-resolution (20 000 < R < 100 000) spectrometer covering 1 – 2.4 μm simultaneously. It is a scientific descendent of NIRSPEC at Keck and CRIRES at the VLT.

PFI (Planet Formation Instrument): an extreme AO high contrast exoplanet imager with spectroscopic (R ≤ 100) capability. The first generation system will obtain 10^6 (goal: 10^7) contrasts while the second generation requirement is 10^8 (goal: 10^9) in H-band for R < 8 mag. PFI is intended to be deployed after GPI at Gemini and SPHERE at the VLT so that lessons learned from those pathfinder high-contrast imagers can be fed back into PFI. Indeed, there is a large overlap between the GPI and PFI development teams.

WIRC (Wide Field InfraRed Camera): a moderate field near infrared imager configuration fed by NFIRAOS to provide near diffraction-limited images through a variety of filters with high photometric and astrometric accuracy. WIRC is expected to deliver Nyquist sampled images (λ/2D = 0.004 arcsec) over a 30 arcsec diameter field-of-view with wavelength coverage 0.8 – 2.5 μm (goal: 0.6 – 5 μm).

3 Fundamental physics and cosmology

One of the most exciting areas of current research lies at the interface between theoretical and high-energy physics and cosmology. Indeed, the discovery of dark matter and dark energy came from astrophysical observations of the Universe. It is these kinds of careful quantitative cosmological and astrophysical measurements that offer the greatest promise for constraining fundamental physical theories. TMT will contribute in this area by providing highly accurate measurements of the most distant sources, large samples of objects probing the Universe at intermediate distances, and precise studies of the dark matter in nearby galaxies, including in the center of our own Milky Way.

3.1 The nature of dark matter

The presence of dark matter was first inferred more than seventy years ago (Zwicky 1933) yet its nature remains a mystery. Cosmological models employing cold dark matter (CDM) predict a bottom-up hierarchical picture of galaxy formation that is in very good agreement with observations over a wide range of scale. However, these models fail in that they predict a sharp concentration of dark matter in the cores of galaxies, and large numbers of dwarf galaxies surrounding larger galaxies such as our own. Both predictions are inconsistent with observations. While the latter might perhaps be explained by astrophysical processes (e.g. star formation efficiency) the former appears to be un-reconcilable. This has motivated many modifications to CDM models, in which the dark matter is either “warm”, self-interacting in some way, or born at late times from the decay of cold particles (see for example Seto and Yamaguchi 2007, Abazajian and Koushiappas 2006, Kaplinghat 2005, Strigari et al. 2007a). The challenge now is to see which, if any, of these models are in accord with reality.

3.1.1 Dwarf galaxy radial mass profiles

Dwarf galaxies are dominated by dark matter, and contain numerous dynamical tracers (stars) that are accessible to large telescopes. Their radial mass profiles can be determined by studying the kinematics of these stars. Precise measurements of the log-slope of the density profile (γ) will allow separation between warm dark matter (WDM) models (that predict $\gamma \sim -0.5$ at the half-light radius of dwarf spheroidal galaxy like Draco) and cold dark matter (CMD) models (that predict $\gamma \sim -1.2$) (Strigari et al. 2007b).

The best current measurements are based on radial velocities of ~1000 stars (Walker et al. 2007). Unfortunately, these are not large enough line-of-sight velocity samples to measure γ precisely enough because of the large degeneracy associated with the unknown stellar velocity anisotropy (Binney & Tremaine 1988). Figure 3-1 shows how the error on γ will be reduced as a function of the number of stars in a kinematic sample. WFOS on TMT will enable the determination of velocities at ~5 km/s accuracies in >~ 10,000 stars in dSphs like Draco, providing a unique and robust constraint on the nature of dark matter.

A different way to overcome the systematic uncertainties in line-of-sight velocity surveys is to add proper motion data. Strigari et al. (2007b) have shown that if proper motion data could be obtained with ~ 5 km/s accuracy for just a few hundred stars, the accuracy of current kinematic studies would be increased five fold. They argue that such data could be provided by the proposed SIM space mission, but the launch of SIM has been deferred indefinitely. TMT, with its wide-field MCAO system, should be able to provide the needed data. Astrometric accuracy of 150 μas has already been demonstrated for galactic center observations with the Keck AO system – TMT should achieve an accuracy of ~30 μas at comparable signal to noise ratio. The magnitude of the RGB tip in local dwarf galaxies is K ~ 18 – 19, comparable to Galactic center stars, and there will be at least a three-fold gain in signal to noise ratio from the larger aperture of TMT. Over a three-year baseline, an astrometric accuracy of 30 μas, for a distance of 100 kpc, corresponds to the required kinematic accuracy of 5 km/s.

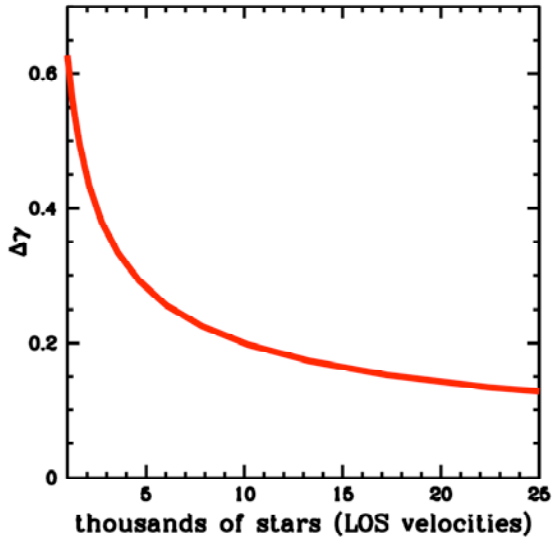

Figure 3-1 – Model error on the ability to determine the log-slope of a dwarf galaxy's dark matter density profile as a function of the number of line-of-sight velocities. The current state of the art samples start at ~1000 stars. TMT will enable samples of ~10,000 stars or more, which will provide a means to discriminate between WDM and CDM predictions for cored vs. cusped profiles. Figure credit: J. Bullock (UCI)

3.1.2 Baryonic power spectrum

The power spectrum of density fluctuations on small scales provides the strongest constraint on the fraction of hot dark matter in the Universe (Hu et al. 1998) as free streaming by this matter reduces the fluctuation power on small scales. Power spectrum data can also provide constraints on a wide variety of potential low-mass particles such as sterile neutrinos, axions and thermal relics (Narayan et al. 2000, Hannestad & Raffelt 2004, Viel et al. 2005).

Amazingly, studies of the distribution of matter can also tell us details about the early inflationary period of the Universe. The power spectrum of density fluctuations is predicted by theory to have arisen from a "scale invariant" primordial spectrum that is a power law with near unity slope. Small deviations from this unity slope are expected and are related to the degree by which the Universe expanded during the period of inflation and hence to the physical properties of the fields that drove inflation. By measuring the distribution of matter over a wide range of scales, one can constrain both the slope and possible deviations to high precision. Measurement of the power spectrum on large scales is limited by "cosmic variance" (there is only one Universe) – the most precise measurements will necessarily come from measures on small physical scales.

In the present-day universe, the memory of the initial conditions on small scales has been erased by the formation of complex structures such as galaxies. However, by studying the details of the distribution of diffuse hydrogen gas in the intergalactic medium at high redshift, it is possible to measure the "primordial" power spectrum of all matter.

The largest data set at present is the SDSS Lyman-alpha forest catalog (McDonald et al. 2005) which comprises about 3000 low-resolution (R ~ 2000) spectra of quasars in the range z ~ 2.2 – 4.2. These data are supplemented by high-resolution observations of a smaller number of quasars, mainly at intermediate redshifts, obtained with 8 – 10 meter telescopes. These data place a tentative upper limit of ~10 keV for the mass of sterile neutrinos (Viel et al. 2006). Since the power spectrum is most sensitive to WDM at high redshifts, future high redshift observations will be of utmost importance in improving these limits.

By using galaxies as probes instead of quasars, TMT will allow for the first time the study of the three-dimensional distribution of diffuse hydrogen in the intergalactic medium, which is directly related to matter

density, thereby increasing the precision of cosmological measurements by an order of magnitude over that possible with current telescopes. Here the distribution of matter is affected by complex physical processes, such as gas dynamics, star formation and feedback. TMT, using WFOS and HROS, will probe the distribution and composition of gas along the lines of sight to distant quasars and galaxies, providing unique high-quality data essential to an understanding of these processes.

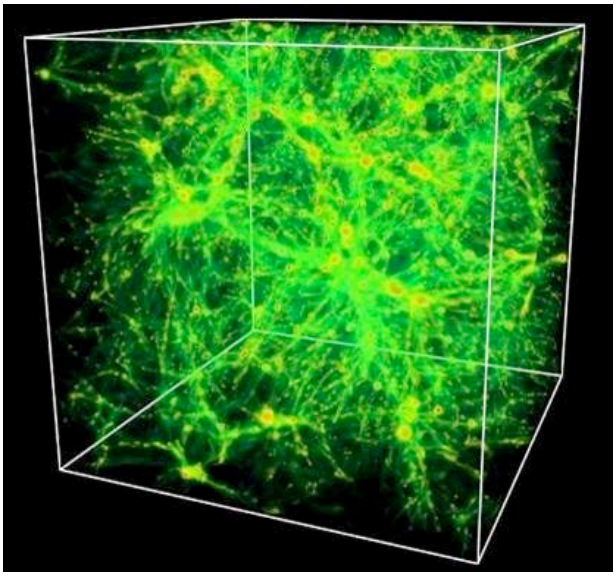

Figure 3-2. Dark matter structure at *z* ~ 3. TMT will probe multiple lines of sight using WFOS and background galaxies as sources. This will provide a more complete understanding of the baryonic power spectrum and interaction of the IGM with baryonic matter in galaxies. (Credit: R. Cen, Princeton U.)

3.1.3 The Galactic Center: a laboratory for dark matter and relativity experiments

Over the last decade, near-infrared monitoring of stars within the Milky Way's central cluster using 10m class telescopes has enabled complete Keplerian orbit reconstructions for ~10 sources which has demonstrated the existence of a central black hole of mass $4.8\pm0.4 \times 10^6$ M_O at a distance of 8.4±0.4 kpc (Schodel, et al. 2002; Schodel, et al., 2003; Ghez et al. 2003, 2007; Eisenhauer et al. 2003). The greater flux sensitivity and spatial resolution of TMT relative to current facilities will allow more stars to be followed, with greater accuracy in both position and velocity measurements. In turn, these more accurate measurements will enable a variety of experiments in relativistic astrophysics.

Relative to the current facilities at 8 – 10m telescopes, diffraction-limited imaging with IRIS on TMT offers a three-fold benefit to stellar-dynamics experiments at the Galactic Center. First, when working at the diffraction limit, source confusion and errors due to crowding are reduced. For the 10m telescope experiments, the region in which orbital motion is detectable has a confusion limit of K ~ 17 mag. With TMT, this limit is extended to K ~ 22 mag and the number of stars with detectable orbital motion is increased by an order of magnitude to 100 stars (see Figure 3-4). Second, the astrometric precision is improved. The astrometric precision limit achieved today at the Galactic Center with the Keck Observatory is $\delta\theta_{10}$ ~ 150 μas. Simulations of MCAO system performance that include realistic models of atmospheric turbulence suggest that TMT can achieve $\delta\theta_{10}$ ~ 30 μas in the Galactic Center (or any other field with high surface density of stars) (Ellerbroek, private communication). Third, the precision of the radial velocity measurements will also be improved. The current experiments achieve radial velocity limits of ~20 – 50 km/s for the orbiting early-type stars. For these stars, one might conservatively expect radial velocities to be measured to within ~10 km/sec. Since the fainter, cooler stars, which will be detected with TMT, have a richer set of spectral features, one might be able to achieve radial velocities of ~1 km/sec as has been done in the case of non-adaptive optics spectroscopy of cool stars in the central parsec of the Galaxy (Figer et al. 2003). Thus the achievable δv may be ten times smaller than the above estimate.

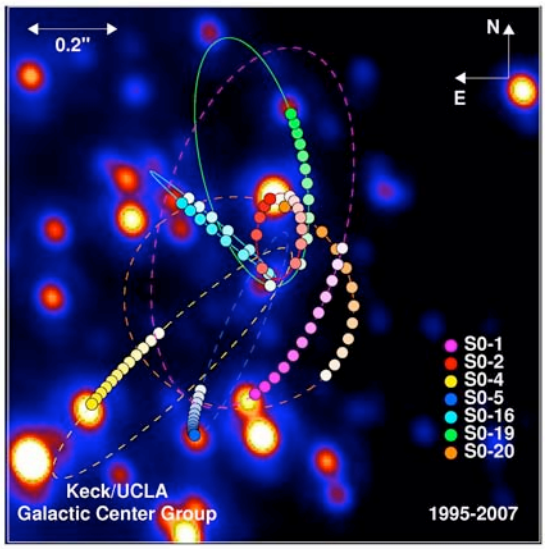

Figure 3-3. Central Milky Way supermassive black hole. Infrared image of the galactic center, with previous positions of stars superimposed. The position of the black hole is indicated by the star-shaped symbol at the center. Ellipses illustrate the derived orbits of seven stars. (A. Ghez, UCLA)

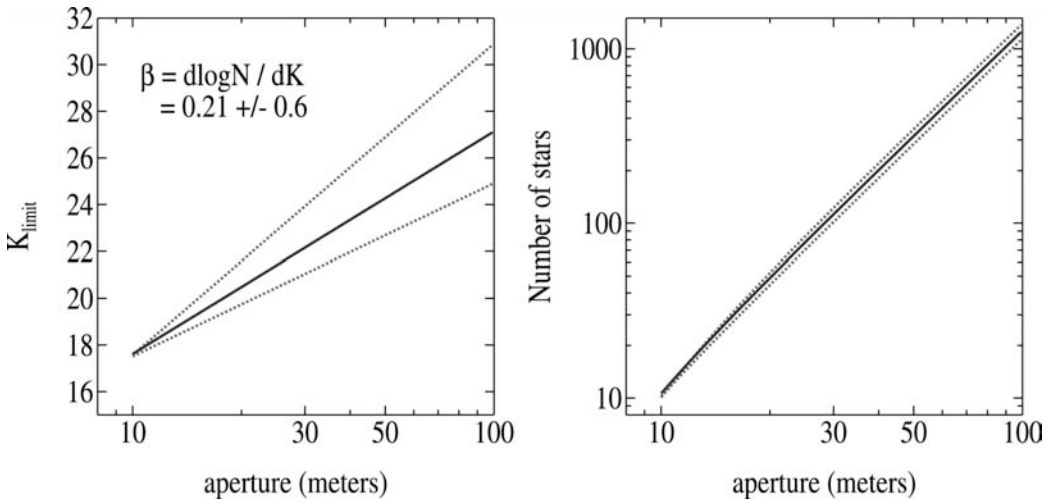

Figure 3-4. K-band magnitude limit vs. stars with detectable motions as a function of aperture. Estimated relationships are shown for K-band limiting magnitude vs. number of stars with detectable orbital motions as a function of aperture size under the assumption of diffraction-limited imaging. Results are shown for power-law K-band luminosity functions normalized to observations by Schodel et al. (2003) with the slopes matching the range found by Genzel, et al. 2003. From Weinberg et al. 2005.

This improvement enables heretofore unachievable astrophysical experiments based on stellar orbits at the Galactic Center (see Weinberg, Milosavljević & Ghez, 2005 for details). Such experiments require long time baselines (e.g. 10 years), roughly monthly sampling intervals, and measurement uncertainties of [$\delta\theta$, δv] = [0.5 mas, 10 km/s] or better. Astrophysical topics include:

- ***Improved M_{BH} and R_O measurement accuracy, a constraint on dark matter:*** fractional uncertainties in black hole mass (M_{BH}) and the distance from the Sun to the Galactic Center (R_0) of less than 0.1% at the 99.7% level are achievable – a factor of ~100 times better than present uncertainties. Measuring these quantities to this accuracy will constrain the shortest-to-longest axis ratio $q = c/a$ of the Galactic dark matter halo to similar accuracy. The shape parameter q is

an important diagnostic of dark matter models and structure formation and is currently poorly constrained in all galaxies including the Milky Way. (Olling & Merrifield 2000; 2001).

- ***Measuring the extended matter distribution:*** modeling the extended matter distribution as a power-law profile, the presence of extended matter is detectable (i.e., observations yield a lower bound) as long as the mass in extended matter within 0.01 pc M_{ext} (r < 0.01 pc) > 1500 solar masses. TMT will measure M_{ext} and the power-law density slope γ to 20 - 30% accuracy (see Figure 3-5). Thus, if the dark matter distribution matches theoretical expectations and forms a density spike (Gondolo & Silk, 1999), its influence on the orbits will be detectable. Such a detection would constitute a measurement of the gravitational influence of dark matter on the smallest scales yet.

- ***Measuring relativistic effects*:** by including post-Newtonian corrections involving terms of order $(v/c)^2$ to the stellar equations of motion, measurements of the extended mass distribution can be coupled with constraints on the speed of light (see Figure 3-5 and Weinberg et al.). Even if only one star with e > 0.96 is monitored over a single period, the orbital pericenter advance due to the relativistic prograde precession will be measured to 5σ accuracy. Several such high eccentricity stars are expected to be detected amongst the ~ 100 stars accessible to TMT. In the favorable event of the discovery of a star on a highly compact and eccentric orbit, it may be possible to also detect such higher-order relativistic effects such as frame dragging due to the spin of the black hole. These measurements require achievable precision in measurements of the speed-of-light as a function of the extended mass distribution (see Figure 3-5).

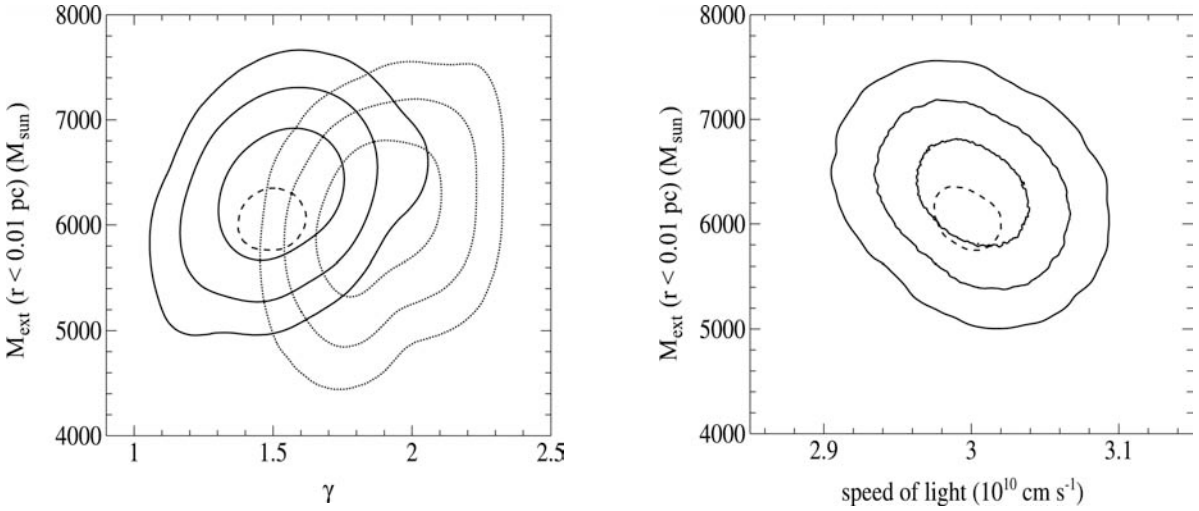

Figure 3-5. Astrophysical experiments with Galactic Center stellar dynamics measurements. Left panel: constraint on the extended mass distribution obtainable with TMT. Shown are the 68%, 95%, and 99.7% confidence levels on the enclosed mass and slope of an extended matter distribution, assuming an astrometric limit of $\delta\theta$ = 0.5 mas and a spectroscopic limit of δv = 10 km s^{-1}. The input models have power-law slope of = 1.5 and 2 and an input enclosed mass of 6000 *M* within 0.01 pc. The dashed contour is the constraint at the 99.7% level for measurement errors that are a factor of 5 smaller. Right panel: TMT sensitivity to post-Newtonian effects. Shown is the uncertainty in the speed of light and the extended matter mass as obtained by including post-Newtonian corrections to the equations of motion of the observed stars. Roemer delay and special relativistic effects are not included in the model in order to demonstrate that general relativistic effects of order $(v/c)^2$, including the prograde precession, are detectable with TMT. The solid contours show the 68%, 95%, and 99.7% confidence levels, assuming an astrometric limit of $\delta\theta$ = 0.5 mas and a spectroscopic limit of δv = 10 km s^{-1}. The dashed contour shows the 99.7% confidence level for smaller astrometric and spectroscopic limits of $\delta\theta$ = 0.1 mas and δv = 2 km s^{-1}. From Weinberg et al. 2005.

- ***Measuring the mass function of stellar-mass black holes:*** the rate of detectable encounters between monitored stars and background stars or stellar remnants is proportional to the mass of the background sources (Weinberg et al. 2005). If the background sources are dominated by stellar-mass black holes, as predicted by estimates of mass segregation in the vicinity of a massive black hole (Morris, 1993; Miralda-Escude & Gould, 2000), approximately 10% of all stars monitored will experience detectable deflections in their orbital motions. Monitoring orbits with TMT therefore provides a viable means of measuring the mass function of stellar-mass black holes in the Galactic Center.

3.2 Dark energy

Understanding the nature of dark energy is arguably the greatest challenge facing cosmology and the quest for a more fundamental theory of the Universe. It is well known that the standard model fails spectacularly to account for the observed small value of the vacuum energy density. The discovery of cosmological acceleration, and its implications for a small but non-zero vacuum energy density were both unexpected, and confounding. Much of the current observational focus hinges on measurements of the energy density, and equation of state of the dark energy. The latter is often reduced to two parameters, *w* and *w'* which can be constrained through combined observations of supernovae, the cosmic background radiation and large-scale structure (see Perlmutter 2005 for a review). A broad range of theoretical models are consistent with the observed data, ranging from theories that involve scalar fields such as quintessence, to modifications of gravity (e.g. Alcaniz and Zhu 2005 and references therein).

Many alternate theories of gravity, such as 5-dimensional "braneworld" theories (e.g. Dvali et al. 2000) predict a saturation of the Hubble parameter when the Hubble distance becomes comparable to the characteristic distance where gravity begins to see the fifth dimension (Zhu and Alcaniz 2005). This results in an effective cosmological constant and consequent acceleration of the Universe without the need for dark energy. On smaller scales, departures from conventional four-dimensional gravity may be detected (Lue et al. 2004). For a radially-symmetric distribution of mass *M*, substantial deviations from the usual Schwarzschild metric (in the form of a repulsive force) will occur at distances greater than

$$r_* = \left(2GM / H_0^2\right)^{1/3}.$$

For a bound system, this corresponds to the distance at which the orbital time is comparable to a Hubble time. This creates a redshift-dependent distortion in the power spectrum since small-scale fluctuations see a different gravitational law than do large-scale fluctuations. Accurate measurements of the expansion history and the power spectrum at low and high redshifts thus have the potential to distinguish between dark energy and modified gravity.

TMT will make several important contributions in this field. The measurement of the power spectrum of the Lyman-α forest has been discussed above. Another approach is to push the supernovae observations to the highest possible redshifts and measure the dark energy density as a free function of cosmic time (see Wang 2005 and Figure 3-6). The D^4 gain afforded by the large aperture and adaptive optics of TMT will provide a 3 – 4 fold improvement in supernovae cosmology at high redshifts (z ~ 2 – 4). Of equal importance, TMT will allow in-depth studies of the astrophysics of high-redshift objects. By studying their properties as a function of redshift, host galaxy properties, environment, etc.

3.3 Physics of extreme objects

The most energetic explosions in the Universe produce gamma-ray bursts that can be seen at great distances. These are believed to be caused by the collapse of massive stars that generate an intense outflow of highly-relativistic particles having energies beyond anything achievable with particle accelerators on Earth. Because these gamma-ray bursts (GRBs) are very rare events, one must look

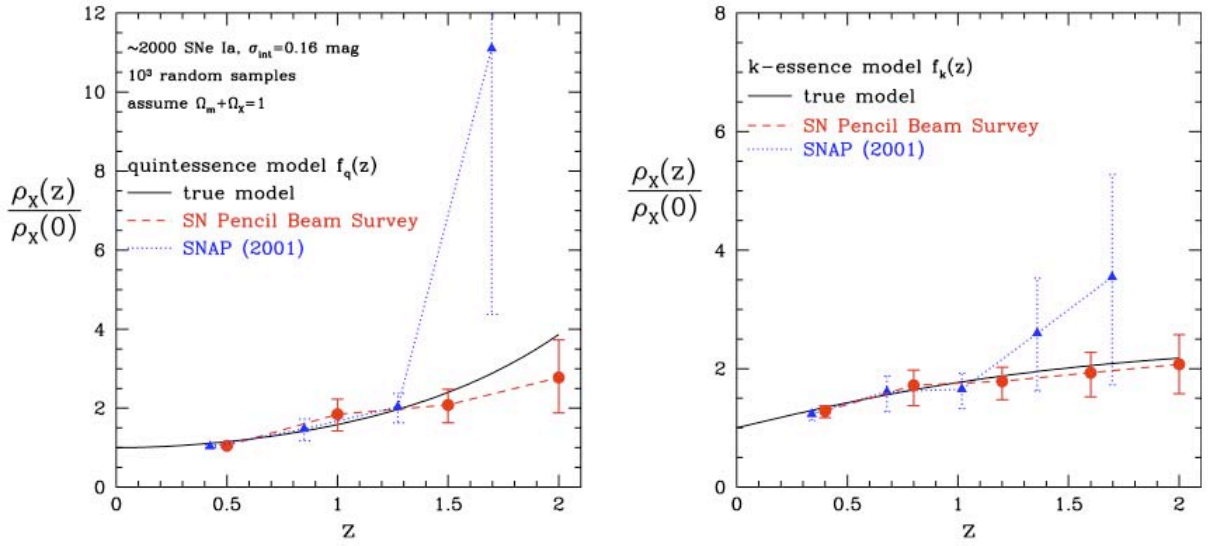

Figure 3-6 Simulations comparing a shallow wide-angle supernova survey (SNAP 2001) with a deep pencil beam survey to z = 2 for two different dark energy models. The deep survey is much more effective at constraining the evolution of the dark energy density (Wang and Lovelace 2001). TMT will be able to detect type Ia supernovae to z ~ 4.

over cosmic distances to find them. Follow-up observations to study their properties require large telescopes. TMT will allow us to study the mechanism that produces the intense radiation beam, and better understand the physical conditions that host the GRB phenomenon.

The optical afterglows of GRB explosions have absolute magnitudes as high as M_V = –36, and are typically brighter than M_V = –21 for hours. This makes them 2 to 4 orders of magnitude brighter than supernovae. TMT will be able detect them to redshifts z ~ 10. The proposed next-generation GRB satellite, EXIST, is expected to find some 600 GRBs per year, with perhaps 10 at z ~ 10.

Another opportunity for TMT is the study of type IIn supernovae. These relatively rare objects (~ 3% of all type II supernovae) exhibit strong emission lines lasting for many months, and are the brightest of all supernovae in the rest-frame UV. The progenitors are believed to be very massive stars (~ 80 M_O), which makes them a unique probe of the high end of the luminosity function. TMT will be able to detect, spectroscopically confirm, and study these supernovae to redshifts z ~ 6.

Tidal flares occur when a massive black hole disrupts a nearby star. Detection and study of such flares in galactic nuclei would allow us to measure the mass of the black hole and study the demographics of the growth rate of massive black holes. For a 10^7 M_O black hole, a typical flare is expected to last several months and have a bolometric peak luminosity of ~ 10^{37} W, most of which is in the X-ray and far UV region of the spectrum. Because of this, flares will exhibit a negative K correction and should be visible to z ~ 10 with TMT. The expected rate is of order 4000 flares per year over the entire sky, to the magnitude limit AB = 25 of the Pan-STARRs medium deep survey.

3.4 Variation of fundamental physical constants

In a large class of fundamental theories, the four-dimensional Universe that we observe emerges from a higher-dimensional space time. In such theories, the fundamental physical constants, such as the fine structure constant and the electron-to-proton mass ratio, are expected to be time dependent (see Uzan 2003 for a review). Time variation of fundamental parameters is also generic in cosmological models of

quintessence. It is possible to search for and constrain any such variations of the constants by accurate measurement of wavelengths of absorption lines seen in the spectra of quasars (Webb et al. 1999). More than a decade of study using 8 and 10-meter telescopes has yielded mixed results (e.g. Murphy et al. 2003, Chand et al. 2004, Tzanavaris et al. 2005), and recent tantalizing evidence for a variation in the electron-to-proton mass ratio (Figure 3-7). The present observations are limited both by signal to noise ratio, and by identification and control of systematic errors (Murphy et al. 2007). While both of these limitations need to be addressed, it is clear that signal-to-noise ratio provided by the current generation of 8-10 m telescopes is at best marginal. In the same amount of observing time, TMT with HROS would provide a three-fold improvement, providing a statistically definitive result.

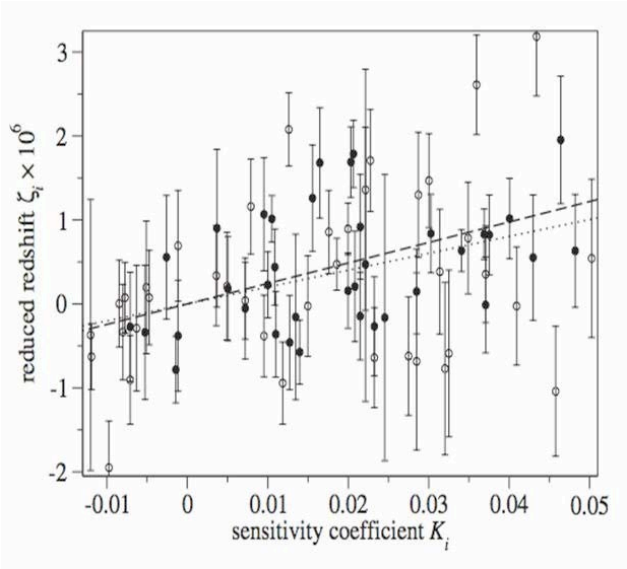

Figure 3-7. Measuring alpha. Wavelength residuals seen in QSO spectra vs. sensitivity coefficient. A positive slope indicates a variation of the ratio of the masses of the proton and electron (Reinhold et al. 2006)

References

Abazajian, K., Koushiappas, S. M. 2006, Phys. Rev. D, 74, 023527
Alcaniz, J. S. and Zhu, Z.-H. 2005, Phys. Rev. D, 71, 083513
Binney, J. and Tremaine, S. 1988, *Galactic Dynamics*, Princeton University Press.
Chand, H., Strianand, R., Petitjean, P., Aracil, B. 2004, A&A, 417, 853
Dvali, G., Gabadadze, G. and Porrati, M 2000, Phys. Lett. B, 485, 208
Eisenhauer, J. et al. 2003, ApJL, 597, L121
Fan, Y. Z., Zhang, B. and Wei, D. M. 2005, ApJ, 628, 298
Figer, D.F., et al., 2003, ApJ, 599, 1139
Genzel, R. et al. 2003, ApJ, 594, 812
Ghez, A.M. et al. 2003, ApJ, 586, L127
Ghez, A.M. et al. 2005, ApJ, 620, 744
Ghez, A.M. et al. 2007, ApJ, submitted.
Gondolo, P. & Silk, J., 1999, PRL, 83, 1719
Hannestad, S. & Raffelt, G. 2004, JCAP, 4, 8
Hu, W., Eisenstein, D. J. and Tegmark, M. 1998, PRL, 80, 5255
Kaplinghat, M. 2005, Phys. Rev. D, 72, 063510
Lue, A., Scoccimarro, R. and Starkman, G. 2004, Phys. Rev. D, 69, 044005
McDonald, P. et al, ApJS, 163, 80
Miralda-Escude, & Gould, 2000, ApJ, 545, 847

Morris, 1993, ApJ, 408,496
Murphy, M. T., Tzanavaris, P., Webb, J. K. and Lovis, C 2007, MNRAS 378, 221
Murphy, M. T., Webb, J. K. and Flambaum, V. V. 2003, MNRAS, 345, 609
Narayan, V. K., Spergel, D. N., Dave, R. and Ma, C. P. 2000, ApJ, 543, L103
Olling & Merrifield 2000, MNRAS, 311, 361
Olling & Merrifield 2001, MNRAS, 326, 164
Perlmutter, S. 2005, Physica Scripta, T117, 17
Reinhold, E. et al. 2006, PRL, 96, 151101
Schodel, et al. 2002, Nature, 419, 694
Schodel, et al., 2003, ApJ, 596, 1015
Seto, O. and Yamaguchi, M. 2007, Phys. Rev. D, 75, 123506
Strigari, L. E., Kaplinghat, M. and Bullock, J. S. 2007a, Phys. Rev. D, 75, 061303
Strigari, L. E., Bullock, J. S. and Kaplinghat, M. 2007b, ApJ, 657, L1
Tzanavaris, P. et al. 2005, PRL, 95, 041301
Uzan, J.-P. 2003, Rev. Mod. Phys., 75, 403
Viel M., Lesgourgues, J., Haehnelt, M. G., Matarrese, S., and Riotto, A. 2005, Phys. Rev. D, 71, 063534
Viel M., Lesgourgues, J., Haehnelt, M. G., Matarrese, S., and Riotto, A. 2006, PRL 97, 071301
Walker et al. 2007, ApJ, 667, 53
Wang, Y. 2005, New Astron. Rev., 49, 97
Wang, Y. and Lovelace, G. 2001, ApJ, 562, L115
Webb, J.K. et al. 1999, PhRvL, 82, 884
Weinberg, N.N., Milosavljevic, M., Ghez, A.M. 2005, ApJ, 622, 878
Zhu, Z.-H. and Alcaniz, J. S. 2005, ApJ, 620, 7
Zwicky, F. 1933, "Die Rotverschiebung von extragalaktischen Nebeln". *Helvetica Physica Acta* **6**: 110–127

4 The early Universe

4.1 Overview

The expansion of the Universe stretches the wavelengths of photons, causing spectral lines to shift to longer (redder) wavelengths. The redshift of a source is thus a measure of its distance, and the epoch at which the light was emitted. In terms of sources for study, the frontier of current exploration is at a redshift of 7, corresponding to a time when the Universe was about 800 million years old.

The motivation for finding yet earlier sources is three-fold. Firstly, astronomers are inspired to undertake a census of the first galaxies seen in the first few hundred million years after the Big Bang. This curiosity for exploration is fundamental to science and has driven astronomy to major discoveries in the past; it also excites great public interest. Secondly, and more fundamentally, hydrogen in intergalactic space is ionized by a redshift of about 5, whereas it was fully neutral soon after the time the microwave radiation emerged. At some point there was a landmark event called *cosmic reionization*, akin to a phase transition in the intergalactic medium (IGM), when hydrogen became ionized. Most astronomers suspect this event was closely related to the birth of the first galactic systems that released copious amounts of ionizing ultraviolet photons. Prior to reionization, hydrogen was still in atomic form and the Universe was devoid of any light emitting celestial sources – a period commonly termed the *Dark Ages*. Pinpointing when and how the Dark Ages ended, and finding the sources responsible for cosmic reionization is necessary to complete the story of galaxy evolution. Thirdly, the physical processes which accelerate or inhibit the cooling and collapse of hydrogen gas clouds into young galaxies at these early times provide the seeds from which later, more massive, galaxies such as our own Milky Way assembled. Although theory makes predictions of how these early systems grew and evolved, it is currently observationally unchallenged.

4.2 Early sources and cosmic reionization

It is thought that the first luminous objects, forming from primordial hydrogen and helium, will be giant short-lived stars, perhaps more than 200 times more massive than the Sun. Their number and brightness is uncertain, in part because it is not known how much of the light will penetrate the IGM. Their detection will be challenging with JWST and TMT even if they lie in an accessible redshift range (redshift $z < 20$ for TMT). As gravity inexorably forces larger hydrogen clouds to cool and collapse, low mass galaxies will begin to shine. Calculations taking into account the transfer of ultraviolet radiation from these early galaxies through the IGM suggest “bubbles” of ionized gas will develop around each prominent source. The bubbles will enlarge and eventually overlap, completing the process of cosmic reionization.

When might this have occurred? The pattern of polarization signals from microwave background photons detected by the WMAP satellite suggests the free electrons responsible reside in ionized gas in the redshift range 8 – 20. Thus it is quite likely there will be an abundance of energetic star-forming sources in this interval. However, it is not known if reionization was an instantaneous or protracted event, or whether the ionizing radiation comes from a highly abundant distribution of feeble sources, or a rarer population of intensely-emitting more massive galaxies. Some cosmologists suspect there may be ionizing contributions from black holes or decaying particles. Only by locating and carefully studying star-forming sources in this era can these important questions be answered.

Soon after the first sources emerge, the heated neutral hydrogen begins to glow more brightly than the microwave radiation. Powerful radio telescopes and interferometers now being planned should trace the topology and growth of the bubbles around these sources by mapping selected regions of the sky using the redshifted 21cm emission line of hydrogen. However, although low frequency radio surveys may improve our knowledge of when cosmic reionization occurred, they will not detect the sources responsible. Our physical understanding of the process will thus rely crucially on observations with JWST and TMT.

JWST should certainly be able to detect the brightest sources lying within each ionized bubble. However, TMT, with adaptive optics, will be able to detect and study objects an order of magnitude fainter. The gain will be particularly dramatic if, as expected, the earliest sources are physically small. TMT may also find the signatures of the much sought after, chemically unevolved, Population III sources expected at these early epochs. In general terms, therefore, we can expect the role of TMT to be one of providing a more detailed story of the properties and influence of earliest sources on the intergalactic medium, building on the basic progress made with radio surveys and JWST.

In the following sections, suggested programs in this area are presented and the expected synergy between TMT and both JWST and the upcoming 21cm surveys is discussed. Inevitably, given how little is known about the properties of the relevant sources, the quantitative details are more speculative than in other areas of this document. Flexibility in survey strategy will be crucial as more is learned about this uncharted era. Some of the performance uncertainties are discussed in a later section in terms of both the unknown size and abundance of star-forming sources.

4.3 Characterizing the first galaxies and their influence on the IGM

This section introduces several areas where TMT is likely to make a profound impact in its early years in addressing the physical processes by which star forming galaxies contribute and define the cosmic reionization process. The programs fall into two broad categories: (i) multi-object surveys of large numbers of line emitting galaxies, where the motivation lies in their statistical distribution and properties, analyzed in conjunction with both JWST and 21cm surveys, and (ii) detailed follow-up studies of individual sources, possibly ones known a priori to be of interest.

4.3.1 Locating Primordial Stellar Systems

The earliest galaxies will contain massive stars formed from primordial gas. As these stars evolve and eject processed material from their eventual supernovae, newly-formed stars containing heavy elements will become more common. Simulations consistent with the WMAP polarization results (Ciardi et al. 2006) suggest primordial (so-called Population III) stars may lie in the redshift range 7 to 20. Verifying their presence and determining the redshift distribution of galaxies containing these early populations would represent a major new constraint on early galaxy evolution.

As massive hot sources, Population III stars are expected to generate radiation fields intense enough to ionize the primordial helium gas. The characteristic emission lines produced by this gas, particularly He II at 1640 Å, can thus serve as a marker for a primordial system. Model atmosphere calculations by Schaerer (2002, Figure 4-1) suggest this helium line could be revealed with a strength of up to ~10% of that of the hydrogen Lyman alpha line in these systems. TMT would be able to see this line in galaxies out to redshift $z \sim 14$. Assuming the sources are physically small, there will be a significant signal/noise gain over JWST (see below).

For a single burst of star formation, the He II line is short-lived (a few Myr) so the practicality of its detection relies on building up a large survey. Both the improved spectral resolution and multiplex advantage of IRMS over the spectrographs on JWST, and the improved sensitivity of TMT to more typical low mass star-forming galaxies, makes this program an important opportunity. Sources known a priori to be of interest, e.g. from JWST data, would be studied with IRIS.

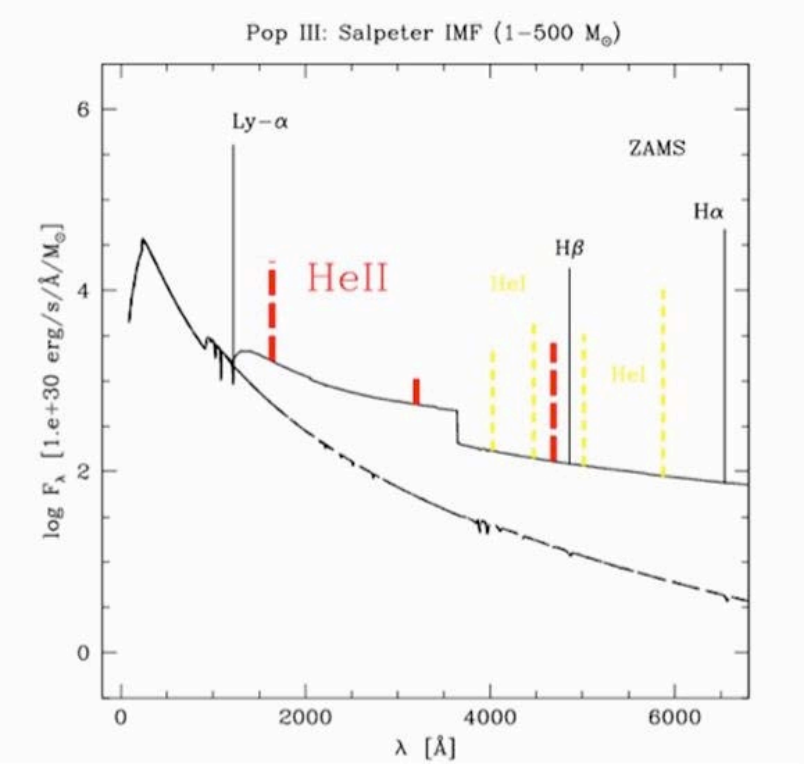

Figure 4-1. Predicted spectrum of first luminous objects. Spectrum of a Pop III ZAMS burst (from Schaerer 2002) based on non-LTE model atmospheres including H and He recombination lines. The dashed line shows the pure stellar continuum (neglecting nebular emission). Note the prominent line of He II 1640 (thick dashed line) and the importance of nebular continuous emission. Simulations indicate the He II line, which decays rapidly within 2 Myr, is a valuable tracer of metal-free stellar populations.

4.3.2 Tracing Star Formation in Ionized Bubbles

Although the detection or absence of He II 1640 Å is a goal in characterizing an early galaxy, most distant sources will be recognized via their Ly-α 1216 Å emission. As much as 8% of the light of a metal-poor young galaxy can emerge in this transition and thus it is clearly the most effective redshift indicator. Unfortunately however, as a resonant transition, the Ly-α line radiation is scattered by neutral hydrogen and so its presence and strength will depend on the extent and geometry of the local ionizing bubble. The faintest Ly-α emitters, detectable only with TMT, will act as valuable tracers of star formation within individual bubbles and indicate clearly the contribution of lower mass galaxies to the reionization process.

A practical strategy is therefore to first locate ionized bubbles either from 21cm surveys or by locating luminous or clustered sources at a given redshift with JWST. The improved sensitivity and multiplex gain of IRMS should be extremely effective in such a program but only if broad-band, near-IR selected targets are available. In this case the ionization bubbles would be isolated in position and redshift space from JWST surveys, and their extent would ideally match the spectroscopic survey field of IRMS. The deployable IFUs of IRMOS would enable blind spectroscopic searching for line emitters within the bubbles, thereby eliminating the need for broad-band selected targets.

Table 4-1 shows the expected evolution in ionized bubble sizes from a recent analytical model that accounts for IGM clump distribution and large scale clustering (Furlanetto & Oh 2005). The largest bubbles will be ~2 arcmin across at z = 10, well-matched to the field of IRMS and its second-generation version, IRMOS. The redshift depth of the largest z = 8 bubbles will correspond to $\Delta z \sim 0.02$.

Table 4-1: Sizes of ionized bubbles (from IRMOS-CIT study).

Redshift	Bubble Radius (comoving Mpc)	Physical (kpc)	Half-angle (arcsec)
10	0.3 – 2.5	27 – 227	6.5 – 54
8	0.6 – 6.0	66 – 666	13 – 138
7	0.5 – 20.0	63 – 2500	12 – 478

It is possible that some luminous emitters, around which such TMT surveys can be undertaken, will be located by present-generation programs on 8 – 10 m class telescopes with such instruments as the FLAMINGOS 2, the Gemini Tunable Filter (F2T2), the CIRCE narrow-band imager at the GTC, and the VLT Dark Ages *z* Lyman Explorer (DAZLE). With its capability to image dust continuum up to $z = 10$, ALMA may also provide additional targets as well as additional information about the baryonic content of candidates selected by other means. Surveying the gravitational lens caustics of intervening galaxy clusters has also been an effective probe of very high-redshift objects (e.g. Stark et al. 2007b), although this technique is largely effective in locating abundant populations of low luminosity candidates.

4.3.3 Ly-α Line Profiles

Although neutral hydrogen in the IGM reduces the visibility of Lyman alpha emission from distant sources, it also affects the line profile in a manner that is well-understood (Miralda-Escude 1998).

Foreground hydrogen clouds resonantly scatter Ly-α photons in both direction and frequency. In a partly-ionized medium, scattering is most prominent in the rest-frame of the cloud, thereby diminishing the blue wing of the Ly-α line. However, in a fully-ionized medium, scattering far from resonance (damping) can occur. Accurate line profiles for representative sources at various redshift can thus constrain the neutrality of the IGM, or conversely (if that is already known from 21cm measures), it can provide valuable insight into the physical properties of the radiating sources, such as the escape fraction of the ionizing photons and the velocity of any outflowing gas. It is particularly advantageous to compare line profiles across sources with a range of intrinsic luminosities as well as in different redshift intervals.

Little headway has been made in this area with present telescopes. Hu et al. (2006) have compared stacked Ly-α profiles for the most luminous known emitters at $z \sim 5.7$ and $z \sim 6.5$ and found no obvious evolution. The program is challenged by the need to achieve a high spectral resolution for individual sources as well as the need to probe systems with less extreme luminosities. Once a large number of high redshift emitters are located, either with JWST or TMT, more detailed follow-up studies will become practical.

As an example, in an 8 hour observation, a SNR of 22 per TMT/IRIS resolution element can be secured for an emitter at $z = 8$ with a Ly-α luminosity of $L = 5 \times 10^{41}$ erg s^{-1}, which is sufficient to clearly resolve the line profile (see Figure 4-2). Such systems have a star formation rate of less than 10 M_O/yr (Le Delliou et al. 2006) and are more representative and likely numerous than the luminous emitters for which this program has been attempted statistically thus far.

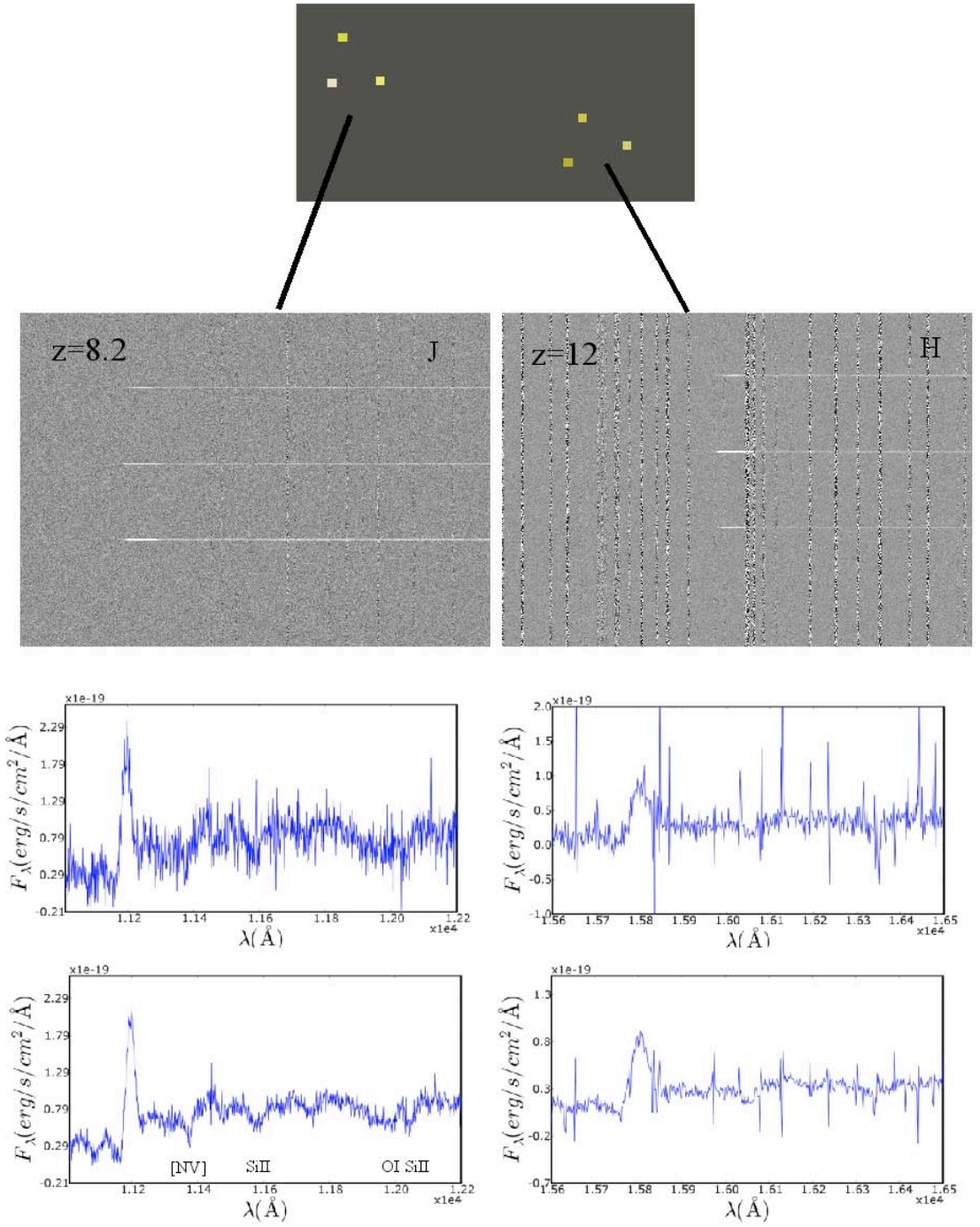

Figure 4-2. Simulated spectra of three high redshift star forming regions with Ly-α luminosities of $7x10^{42}$, 1 x 10^{42}, and 5 $x10^{41}$ erg/s, respectively, at z = 8.2 (left panels) and z = 12 (right panels). Input data is an actual STIS spectrum of Haro 2 (Mas-Hesse, private communication). The top 1-D spectra correspond to a total integration time t = 1hr, while the bottom 1-D spectra correspond to t = 8 hrs. From IRMOS-UFHIA study.

4.3.4 The intergalactic medium beyond $z = 7$

At redshifts $z > 6$, line blanketing in the Ly-α forest essentially removes nearly all the light below the redshifted Ly-α position. Very small amounts of light still penetrate at $z = 6.5$ and can be analyzed using the separation between their positions (the "dark gap" statistics) to analyze the structure and neutral fraction of the intergalactic medium (Songaila & Cowie 2002; Paschos & Norman 2005; Gallerani et al. 2006). However, nearly all of the information at these redshifts must come from metal lines longward of Ly-α. At $z > 6.5$ all of these lines lie in the near infrared – the domain of TMT/NIRES.

Only a handful of bright quasars have been found at $z > 6$, all from the Sloan survey (e.g. Fan et al. 2006). These objects have AB magnitudes of around 20 above the Ly-α line. The highest redshift quasar SDSS 1148+5251 has a redshift of 6.49. However, the limit on the redshift is set by the wavelength coverage of the Sloan survey, and while the numbers are falling rapidly at increasing redshift, we may expect to find a number of $z > 7$ quasars with wide-sky near infrared surveys such as UKIDSS with only slightly fainter magnitudes.

Currently high redshift searches are limited by both the wavelength coverage and the sensitivity of the 10m telescopes. At $z >> 5$ the fundamentally important CIV 1550 doublet, which is the crucial tracer of metals in the diffuse intergalactic medium, moves beyond the optical wavelengths. Up to this point the density of this ion in the intergalactic medium is almost constant (Songaila 2001), providing one of the most fundamental constraints on early galaxy formation. With TMT/NIRES we can extend this measurement to the highest redshifts at which quasars or GRB targets can be found. The b-values of the CIV lines are about 8 km s^{-1}, typically, and are best mapped with resolutions at or above R = 30,000. Mapping the weakest absorption features in the CIV forest requires a SNR > 100 which can be achieved on J ~ 20 quasars in 5 hours.

It is also possible that the ionization may drop as the intergalactic gas becomes progressively neutral and searches may then have to focus on the strong OI and CII lines (e.g. Becker et al. 2006). At $z >> 6$ these lines also move into the near infrared. However, extending the coverage (with NIRES, for example) to 0.9 μm would be extremely useful in allowing us to cover both the high and low ions at the $z = 5 – 7$ redshifts. Such studies will also pick out the high redshift analogs of the $z < 4.5$ DLAs where many other metal lines will be measurable and where relative abundances can be determined.

Figure 4-3. In planning for coordinated TMT and JWST surveys of early galaxies, it is important to estimate their angular sizes. The role of TMT is particularly important for small galaxies given the improved angular resolution over JWST provided by its larger aperture and AO capability. Most known distant galaxies are unresolved, even with HST. However, a few have been studied via the gravitational lensing of a foreground cluster such as this system at z ~5.7 (Ellis et al. 2001). As such sources are physically enlarged by factors of × 20 – 30, their intrinsic size can be reliably measured. Several with prominent Ly-α emission have star forming regions whose physical sizes is ~150 pc, corresponding to < 30 mas. At this angular scale, TMT outperforms JWST in both imaging and spectroscopic detection by factors of × 10 – 100.

4.4 Angular sizes and the synergy with JWST

The oft-quoted present synergy between HST and ground-based 8-10 meter class telescopes (i.e. resolved imaging in space, spectroscopy on the ground) is not really applicable for TMT and JWST as both have impressive imaging and spectroscopic capabilities. However, they are largely complementary in their performance. JWST has the advantage of a reduced background and a sensitivity to sources beyond redshift z ~ 20, whereas TMT has, with its larger aperture and adaptive optics, an improved sensitivity to physically-small, faint sources.

It is very important to know how small these early galaxies might be. Unfortunately, few galaxies with z > 7 have been resolved, even with HST. Objects detected at z ~ 6.5 have angular sizes at or below the 80 – 100 mas range. Le Delliou et al. (2005) have argued that the earliest galaxies will have projected angular sizes of 50 mas. Fortunately, with the aid of gravitational magnification, it is possible to demonstrate that at least some star forming regions have (unlensed) angular sizes as small as 30 milliarcsec or less (Figure 4-3). Such tiny sources will be much more effectively charted with TMT.

As TMT observations in this regime will be background-limited, the sensitivity is a strong function of source angular size. For various assumptions the spectroscopic efficiency of detecting Ly-α is considered for the 6 < z <10 redshift range in Figure 4-4. It is illustrative to compare the detection limits with those currently practical with 8 – 10 meter telescopes as well as that possible with JWST.

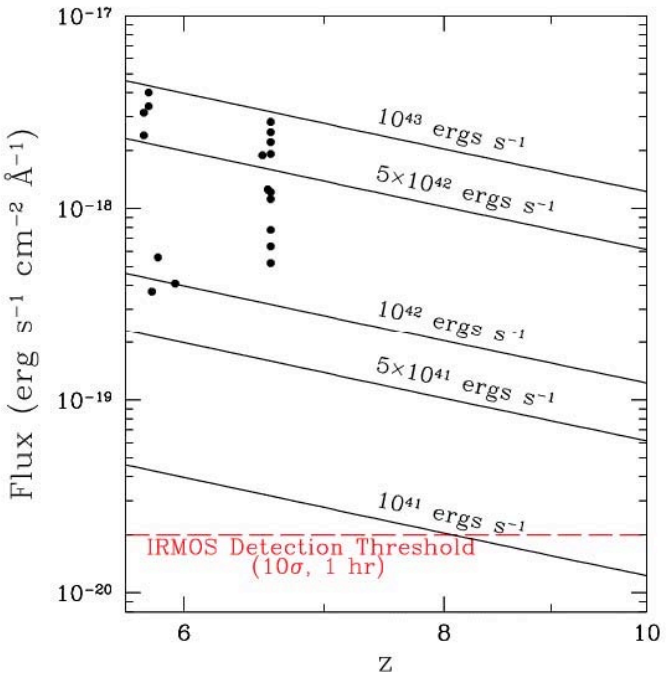

Figure 4-4. Flux vs. redshift for fixed angular size. Curves show the flux expected from galaxies with a fixed projected angular size of 50 mas but different intrinsic Ly-α luminosities. The data points are emitters (with projected sizes between 80 and 100 mas and z ~ 6.5) detected by Kodaira et al. 2003, Rhoads et al. 2004, Stanway et al. 2004, Ajiki et al. 2004, and Taniguchi et al. 2005). The curves assume that emission line is spread over 20 Å, while for most of the data points the actual line width is smaller. The one (1) hour, 10σ TMT/IRMOS detection limit is shown for 100 mas sized objects and 50 mas spatial pixels. From the IRMOS-UFHIA study.

Consider a Ly-α source with the line emission distributed over 20 Å (e.g. Stanway et al. 2004) with a half-light radius of 50 mas. Whereas current programs are restricted to studying the bright tip of the Ly-α emitter luminosity function (L > 10^{42} erg/s) at z < 7, a 1-hour TMT/IRMOS observation is sufficient to detect emitters as faint as $f = 10^{-18.4}$ ergs s^{-1} cm^{-2} ($L = 10^{41}$ erg s^{-1} at z = 8) with SNR = 10 and to study the winds and outflows via line profile measures for sources as faint as $f = 10^{-17.9}$ ergs s^{-1} cm^{-2} with SNR = 10 per spectral resolution element. Thus, in a single hour TMT/IRMOS can detect systems at z = 8 with intrinsic luminosities an order of magnitude fainter than the faintest emitters currently studied at z = 6.5

Likewise, there are impressive gains over JWST for the smallest sources. As a guideline, using an R ~ 100 spectroscopic survey mode, JWST is expected to reach a 10σ flux limit of ~ 2 x 10^{-18} ergs s^{-1} cm^{-2} in ~ 4 hours of integration time. Thus, TMT can probe systems whose flux is at least 20 times fainter per unit integration time. The gain rises to × 50 – 100 for sources in the 30 – 50 mas range.

4.5 Source densities and survey requirements

A major source of uncertainty in planning TMT observations in this era is a fundamental one. How many sources are there? What is their luminosity and surface density? The likely presence of star forming galaxies in the 7 < z < 20 redshift range follows from a number of deductions, in addition to the presence of ionized electrons inferred from the WMAP polarization study. Galaxies with well-established (>100 Myr old) stellar populations are being readily found at z ~ 6, suggesting their progenitors were more luminous or perhaps comprised of smaller, more abundant sub-units (Stark et al. 2007a). Carbon is likewise detected in absorption in the highest redshift quasars, suggesting early enrichment from supernovae (Ryan-Weber et al. 2006). But what is the likely form of the luminosity function of the earliest galaxies?

Numerical predictions by Barton et al. (2004), based on hydrodynamical simulations by Springel & Hernquist (2003) as detailed in Table 4-2 are plotted in Figure 4-5. These allow us to contemplate the practicality of conducting surveys of line emitters in ionization bubbles at various redshifts..

Table 4-2: Model Ly-α luminosity function prescriptions (from Barton et al. 2004).

Model	IMF (M_O)	Metallicity (Z_O)	f_{IGM}	f_{esc}	F(Ly-α) (ergs/s)	F(HeII) (ergs/s)
Optimistic	300 –1000	0	1.0	0.35	2.1 x 10^{43}	3.7 x 10^{42}
Plausible	50 – 500	0	0.25	0.1	6.4 x 10^{42}	6.1 x 10^{41}
Heavy Salpeter	1 – 500	10^{-5}	0.25	0.1	1.8 x 10^{42}	3.0 x 10^{39}
Salpeter	1 – 100	0.2	0.25	0.1	7.3 x 10^{41}	…

Table notes: The parameters are (1) model name, (2) the range of stellar masses, where the slopes are Saltpeter (except in the Optimistic case, where the slope is irrelevant), (3) the metallicities of the stars, (4) the fraction of Ly-α photons that escape from the IGM, (5) the fraction of ionizing photons that escape from the galaxy (without becoming Ly-α or HeII photons), (6) the Ly-α luminosity per unit of star formation and, (7) the He II (1640) luminosity per unit of star formation. From the IRMOS-CIT instrument feasibility study.

Figure 4-5 (left panel) shows the source counts could span a considerable range per unit redshift interval at z ~ 8.2 with a consequent uncertainty for the number of observable sources in the proposed *blind spectroscopic search* possible within a contiguous array of IRMOS IFUs (36 $arcsec^2$). For example, the least-optimistic Saltpeter model assumes we can choose lines of sight along enough projected large-scale structures that an average of 25% of the Ly-α photons escape. If we assume the attenuated photons sample the luminosity function fairly and the sources are small, the associated flux limit is 7 x 10^{-20} ergs cm^{-2} sec^{-1}, yielding only two (2) sources contiguous field in 4 hours. However, for more optimistic scenarios, even with larger sources, the yield could be ~10 per field. ~15 TMT/IRMOS pointings would thus be needed to map a 10 Mpc (comoving) bubble at z = 7.2. A survey sampling 5 – 10 bubbles over a range of different central source luminosities would require ~900 hours.

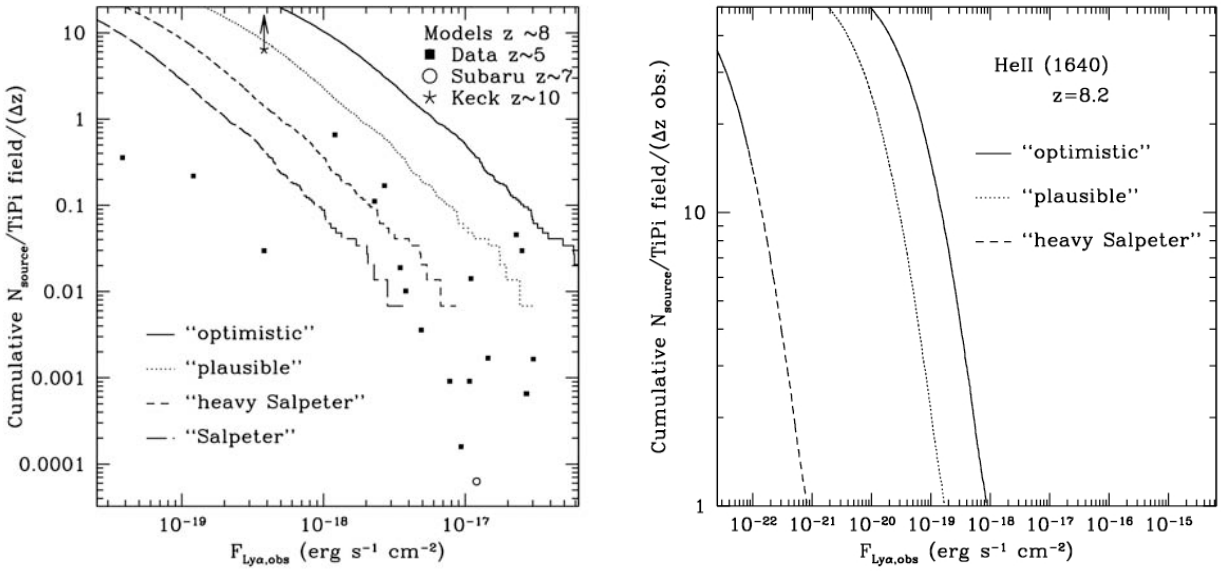

Figure 4-5. Surface density of Ly-α and He II emitters. Cumulative surface density of *z* = 8.2 Ly-α emitters (left) and He II emitters (right) per 36 arcsec^2 field within a unit redshift interval as calculated for various assumptions (see table above, adapted from Barton et al. 2004) using the hydrodynamic simulations of Springel & Hernquist. Solid squares are *z* ~ 5 data from the compilation of Santos et al. (2004) with non-detections omitted, the star is from the gravitational lens survey of Stark et al. (2007b), and the open circle is the Subaru z~7 survey of Ota et al. (2007). All the data points are corrected to the luminosity distance at *z* = 8.2 assuming (Ω_M, Ω_Λ, H_O) = (0.3,0.7,70 km/s/Mpc). In a 4-hour exposure, TMT/IRMOS should detect line fluxes to 3 x10^{-19} erg s^{-1} cm^{-2} (5σ). Only the zero metallicity models yield detectable He II (1640 Å) emission – the *smoking gun* for Pop III star formation. From the IRMOS-CIT (TiPi) instrument feasibility study.

References

Ajiki, M. et al. 2003, AJ, 126, 2091
Barton, E. et al. 2004, ApJ, 604, 1
Becker, G.D. et al. 2006, ApJ, 640, 69
Bunker, A. et al. 2004, MNRAS, 355, 374
Ciardi, B. et al. 2006, MNRAS, 366, 689
Ellis, R. et al. 2001, ApJ, 560, L119
Ellison, S. et al. 1999, ApJ, 520, 456
Eyles, L. P. et al. 2005, MNRAS, 364, 443
Fan, X. et al. 2006, AJ, 132, 117
Furlanetto, S.R. & Oh, S.P. 2005, MNRAS, 363, 1031
Gallerani, S. et al. 2006, MNRAS, 370, 1401
Gwyn, S.D.J. & Hartwick, F.D.A. 2005, AJ, 130, 1337
Horton, A. et al. 2004, SPIE, 5492, 1022 (astro-ph/0409080)
Hu, E., Cowie, L.L., and Kakazu, Y. 2006, IAU General Assembly 26, JD07, 10.
Kodaira, K. et al. 2003, PASJ, 55, 17
Le Delliou, M. et al. 2005, MNRAS, 357, 11
Le Delliou, M. et al. 2006, MNRAS, 365, 712
Miralda-Escude, J. 1998, ApJ, 501, 15
Ota, K., et al. 2007, ArXiv e-prints, 707, arXiv:0707.1561
Paschos, P. & Norman, M. L. 2005, ApJ, 631, 59

Rhoads, J. et al. 2003, AJ, 125, 1006
Rhoads, J. et al. 2004, ApJ, 611, 59
Ryan-Weber, E.V. et al. 2006, MNRAS, 371, 78
Santos, M.R. et al. 2004, ApJ, 606, 683
Schaerer, D. Astron. Astrophys. 382, 82 2002
Songaila, A. 2001, ApJ, 561, L153
Songaila, A. & Cowie, L. L. 2002, AJ, 123, 2183
Spergel, D. N. et al. 2003, ApJS, 148, 175
Springel, V. & Hernquist, L. 2003, MNRAS 339, 289
Stanway, E. R. et al. 2004, ApJL, 604, 13
Stark, D.P. et al. 2007a, ApJ, 659, 84
Stark, D.P. et al. 2007b, ApJ, 663, 10
Steidel, C.S., Pettini, M. & Adelberger, K. L. 2001, ApJ, 546, 665
Taniguchi, Y. et al. 2005, PASJ, 57, 165
Thommes, E. & Meisenheimer, K. 2005, A&A, 430, 877
Yan, H. & Windhorst, R. A. 2004, ApJ, 600, L1

5 Galaxy formation and the intergalactic medium

5.1 Overview

Tremendous progress has been made over the last decade in establishing a broad cosmological framework in which galaxies and large-scale structure develop hierarchically over time, as a result of gravitational instability of material dominated by dark matter. However, there remain many unanswered questions about how the observable universe of galaxies is related to the growth of the underlying distribution of dark matter; most of this uncertainty relates to our poor understanding of the complex baryonic processes that must be included in any successful theory of galaxy formation: cooling, star formation, feedback, merging. Understanding how these processes operate on galaxy scales is an inherently multi-wavelength observational problem that is limited at present by the sensitivity of our tools for extracting detailed physical information, for both stars and gas, as a function of cosmic time.

Observations of galaxies beyond $z \sim 1$, selected using initial surveys at UV, optical, near-IR, and far-IR rest-frame wavelengths, have begun to establish in broad-brush what the universal history of star formation has been like over the last ~90% of the age of the Universe. As Figure 5-1 shows, the current census paints a picture in which the peak era for star formation in galaxies occurred in the distant past; indeed, while precise numbers remain somewhat controversial, there is now little doubt that star formation peaked at redshifts between $z \sim 2$ and $z \sim 3$, and that a large fraction of the stars observed in present-day formed during a relatively brief, but incredibly active, period of time between $z \sim 6$ and $z \sim 2$, or an interval when the Universe was ~1 – 3 billion years old. Very similar behavior with cosmic time is observed for the growth of supermassive black holes — a broad peak near $z \sim 2 – 3$ with a rapid ramp-up before $z \sim 3$ and a rapid decline after $z \sim 1$.

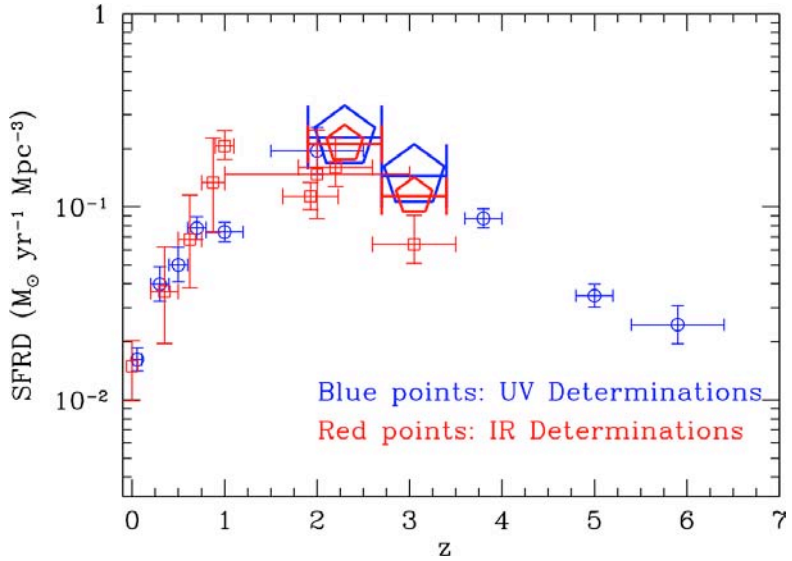

Figure 5-1 – Current census of the integrated star formation rate per unit co-moving volume since redshift $z \sim 6$. The star formation rate density (SFRD) is ~15 times higher at $z \sim 2$-3 than at $z \sim 0$, and increases by a factor of ~10 from $z \sim 6$ to $z \sim 2$. Approximately 50% of the stars in the present day universe were formed over the ~2.5 billion year interval between $z \sim 1.5 – 3.5$ (from Reddy et al. 2007).

During this ``epoch of galaxy formation'', most of the baryons in the Universe are actually *outside* of galaxies, in the intergalactic medium (IGM). The IGM is thus a vast reservoir of normal material acting as both a source of gas to fuel galaxy formation, and a ``sink'' of the waste products of that process. The structure of the IGM, which is dictated in part by the underlying dark matter distribution, and, with time, increasingly modified by the energetic processes occurring in forming galaxies, also acts as a laboratory where the most sensitive measurements of the physics of the galaxy formation process may be made. For these reasons, understanding structure formation in the Universe requires measurements of all

material, both inside and outside of galaxies. Fortuitously, observational access to both galaxies and the IGM during this crucial epoch is excellent for large-aperture telescopes placed at the very best terrestrial sites.

TMT will thus play a fundamental role in providing the detailed physical measurements necessary to understand the development of the modern universe. TMT will provide rest-frame UV spectra of unprecedented sensitivity and depth: WFOS and HROS will together provide exquisite information on the physics of gas associated with forming galaxies and the IGM using the rich rest-frame far-UV transitions made observable from the ground by the redshift of the sources. IRIS, IRMS, and IRMOS, all taking advantage of the diffraction-limited capabilities of TMT in the near-IR, will provide spectra of extremely high sensitivity and spatial resolution, allowing the first detailed studies of galaxy structure, dynamics, and chemistry while they are in the process of forming the bulk of their stars. The near-IR observations with TMT will provide observational access to the same rest-frame optical diagnostic spectral features, of both stars and gas, that have been used for decades of research on nearby galaxies — but for distant galaxies observed as they are forming.

5.2 TMT and galaxy formation

Over the last several years, there have been a number of surprising observations that would be quite unpredictable based solely on an understanding of the underlying cosmology and the overall distribution of dark matter. In hierarchical structure formation, gravitationally bound structures begin on small scales, and the largest bound objects are expected to be the last to form. A universal peak in overall star-formation and black hole accretion, as observed, is not necessarily expected. Neither is the observation that the most massive known galaxies appear to finish forming their stars earliest nor that typical galaxies at redshifts $z \sim 2 – 4$ appear to be forming stars at rates that are 10 – 100 times higher than for typical galaxies in the local universe. The symbiotic relationship between the formation of galaxy spheroids and central black holes also does not follow directly from a cosmological framework alone. The complexity of galaxy formation requires following the behavior of dark matter *and* the “gastrophysics” of star formation, feedback of energy, accretion and expulsion of gas, and effects of environment.

Among the many remaining unanswered questions in galaxy formation are:

- Why does galaxy formation apparently proceed in an “anti-hierarchical” fashion, in spite of broad agreement that cosmological large scale structure develops hierarchically?
- Is star formation inherently different in the distant universe compared to locally?
- How do galaxies acquire their gas, and how much cross-talk and exchange is there between galaxies and the intergalactic medium?
- What are the primary drivers of galaxy-scale star formation during the epoch of galaxy formation? What shuts it off?
- How do energetic processes (star formation, black hole accretion, supernovae) influence the galaxy formation process?
- What is the nature of any environmental influences that modulate how rapidly galaxy formation occurs?
- How does the distribution of dark matter relate to the luminous stars and gas we see?
- What are the details of the connection between galaxy formation and the formation and growth of supermassive black holes? What are the relevant physical processes?

Answers to these questions will come from detailed studies of galaxies and the intergalactic medium at high redshift. One needs to measure the distribution and metallicity of gas inside and outside of galaxies, the star formation rates, internal structure, stellar content, and dynamical states of galaxies, all as a

function of environment and of cosmic time. The combination of WFOS, IRIS, IRMS, and (later) IRMOS and HROS mounted on TMT provides a near ideal instrument suite for attacking the problem of structure formation in the distant universe. Across a wide wavelength range (0.3 – 2.4 μm), TMT complements or exceeds the spectroscopic capability of JWST while providing higher spatial resolution. With ALMA providing information on the molecular gas content and kinematics of galaxies, as well as tracking the rest-frame far-IR emission from dust during the same cosmic epoch, TMT will remain the most powerful tool for tracking the process of the galaxy formation during the most active period in the history of the Universe.

Broad wavelength coverage (0.3 – 2.4 μm) is key to probing the critical spectral diagnostics, from the far-UV stellar, interstellar, and intergalactic lines of H and metals, to the nebular emission and stellar absorption features in the rest-frame optical. Figure 5-2 shows examples of low-resolution spectra obtained using current 8m-class telescopes for some of the brightest star-forming galaxies at redshift $z \sim 2$, in order to illustrate some of the spectral features of interest.

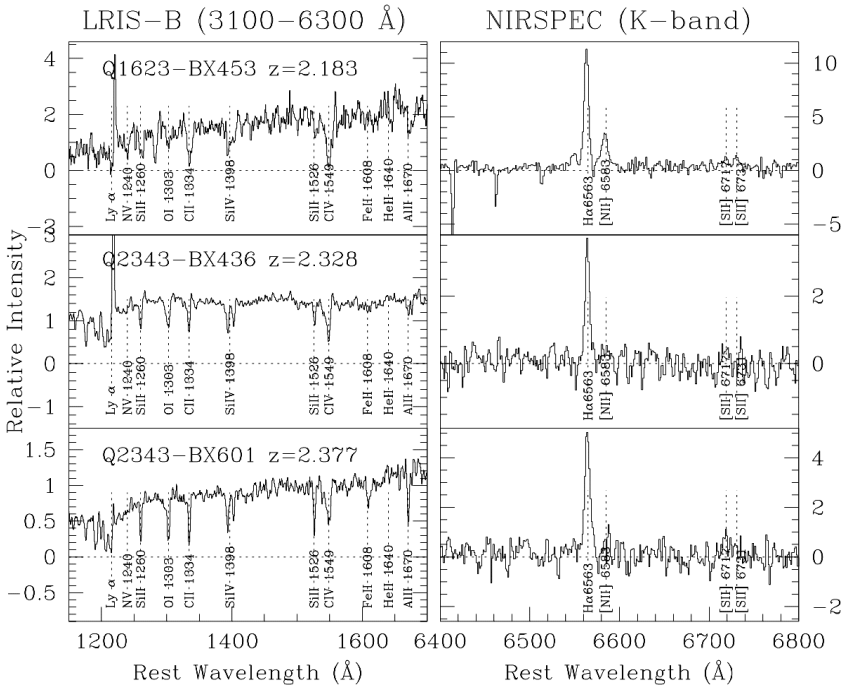

Figure 5-2 – Example low-resolution spectra of 3 high redshift galaxies, where the left panels show the rest-frame far-UV spectra observed in the optical (0.31-0.6 μm), and the right panels show the Hα [NII], and [SII] lines observed in the K-band (2.2 μm) window. The far-UV spectra contain a wealth of interstellar absorption features, and nebular emission lines, as well as stellar wind and photospheric features from massive stars. The rest-optical spectra are used for measuring kinematics, chemistry, and star formation rate. Credit: C. Steidel (CIT)

The envisioned TMT instruments are expected to play complementary roles in addressing these fundamental issues:

- WFOS provides highly multiplexed, moderate resolution, slit spectroscopy in the optical window (0.31 – 1μm). It is optimal both for obtaining identification-quality spectra of the faintest galaxies and AGN throughout the epoch of galaxy formation, and for high quality rest-frame UV spectra of large samples of galaxies and AGN that will provide diagnostics of gas and stars in galaxies, as well as the distribution, metallicity, and physical conditions of the IGM.
- IRMS provides analogous capabilities (albeit with a smaller field of regard) in the near-IR windows, allowing study of key diagnostic nebular and stellar lines in the rest-frame optical (e.g. [OIII], Hβ, Mgb, Hα, [NII]). IRMS takes advantage of the AO power of TMT+NFIRAOS to obtain extremely sensitive multiplexed spectra in both emission lines and stellar continua in the observed frame near-IR, providing information on chemistry, kinematics, and stellar populations.

- Using integral-field spectroscopy, IRIS allows the three-dimensional (X, Y, velocity) dissection of individual galaxies. IRIS will bring the full power of 30m diffraction-limited performance during early light, providing near-IR spectral information on physical scales as fine as 50 – 70 pc at any redshift in the range z = 1 – 6.
- IRMOS will combine the diagnostic power of IRIS and the multiplexing capabilities of IRMS, providing integral field spectroscopy in the near-IR (0.8 – 2.5 μm) for up to 20 objects distributed over a 5 arcmin field of regard.
- HROS, with a factor of >20 gain in sensitivity over the best current-generation high resolution spectroscopic capabilities, will vastly increase the number of lines of sight that can be used for the most detailed studies of the IGM and of individual galaxies and AGN.

5.3 Multiplexed spectroscopy of distant Galaxies: the rest-UV

Somewhat ironically, a large fraction of what we currently know about galaxies at redshifts z > 1.5 comes from observations made in their rest-frame UV light. The main reason for this is practical — it is easy to identify high redshift (star forming) galaxies based on their distinctive far-UV colors as the Lyman limit of hydrogen passes through the observed passbands, and once flagged, the naturally dark terrestrial background in the optical (defined for the present purposes as 0.31 – 1μm) makes spectroscopy of faint objects feasible for at least the brightest examples with 8 – 10m telescopes. Practicalities aside, as illustrated above in Figure 5-2 the rest-UV spectra of galaxies contain a vast amount of information because of the very large number of ground-state transitions of astrophysically abundant ions at these wavelengths, including hydrogen Lyman-α, CII, CIII, CIV, NI, NV, OI, OVI, SiII, SiIII, SiIV, FeII, AlII, AlIII, to name a small subset. At the redshifts of interest, z ~ 1.5 – 6, essentially all galaxies spectroscopically observed to date have extremely strong, broad absorption lines which arise in interstellar gas associated with the galaxy itself, stellar wind P-Cygni lines of CIV, HeII, and SiIV from O-stars, as well as O and B star photospheric features. With sufficiently high quality data (as illustrated below), one can extract information on the stellar initial mass function (IMF) shape at the high mass end, stellar chemical abundances, the chemistry of the interstellar gas, and the kinematics of gas motions within the galaxy. For redshifts z > 2.5, the hydrogen Lyman limit is redshifted above the atmospheric cutoff so that a direct measurement of the ionizing radiation escaping from the galaxy (highly relevant for the physics of the IGM, including the process of re-ionization), and for redshifts z > 1.6, galaxy spectra will contain information on the ``Lyman α forest'' (and associated lines of heavier elements) from the IGM along the line of sight.

A relevant example of what is possible is shown in Figure 5-3 — the z = 2.723 gravitationally-lensed galaxy cB58 (Pettini et al. 2002) is one of a handful of high redshift galaxies bright enough to obtain R = 5000 spectra on an 8m-class telescope. From this spectrum alone, one obtains a measure of the stellar metallicity (~0.25 solar); constraints on the slope of the high mass end of the IMF (top-heavy mass functions appear ruled out); the interstellar abundances of 8 different elements, showing clear enhancement of alpha elements, and a N abundance indicating that cB58 is very chemically young; velocity profiles showing the clear presence of a galaxy-scale outflow, with systemic velocities of the gas relative to the stars of up to ~800 km s^{-1} , and an inferred mass outflow rate of the same order as the star formation rate (50 solar masses per year).

Unfortunately, the typical spectra of even bright (but un-lensed) star forming galaxies at similar and higher redshifts do not approach the quality of the cB58 spectrum, and generally many spectra (of separate objects) must be co-added in order to measure any spectral feature with reasonable SNR (e.g., Shapley et al. 2003). The problem is that the characteristic apparent magnitude in the optical of galaxies at z = 2, 3, 4, and 5 are R = 23.9, 24.5, 25.0, and 25.6, respectively (this is the magnitude brighter than which the space density falls exponentially) — whereas cB58 has an apparent magnitude of R = 20.5, ~4 magnitudes brighter than its unlensed (~L*) magnitude of R = 24.4.

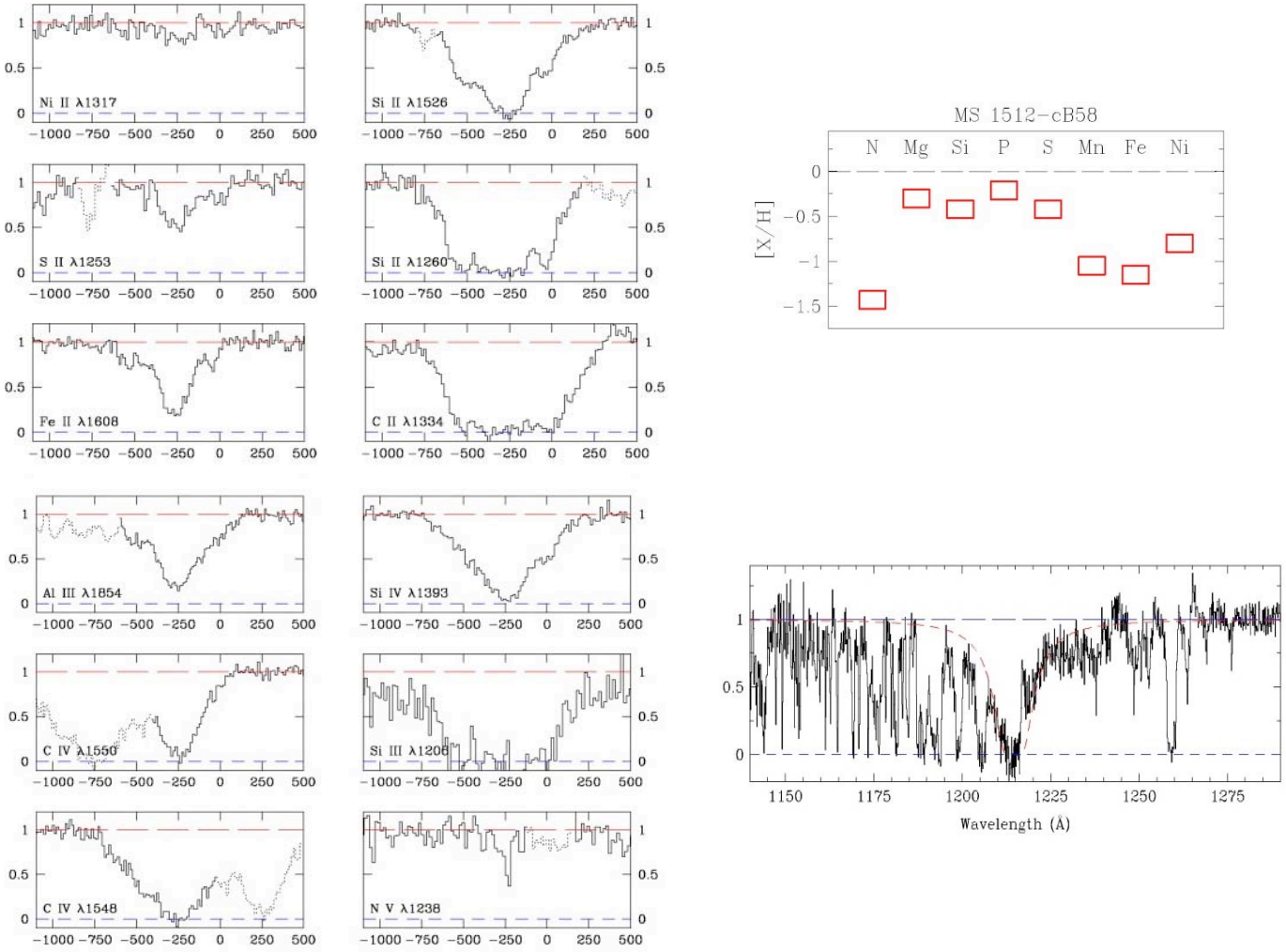

Figure 5-3 – Spectrum of the graviationally lensed high redshift galaxy cB58, as an example of the quality of data that can be expected for typical (unlensed) galaxies using TMT/WFOS. The left panels show various interstellar absorption lines, with velocities in km s^{-1} relative to the galaxy systemic redshift. Note that almost all of the absorption is blue-shifted by up to 800 km s-1, implying very strong outflows on galaxy scales. The bottom right panel shows the spectrum near Lyα, which has a damped profile; at the top right are the inferred chemical abundances of various elements in the ISM of the galaxy, showing a combination of alpha enhancement and mild depletion onto dust grains.

Fortunately, spectra of the quality and diagnostic power of the cB58 spectrum will be within reach for relatively typical ~L* (in the far-UV luminosity function; see Reddy et al. 2007) using TMT/WFOS, while obtaining spectra of high quality but lower resolution will be possible for objects significantly fainter than L* even at z ~ 6 with modest ~1 hour integration times – the gain in sensitivity over current 8m telescopes for spectroscopy over the 0.31 – 1 μm wavelength range will be a factor of at least 14. The sensitivity gain will bring intrinsically faint galaxies during the epoch of galaxy formation within spectroscopic reach for the first time, and will vastly increase the fraction of the high redshift populations for which extremely high quality spectra will be achievable.

5.4 Multiplexed spectroscopy of distant Galaxies: the rest-frame optical

Compared to the observed-frame optical, spectroscopy of faint objects in the near-IR faces substantial obstacles. First, the integrated sky background in the 1 – 2.5μm wavelength range is 250 – 1500 times brighter per sq. arcsec on the sky than at 0.4μm, even for a near-IR optimized telescope, AO system, and instrument. For wavelengths shorter than 2.2μm, the background is dominated by extremely strong OH emission features, making clean subtraction of the background for spectroscopic observations a challenge. Longward of 2.2μm, thermal emission from the sky and the telescope begin to rise precipitously. However, the scientific rationale for obtaining faint galaxy spectra in the near-IR becomes increasingly compelling as one moves to higher redshift: some of the oldest and most massive galaxies present at redshifts $z > 2$ are either heavily obscured by dust, or have little or no current star formation, so that they may only be observed in the near-IR (there is no rest-UV flux); the familiar rest-frame optical diagnostic spectral lines used for measurement of star formation rates, kinematics, metallicities, dynamical masses, and evaluation of stellar populations are all redshifted into the near-IR. For galaxies at $z \sim 1 – 5$, the physical parameters accessible in the near-IR windows include star formation rates and gas surface density through Hα/Hβ flux and surface brightness, kinematics and dynamical mass measurements from nebular emission lines tracing ionized gas or from stellar absorption features, and the measurement of accurate systemic redshifts that are often difficult to measure in the rest-frame UV for reasons outlined above.

Potential targets within the sensitivity range of TMT have a very high surface density on the sky; even to the relatively bright flux limit of $K_{AB} = 24$, the surface density of star forming galaxies in the redshift range $1.5 < z < 3.5$ is >10 arcmin^{-2}, and that of near-IR bright but optically faint galaxies to $K_{AB} = 23.0$ is > 2 arcmin^{-2} in the same redshift range.

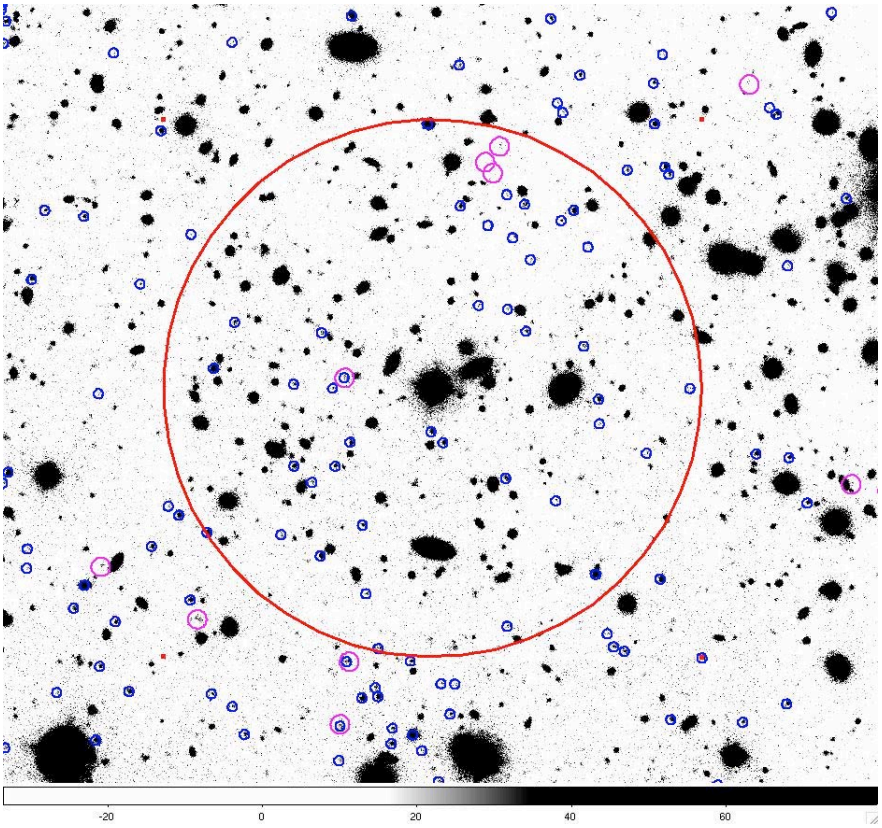

Figure 5-4 – An illustration of the surface density of galaxies with $K_{AB} < 24$ and redshifts in the range $1.7 < z < 3.2$ galaxies within a portion of an extragalactic survey field. Blue circles are objects that are likely to have strong nebular emission lines in the near-IR bands, while magenta circles are objects to $K_{AB} = 22.9$ with near-IR colors indicating heavy UV obscuration in the same range of redshifts or a complete absence of current star formation. The red circle shows the 2.3' diameter field of regard of IRMS behind NFIRAOS. There are a total of at least 40 potential targets within the 3.5 sq. arcmin region to the stated limits.

Because observations in the near-IR are in all cases severely background-limited, the gain in sensitivity achieved by moving to a larger aperture telescope is affected as much by an object's footprint on the sky as by the collecting area of the aperture. Together, in the limiting case that targets appear as point sources at the diffraction limit of the telescope, the sensitivity gain will be proportional to D^4, or a factor of ~200 as compared to an 8m telescope. Many objects of interest in the z ~ 1 – 5 range will not be point sources at TMT spatial resolution, but they almost invariably have characteristic angular sizes (i.e., the angular diameter enclosing >50% of the light) smaller than the typical natural near-IR seeing disk of ~0.5". For this reason, taking advantage of TMT AO to reduce the size of the focal plane aperture needed to enclose most of the galaxy light is compelling. Because so much of the astrophysics of galaxy formation depends on near-IR spectroscopy, and significant samples are required to extract fundamental results, multiplexing is essential. Ultimately, one would like a near-IR instrument on TMT that simultaneously provides a multiplex advantage and takes full advantage of AO corrected images over a wide field with full 2-D image sampling at the position of each target (as described in section 1.5). This capability will be provided by IRMOS, for which (at the time of this writing) the necessary AO developments look promising for the future.

In the shorter term, for multiplexed near-IR spectroscopy of faint objects during TMT early operations, the combination of the facility AO system (NFIRAOS) and IRMS will deliver a potent combination: the projected performance of NFIRAOS over the full 2.3 arcmin diameter field of IRMS will allow observations of faint galaxies using typical 200 mas slits, providing an estimated gain in sensitivity of a factor of 50 over existing near-IR faint object spectrometers on 8-10m class telescopes. A summary of the estimated sensitivity of this combination is provided in Table 5-1.

Table 5-1 TMT/IRMS predicted sensitivity

Passband	Spec. Sky Brightness, mag arc sec^{-2} Vega (AB)	Vega (AB) mag for SNR = 10 in 1 hour, R = 3270 with 0.23" slit	Line flux for SNR = 10 (unresolved line) in 1 hour, R = 3270 (erg s^{-1} cm^{-2})
Y (0.97 to 1.13μm)	17.3 (17.9)	23.4 (24.0)	7.0 x 10^{-19}
J (1.15 to 1.35μm)	16.8 (17.7)	23.0 (23.9)	7.4 x 10^{-19}
H (1.48 to 1.80μm)	16.6 (18.0)	22.7 (24.1)	4.7 x 10^{-19}
K (1.95 to 2.40μm)	14.4 (16.3)	21.2 (23.1)	8.5 x 10^{-19}

Table notes: spectroscopic limits assume 0.05 e^-/s dark current and effective read noise of 4e^-/pixel, with background for spectral regions between OH lines, evaluated over a 3 pixel resolution element and assuming a 0.05 arcsec^2 extraction aperture.

As an example, the limiting line flux in the K-band (10σ in a 1-hour integration) corresponds to a star formation rate of only 0.3 solar masses per year at z = 2.5; the same galaxy would have an apparent magnitude m_{ab} = 27 at rest-frame 0.15 μm (observed frame 0.5 μm) even if it were completely dust-free — this would be at least 1 magnitude fainter in the UV continuum than the faintest objects indicated on Figure 5-4. Continuum spectra suitable for measures of stellar velocity dispersions and detailed stellar population analyses will reach K_{AB} ~ 24, roughly equivalent to passive galaxies with stellar mass of only 10^{10} solar masses at z ~ 2.5. At present, on 8m-class telescopes, even the brightest such galaxies at similar redshifts (K_{AB} ~ 21 @ z = 2.5) require several nights integration time per object, making representative samples completely impractical and multiplexing of little use (due to the very low surface density). Using IRMS, it will be practical to obtain nebular spectra of hundreds of high redshift objects within a survey region, where every spectrum will be of high enough quality to measure velocity dispersion, chemical abundance, star formation rate, stellar excitation, and characteristic electron density

— and to evaluate whether or not active AGN are present--for galaxies at the limits of current *imaging* surveys.

5.5 Spatial dissection of forming galaxies

A major breakthrough scientific application will be the spatial dissection of galaxies during the peak epoch of galaxy formation. Observations of these galaxies will exploit both the light gathering power and the unique angular resolution at near-IR wavelengths provided by TMT. Large samples of galaxies throughout the redshift range z = 1 – 5 are already known, and the current generation of 8 – 10m telescopes will help us learn a great deal more in the coming decade. However, spatially resolved spectroscopy, allowing differences in chemistry, kinematics, and physical conditions to be mapped as a function of spatial position within the galaxies, is required to go beyond measurements of crude global properties, and thereby gain fresh understanding into the physics of galaxy formation.

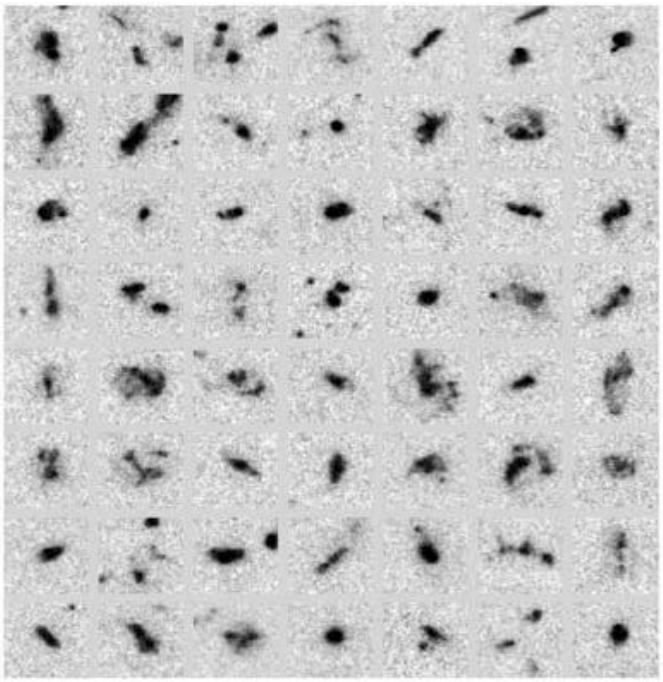

Figure 5-5 – Postage stamp images of 56 GOODS-N galaxies with z = 1.5 – 2.0., observed with the ACS on board HST. Each box is 3 arcsec on a side. Note the complex morphologies of these systems. With IRIS in both imaging and IFU modes it will be possible to observe systems of this nature with unprecedented angular resolution in the rest-frame visible. Courtesy C. Steidel, CIT.

Galaxies at z = 1 – 5 generally exhibit apparently complex spatial structure in the highest spatial resolution images such as those recorded with the Hubble Space Telescope Advanced Camera for Surveys (ACS) (see Figure 5-5). The apparent morphological complexity of most galaxies while they are forming the bulk of their stars at high redshift suggests that most of the star formation in this epoch is stimulated by galaxy mergers and major accretion events, and does not occur in rotating disks of gas as observed in the relatively nearby universe.

The physics of the galaxy formation process are far too complex to allow physical inferences to be drawn from images alone, even those obtained at high spatial resolution. To truly understand this process, it is essential to have 3-dimensional information about the velocity field of the gas and stars within it. As in the local universe, the most sensitive measures of galaxy kinematics come from measurements of the narrow nebular emission lines such as those illustrated in Figure 5-6. These lines, whose diagnostic power has been calibrated through decades of work in the local universe at rest-frame optical wavelengths, also provide information on chemistry, density, and excitation in the regions where stars are forming.

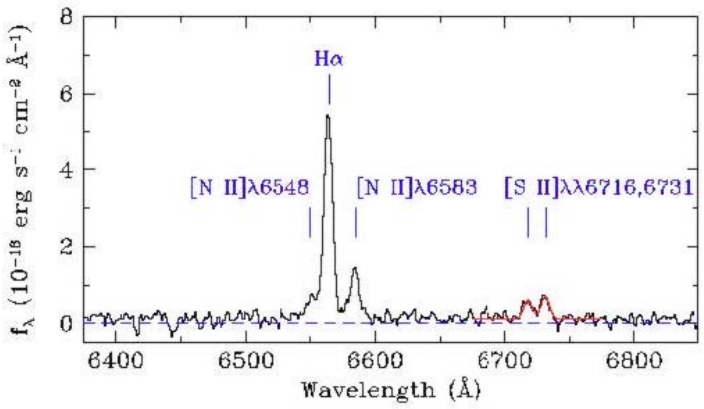

Figure 5-6 – The composite spectrum for a sample of 10 galaxies at <*z*> ~ 2.3, obtained in seeing-limited mode for whole galaxies using Keck/NIRSPEC. The [NII]/Hα ratio indicates approximately solar metallicities in the HII regions, and the ratio of the [SII] lines suggests densities of ~1000 cm^{-3}. Using IRIS/IRMOS, spectra of this quality could be obtained for positions in individual galaxies at a spatial scale of 0.1 – 0.2 kpc at any redshift < 4. Courtesy D. Erb, C. Steidel, (CIT), A. Shapley (Princeton), M. Pettini (IoA.)

As illustrated in Figure 5-7, integral-field spectroscopy can be used to obtain spectral and spatial information over contiguous regions simultaneously. Initial attempts using AO-equipped 8m-class telescopes and IFU spectroscopy (e.g., Genzel et al. 2006, Law et al. 2007) to observe galaxies at *z* > 2 have shown the promise, but revealed the limitations, of this technique with current facilities. TMT, with IRIS and IRMOS, will represent sensitivity gains of a factor of between 10 and 100, with angular resolution gains of a factor of > 3 – 5, over current capabilities. The gains will vastly expand the range of targets that may be observed, making it feasible to construct the statistically representative samples needed to connect individual galaxies to the larger framework of cosmological evolution.

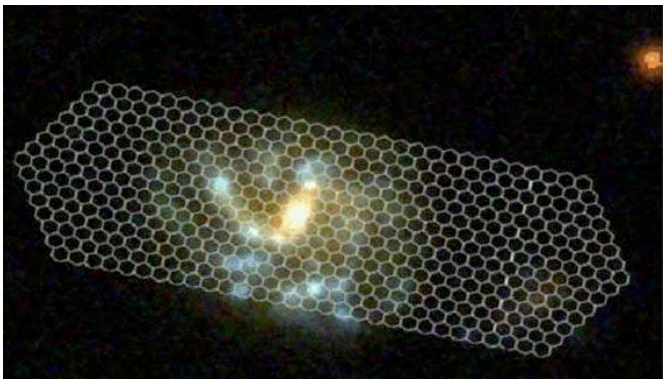

Figure 5-7. Image of distant galaxy superimposed on a TMT integral field unit. Individual spectra are produced for every hexagonal element, allowing an in-depth study of the physical properties of the galaxy with a spatial resolution of 50-100 pc at all redshifts z=1 – 5 (J. Larkin, UCLA).

When the information is collected at extremely high spatial resolution, as will be possible with IRIS and IRMOS, the structure, velocity field, abundances, and excitation of forming galaxies may be examined at 50 – 100 pc resolution (8 – 15 mas or 6 – 12 times higher better than HST/ACS) throughout the redshift range of interest. At such scales, even individual giant HII regions and the largest rich star clusters within galaxies at high-redshift may be resolved and detected (see Figure 5-8), providing a level of astrophysical detail currently only accessible in nearby, bright galaxies.

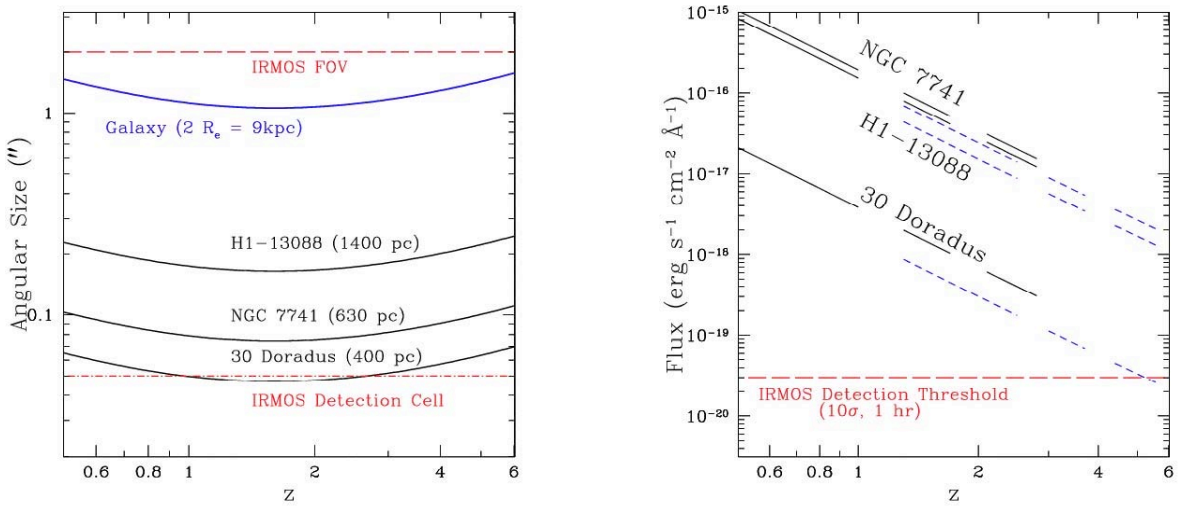

Figure 5-8 – Angular size and flux vs. redshift. Left Panel: Angular diameter of three giant star forming regions as a function of redshift. The two dashed lines at the bottom correspond to the angular size of the IRMOS detection cell. Also shown is the angular effective diameter of a typical high-redshift starburst galaxy compared to the FOV of a single IRMOS IFU. Right panel: Hα (black solid lines) and [OII] 3727 (blue dashed lines) fluxes of the same three giant star-forming regions as a function of redshift, compared to the IRMOS limiting flux per detection cell (SNR = 10, t = 1hr). The gaps correspond to terrestrial atmospheric absorption bands. Courtesy: IRMOS-UF/HIA team.

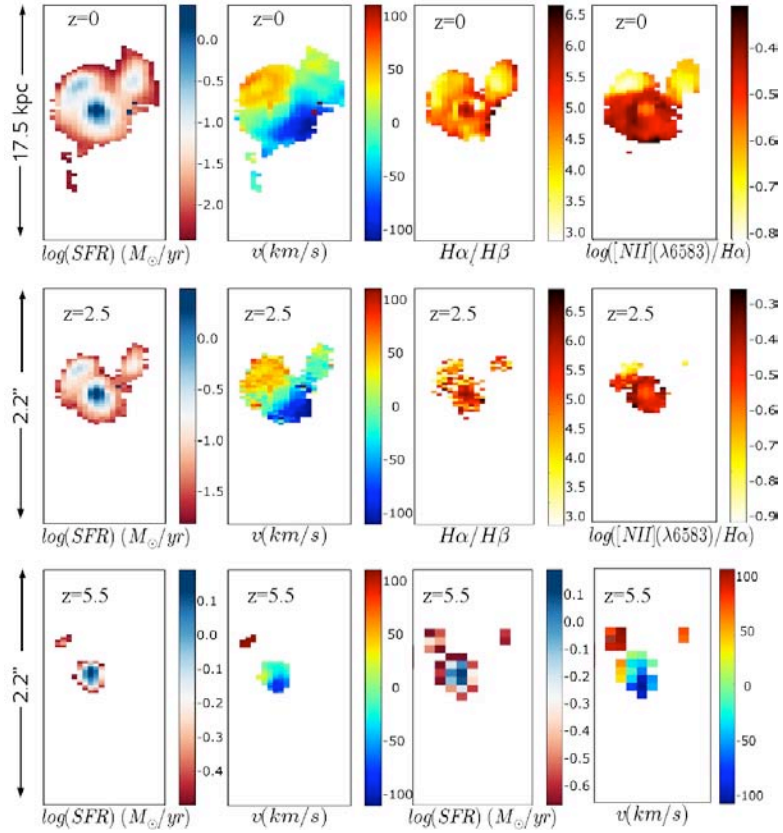

Figure 5-9 – Simulated IFU observations of starburst galaxy at various redshifts. Top panels: actual SFR, velocity, extinction, and metallicity maps for Mrk 538, a nearby L* starburst galaxy, scaled up to L = 4L*, R_e = 4.5 Kpc, and L(Hα) = 10^{43} erg/s. Middle panels: same galaxy at *z* = 2.5, after 1-hour of integration with 50 mas pixels and *R* = 4800. Regions with SFR as low as 0.01 M_O per year per resolution element have been detected. Bottom panels: same galaxy at *z* = 5.5, after 4-hour integration with 50 mas pixels and *R* = 4800. Regions with SFR > 0.05 M_O per year have been detected. Courtesy IRMOS-UF/HIA team.

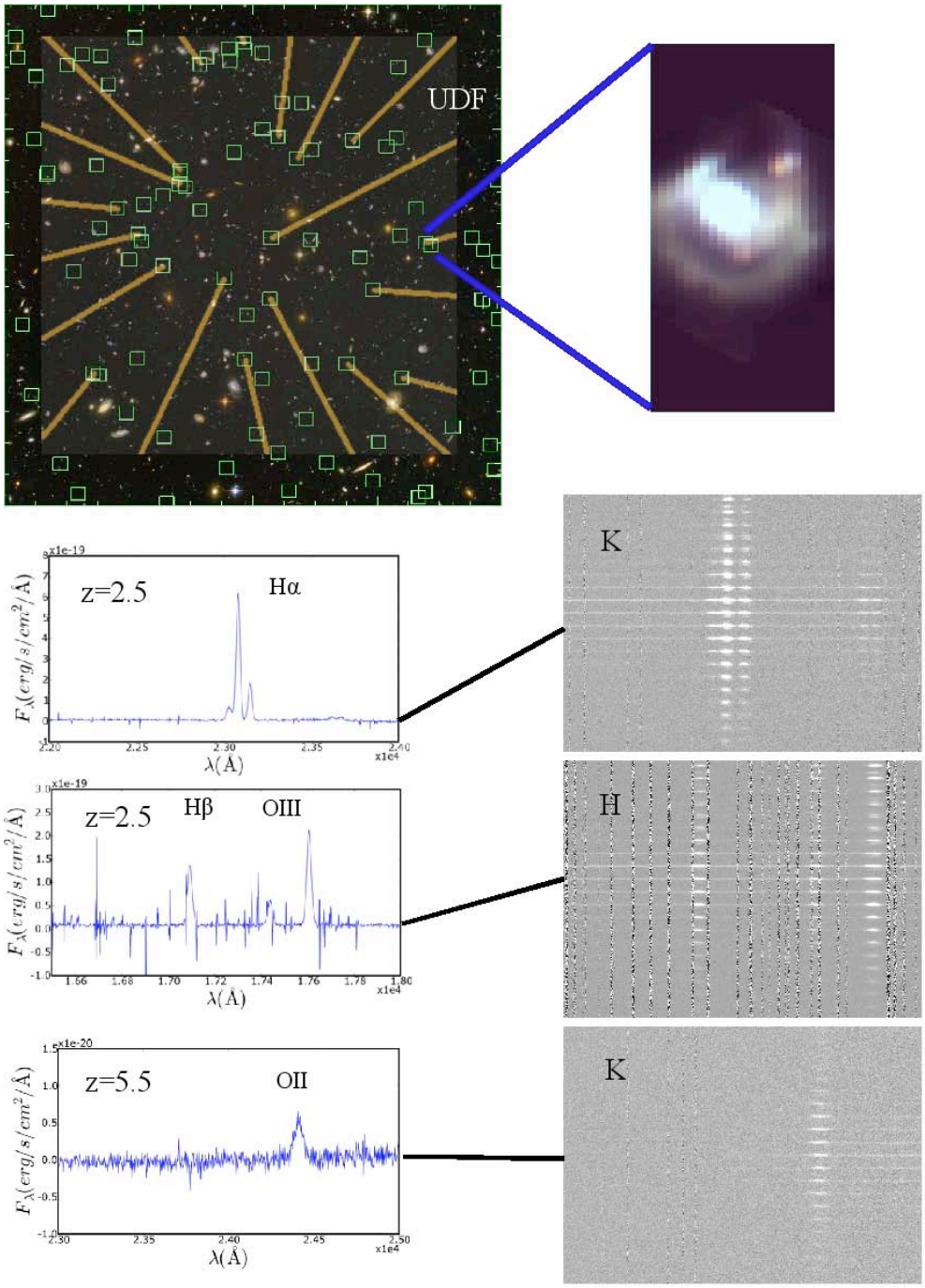

Figure 5-10 – Simulated IRMOS observations of Lyman-break galaxies. Simulated IRMOS observations of a typical Lyman-break galaxy at redshifts *z* = 2.5 and *z* = 5.5. Top right panel: image of the Hubble Ultra Deep Field (UDF). Lyman-break galaxy candidates at *z* = 2 – 6 are identified with green squares. An actual MOS probes configuration is shown in yellow lines. Top left panel: simulated deep near-IR image of a typical Lyman-break galaxy as seen in a single IRMOS IFU. Middle panels: simulated 2-D and 1-D spectra showing characteristic emission lines of Lyman-break galaxies at *z* = 2.5 and 5. Courtesy: IRMOS-UF/HIA team.

Figure 5-9 shows simulated examples of the type of spatially-resolved information that will be recovered in a typical IRMOS observation of a distant galaxy based on emission line measurements. The examples use spatial sampling that is optimized for spectroscopy of galaxies that have typical total angular extents of ~0.5 – 2 arcsec (4 – 15 kpc at z = 1 – 5). Even for the faintest objects at high-redshift, IFU spectroscopy should be the most sensitive means of obtaining near-IR spectra independent of their morphology, since the aperture used for extraction of spectra may be optimized to achieve the highest possible SNR (see Figure 5-10).

5.6 The intergalactic medium: taking core samples during the epoch of galaxy formation

Most baryonic matter, particularly during the early history of the Universe, is actually outside of galaxies. Intergalactic space is filled with a tenuous gas that provides "fuel" for forming galaxies, and is a repository for material expelled by galaxies by energetic processes such as supernova explosions and accretion onto supermassive black holes. The interplay between the galaxies and the intergalactic medium is of prime importance for understanding the history of normal matter in the Universe, the process of galaxy formation, and the effects of the "feedback" of energy produced by forming galaxies. From observations of high redshift QSOs using high resolution echelle spectrometers on 8 – 10m class telescopes, combined with state-of-the art hydrodynamical simulations of the high redshift universe, we have learned to picture the IGM as a "web" of diffuse, highly ionized gas of varying density, much like the picture in the left panel of Figure 5-11. Because the physics of diffuse gas can be very simple, the theory has told us that the neutral hydrogen (HI) optical depth, as well as the gas temperature, is controlled by the gas density and the intensity and spectral shape of the metagalactic ionizing radiation field. This simplicity makes it possible to turn a Lyman α forest spectrum, as in Figure 5-11, into a one-dimensional map of the density along the line of sight, as a function of redshift. Because high resolution spectra of QSOs have the remarkable capability of detecting column densities of HI associated with regions of the Universe that are at or even below the mean density, these density fluctuations can provide information on the spectrum of initial density fluctuations without the non-linear gravitational processing that affects denser regions of the Universe, and thus the Ly-α forest may offer the best means of measuring the spectrum of these perturbations on small scales where other techniques cannot (the cosmological uses of the Ly-α forest are discussed in the *Fundamental Physics* section of this document).

Of course, random lines of sight to distant QSOs also intersect dense gas associated with galaxies and their environs, and everything else in between. High-resolution spectra are capable of detecting trace amounts of metals, down to metallicities as low as 1/5000 of the solar abundances. In fact, such lines of sight provide a very high quality ``core sample'' of the intervening universe, from which we have learned (e.g.) that there may be no gas, anywhere in the Universe, that was not "polluted" with the products of stellar nucleosynthesis at some early epoch.

The highest quality data on the physical properties of the IGM have been recorded for the redshift range z = 1.6 – 3.5, for several reasons: first, Ly-α must be redshifted above the atmospheric UV cutoff of 0.31μm, setting the minimum redshift; second, the Lyα forest evolves extremely rapidly with redshift, so that by z>3.5, it is so dense with absorption that it loses dynamic range for measuring weak spectral features; third, QSOs bright enough for echelle observations (m < 19) are very rare even at their peak near z = 2.5, and by z = 6 there is only a handful currently known in the entire sky. Thus, in general, our current view of the IGM is "one-dimensional", in the sense that we do not get the picture on the left panel of Figure 5-11, but only the one on the right.

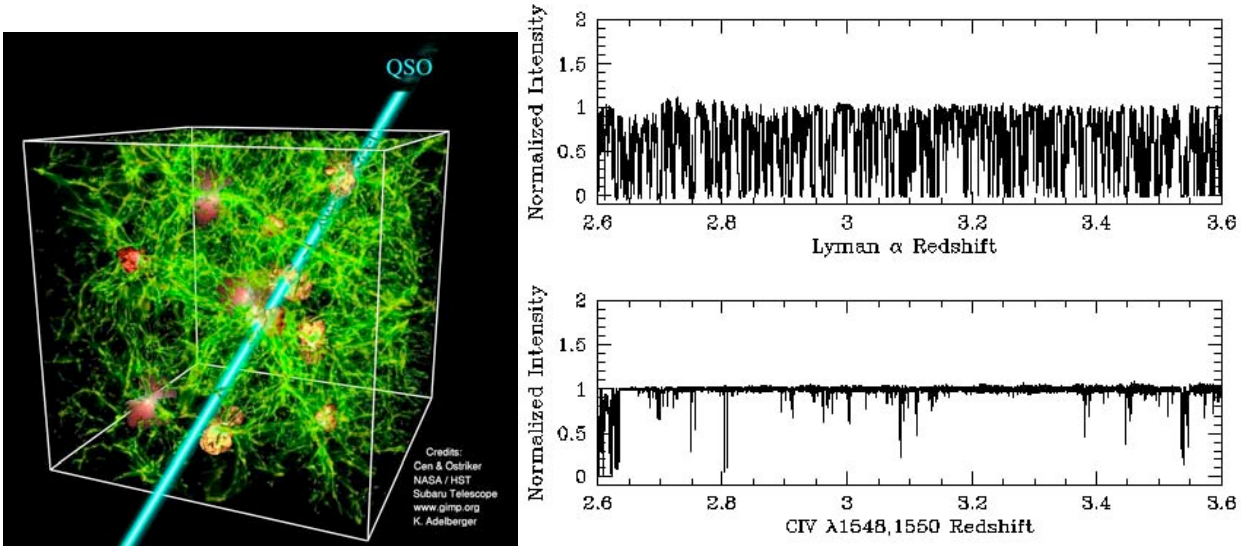

Figure 5-11. The "cosmic web" of the baryon distribution in a cosmological simulation. Here, HI in the IGM traces the dark matter distribution even in regions with low density contrast. A line of sight through the volume yields a one-dimensional map of both the HI and metallic species along the line of sight, as shown in the right-hand panel. Regions disturbed by galaxy formation processes are schematically indicated. In such regions, sightline probes will reveal the extent to which galaxies alter the physical state of the IGM: their sphere of influence, mass outflow, ionization effects, deposition of mechanical energy, etc. Densely sampled sightlines through a survey volume, together with detailed maps of the galaxy distribution, will provide unprecedented views of the distribution of baryons in the Universe, and their relation to the sites of galaxy formation.

There is no doubt that next generation QSO surveys will increase the numbers of QSOs at the highest end of the redshift range, by reaching fainter apparent magnitudes than current surveys. With HROS on TMT, which will represent a gain of a factor of ~20 in sensitivity compared to the best available system at present (Keck+HIRES), much fainter QSOs will be useful for obtaining additional lines of sight through the high redshift universe, and of course significantly better spectra of currently known QSOs will be easily obtained.

5.7 The epoch of galaxy formation in 3-D

One of the most exciting possibilities enabled by TMT is to combine the precision measurements of the astrophysics of the IGM using relatively bright background sources with direct observations of the luminous material — galaxies and AGN — in the same volumes of space, providing for the first time the first three-dimensional view of the distribution of baryonic material in the high redshift universe.

Historically, the spectra of QSOs have been the only available means to study the IGM at high redshifts, since they have been the only suitably bright background sources. The problem is that bright QSOs are rare, and so information on the IGM is difficult to extend to three dimensions. The situation is very different when the light-gathering power of TMT is brought to bear on the problem. While the surface density of QSOs with apparent magnitudes suitable for IGM studies increases significantly, the space density of compact, UV-bright star forming galaxies at apparent magnitudes sufficient to yield very high quality spectra easily overtakes QSOs (by number) as background sources. For galaxies with R ~ 24.5 (~0.6μJy), approximately the apparent magnitude at which TMT/WFOS can obtain a spectrum at R ~ 6000 with SNR ~ 30 (see Figure 5-12), galaxies in the appropriate redshift range (z = 1.8 – 4) outnumber QSOs by more than a factor of 30. More importantly, the surface density of useable background sources increases by more than 2 orders of magnitude over the current situation for 8m-class telescopes, exceeding 2 arcmin^{-2} (see Figure 5-13). This means that the IGM properties can be densely sampled on

physical scales of < 300 kpc, approximately the maximum sphere of influence of individual galaxies on the IGM and comparable to the expected coherence length of the undisturbed IGM. Thus, the 3-D IGM can be effectively reconstructed tomographically over the range 1.6 < *z* < 3.5 where the Lyman-α forest can be observed from the ground with good dynamic range (at higher redshifts the forest becomes so thick that the information content decreases substantially).

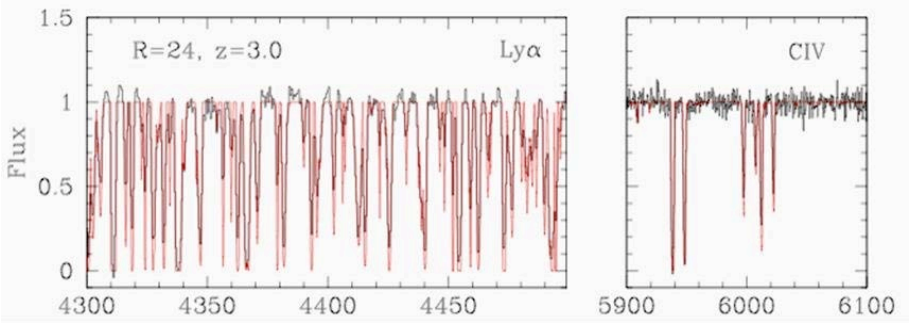

Figure 5-12. Simulated spectrum of an R = 24 galaxy observed with WFOS on TMT. Both structure in the Lyα forest and intergalactic metals will be revealed. (Credit: WFOS-HIA Team)

Fortuitously, this redshift range also encompasses what we believe to be the most important era for galaxy growth, star formation and massive black hole accretion in the history of the Universe.

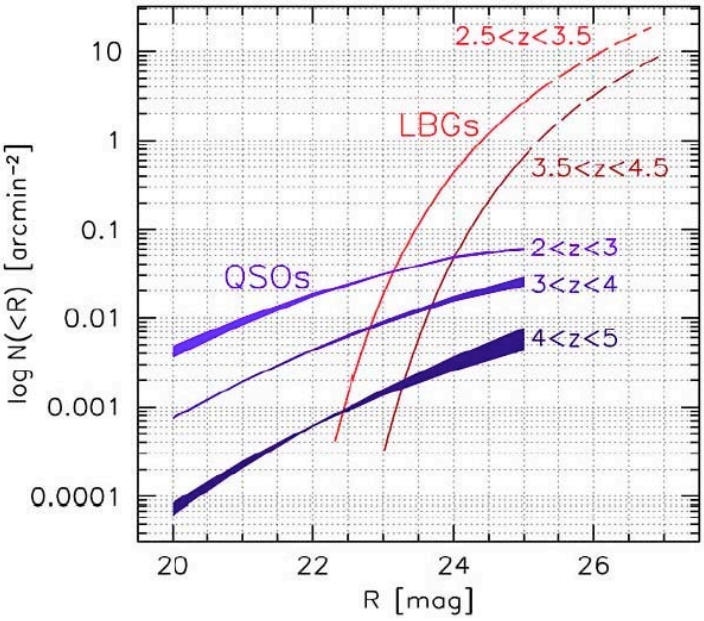

Figure 5-13. The cumulative surface density of QSOs and UV-bright galaxies as a function of R mag. The surface density of suitable IGM probes increases exponentially for R > 22 due to the very steep rest-UV luminosity function of star forming galaxies. By R ~ 24, the surface density of galaxies+QSOs exceeds 1 arcmin^{-2}, sufficient for tomographic mapping of the IGM.

Star-forming galaxies with R < 24.5 represent only the "tip of the iceberg" for the high redshift galaxies- the sensitivity of the combination of WFOS and TMT allows for spectroscopy of much fainter galaxies (to R ~ 27, albeit with lower spectral resolution than for the IGM probes) with a high degree of completeness. Galaxies at such apparent magnitudes have surface densities of >20 arcmin^{-2} for each interval in redshift of Δz ~ 0.5 from *z* ~ 2 to *z* ~ 3.5. Thus, with TMT, it will be possible to simultaneously obtain a densely sampled map of the distribution of galaxies and the diffuse material between them, in 3-D, providing the most complete possible census of all normal matter, and its relationship to dark matter. For the first time, the empirical picture of the high redshift universe would be of as high fidelity as those that currently exist only inside simulations.

More importantly, the observations will reveal the inner workings of all of the poorly understood physical processes that must be incorporated in order to understand how galaxies form — feedback (both hydrodynamic and radiative) from AGN and galaxies, gas accretion, details of the relationship between structure in diffuse gas versus that traced by galaxies. Once these "complications" are understood, the same data could be used successfully for measurement of the small-scale matter power spectrum with the Lyα forest.

Table 5-2: WFOS survey of baryonic structure in the high-redshift universe

Survey	Sky Area	#Targets	Exp	λ Range	#tiles	Total
Galaxies: z = 1.6 - 3.5	4 x (2° x 0.56°)	120,000 @ AB < 26.5	1 hour for SNR > 5 @ R = 500	0.32 - 0.65 μm	1000	1000 hours
IGM z = 1.6 - 3.5	4 x (2° x 0.56°)	15,000 @ AB < 24	4.5 hours for SNR > 35 @ R = 5000	0.31 - 0.60 μm	100	450 hours

An example of the type of ambitious survey that could be mounted with TMT would be an TMT/WFOS observing program to survey both galaxies and the IGM over a volume of the z = 1.8 – 3.5 universe that is as statistically representative as the Sloan Digital Sky Survey (SDSS) redshift survey at z ~ 0.1, which could be accomplished in a reasonable amount of telescope time. The relationship between angular scale on the sky and co-moving scale at the targeted cosmic epoch is vastly different between z ~0.1 (SDSS) and z ~ 2.5 (TMT). The SDSS was carried out with a telescope+instrument combination capable of observing over a field of view with a diameter of 2.5 degrees, or a transverse scale of ~18 Mpc (co-moving) at the median redshift of the survey. At z ~ 2.5, the same 18 Mpc co-moving scale is subtended by an angle of 10.6 arcmin on the sky. Thus, WFOS can be thought of as a wide-field spectrograph for studies of the distant universe. A survey of a representative volume of the Universe (~10^8 co-moving Mpc^3) covers a solid angle of π steradians at z ~ 0.1; for the proposed TMT/WFOS baryonic structure survey, the same volume is covered by ~4.5 square degrees on the sky. Within a total survey area of 4.5 sq. degrees, there would be ~650,000 star forming galaxies brighter than R ~ 26.5 in the redshift range 1.6 < z < 3.5 that could be selected for spectroscopy using simple photometric criteria to within Δz ~ 0.4. The total number of targets with R < 24.5 and 1.6 < z < 3.5 in the same volume would be ~30,000. A summary of the observing parameters, assuming a total WFOS slit length of 10 arcmin, is given in Table 5-2.

The WFOS survey products would include:

- Identification in redshift space of ~1000 over-dense regions that will become clusters by the present-day. The physical state of potential hot gas in the proto-intracluster media can be matched against Sunyaev-Zeldovich signatures in future high resolution CMB maps, providing a complete census of baryons in all phases within the densest regions in the Universe.
- Exquisite far-UV spectra of a large number of galaxies in the same redshift range for which IRIS and IRMOS can obtain rest-frame optical spectra. The far-UV spectra will provide measures of outflow kinematics, chemistry, stellar IMF, and in some cases mass outflow rate (e.g., Rix et al., 2004; Steidel et al., 2004).
- The 15,000 high quality sightlines through the IGM will map intergalactic HI and metals in 3-D, to be compared with the galaxy distribution in the same cosmic volumes (e.g., Adelberger et al., 2003, 2005). Even the lower resolution galaxy spectra will allow the mapping of inhomogeneities in the UV ionizing radiation field and measurement of the lifetime of bright UV sources via the transverse proximity effect (e.g., Adelberger, 2004).

- The information content of the survey could be greatly enhanced with HROS observations of the brightest background sources in the survey regions, providing exquisite information accessible only with high SNR R~50,000 spectra, as well as selected IRMS/IRMOS observations of UV-faint galaxies at the same redshifts in the same survey volumes.

References

Adelberger, K. L. et al. 2003, ApJ, 584, 45
Adelberger, K. L. 2004, ApJ, 612, 706
Becker, G., D., Sargent, W. L. W., Rauch, M. & Simcoe, R. 2005, astro-ph/0511541
Gallerani, S., Choudhury, T. R. & Ferrara, A. 2005, astro-ph/051212
Genzel, R. et al. 2006, Nature, 442, 786
Law, D. R. et al. 2007, ApJ, in press, arXiv:0707.3634
Paschos, P. & Norman, M. L. 2005, ApJ, 631, 59
Pettini, M. et al. 2002, ApJ, 569, 742
Reedy, N. et al. 2007, ApJ, in press, astro-ph/0706.409
Rix, H. W. et al., 2004, ApJ, 615, 98
Shapley, A. E., Steidel, C.C., Pettini, M., & Adelberger, K.L. 2003, ApJ, 588, 65
Songaila, A. 2001, ApJ, 561, L153
Songaila, A. & Cowie, L. L. 2002, AJ, 123, 2183
Steidel et al., 2004, ApJ, 604, 534

6 Extragalactic supermassive black holes

Over the last 10 years, a large body of observational work has pointed to the presence of supermassive black holes (SMBH) in the centers of many nearby galaxies (including our own Milky Way, see Section 3.1.3). SMBH are also assumed to be the central engines of active galactic nuclei (AGN) and quasars seen at cosmological distances. These observations point to a symbiotic relationship between the mass of a galactic spheroid or bulge and its central black hole. However, the physical processes that produced the observed relationship are not understood. It is possible that the energy produced by material accreted during black hole growth may be responsible for controlling the ultimate size a galaxy can attain, or that whatever processes are responsible for terminating star formation in galaxies also shut down further growth of supermassive black holes. In the last 10 years, characterizing the relationship between SMBHs and their host galaxies has emerged as a key problem on the road to understanding galaxy formation and evolution.

The spatial resolving power and sensitivity of TMT will make it possible to break several barriers, allowing researchers to study SMBHs across the entire Hubble sequence, study the demography of SMBHs as a function of environment, and extend the SMBH mass function by a factor two in M_{BH}. TMT observations will extend dynamical measurements of massive (10^8 to $10^9 M_O$) SMBHs to $z \sim 0.4$ (and possibly beyond), and very massive ($>10^{10}$ M_O) SMBHs throughout the Universe. It will anchor the calibration of reverberation mapping as a mass estimator, and allow investigators to study the redshift evolution of SMBH scaling relations up to $z \sim 2.5$. TMT will enable the next giant leap in SMBH research, comparable in magnitude to the one that followed the launch of the Hubble Space Telescope (HST).

6.1 SMBH in nearby galactic nuclei

Ten years of research with HST have produced almost three dozen detections of SMBHs in galactic nuclei. These detections suggest the existence of a symbiotic relationship between SMBHs and their host galaxies. In particular, the relation between SMBH masses and the velocity dispersion of their host bulge

$$M_{BH} = 1.7 \times 10^8 (\sigma / 200\ km\ s^{-1})^{4.6}$$

(Ferrarese & Merritt 2000, Gebhardt et al. 2000) has proven invaluable in the study of SMBH demographics and has generated intense activity on the theoretical front, changing the view of how SMBH and galaxy formation are related.

Nevertheless, there is considerable scatter in the observed M_{BH}–σ relationship and the overall slope and power-law behavior are still disputed (Ferrarese & Ford 2005, Wyithe 2006). It is also not known if a single relationship applies universally to all galaxy types across the full range of galaxy/spheroidal masses. Of the 31 galaxies examined by Tremaine et al. (2002), 18 are ellipticals, 9 are lenticular (S0), and 4 are spiral. Is the M_{BH}–σ relation really the same for giant ellipticals, dwarf ellipticals, S0s, and the bulges of spirals with or without bars – even though these galaxy classes have significantly different structural properties? And what is the role of local environment – are there different relationships for field and cluster galaxies? Clearly, much larger and less biased samples of galaxies are needed to understand how different M_{BH}–σ relationships might occur among different galaxy types, in different cluster/field environments, and in different extremes of galaxy/SMBH mass.

Measuring SMBH mass relies on spatially resolved measurements of central stellar (or gaseous) kinematics coupled with modeling of the three-dimensional velocity field. Spatial resolution must be good enough to map out the so-called sphere of influence, i.e. the region of space within which SMBH dominates the gravitational potential and therefore the kinematics of the surrounding material. This sphere of influence has radius

$$r_h = \frac{GM_{BH}}{\sigma^2} \approx \frac{11.2(M_{BH}/10^8\,M_O)}{(\sigma/200\ km\ s^{-1})^2}\,pc$$

Hence, for any given spatial resolution, only a finite range of SMBH masses are detectable at a given distance. Measurement of r_h is further complicated by intrinsic variations in surface brightness between galaxies – for any given telescope aperture size, spatial resolution may be good enough to resolve a given r_h but an individual galaxy may have too low central surface brightness, making the observation impossible.

At present, further progress is impeded by three main shortcomings:

- The resolution of HST has been exploited to its fullest. However, the smallest (< 10^6 M_O) SMBH remain unexplored because their spheres of influence are smaller than the spatial resolution of HST in local galaxies. Conversely, largest (> 10^9 M_O) SMBHs remain unexplored because they are found in massive, rare galaxies at large distances, also placing their sphere of influence below the spatial resolution of HST.
- The relatively small collecting area of HST confines stellar dynamical studies to high surface brightness objects. For instance, an HST stellar dynamical study of the nuclear region of M87 is not feasible because of its low stellar surface brightness.
- The lack of an integral field unit (IFU) onboard HST limits the accuracy with which the intrinsic dynamical structure of a galaxy can be derived. Many nuclei exhibit complex and asymmetric kinematics; therefore, long slit spectroscopy almost always fails to produce an unambiguous dynamical picture of galactic cores.

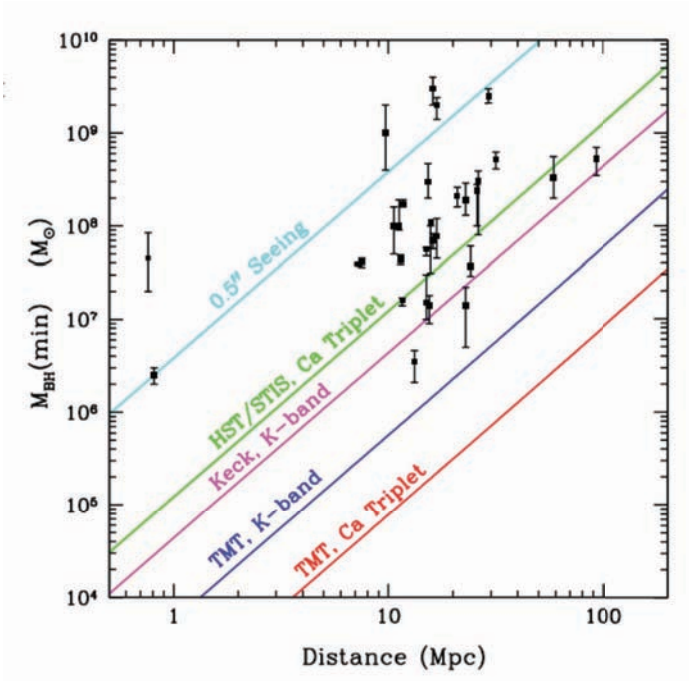

Figure 6-1 – Minimum detectable black hole mass vs. distance at various wavelengths for HST, Keck, and TMT. At any given distance, actual detectable black hole mass will depend on the central surface brightness of the galaxy. More detailed simulations that include surface brightness suggest that hundreds to thousands of candidate galaxies will be available to populate the TMT K-band trend line. The black data points come from Tremaine et al. (2002). Figure courtesy A. Barth (UCI).

All three of these problems are currently under attack from ground-based 8 – 10m telescopes using IFU spectrographs fed by laser guide star (LGS) assisted adaptive optics systems. With their increased spatial resolution and collecting areas, progress can be expected in the near future. Absolute progress relative to HST will be limited, however, by two factors. First, ground-based observations will be made at longer wavelengths than HST observations (to take advantage of the best possible LGS AO natural seeing improvement); hence, the relative resolution gain will not scale directly with relative aperture diameters. Second, the effective background surface brightness is higher at the ground-based observatories, which in turn eliminates some candidate galaxies because their central surface brightness is too low. Working at longer wavelengths does have the advantage of being less sensitive to the presence of dust, particular important for probing the low-end of the M_{BH}–σ relation, likely to correspond to the centers of dusty spirals.

The improved spatial resolution and increased flux sensitivity of TMT open the door to more complete galaxy samples in a larger range of environments than is currently possible. As illustrated in Figure 6-1, this implies that a larger range of SMBH mass can be explored than is currently possible. The combination of NFIRAOS (to produce diffraction-limited images in the near-IR) with the IFU in IRIS creates the near-ideal system for exploring this crucial problem in galaxy formation.

6.2 SMBH beyond the local neighborhood

Has the relationship between SMBH mass and central velocity dispersion evolved with time? This question directly probes the mechanisms that regulate the joint evolution of galaxies and SMBHs. Answering it requires measurements of MBH beyond the local neighborhood. What is possible with TMT?

Measuring central velocity dispersion requires a strong spectral feature redshifted to an accessible wavelength. For example, the Ca II triplet lies at 0.85 μm in the rest-frame. Centering this feature in the JHK bands corresponds to redshifts of 0.40, 0.87, and 1.58, respectively. Given the expected spatial resolution of IRIS in each these bands, the minimum resolved SMBH radius of influence corresponds to 60, 100, and 150 pc at these redshifts. For comparison, note that the radii of influence for M87 (M_{BH} ~ 3 x 10^9 M_O) and M31 (M_{BH} ~ 7 x 10^7 M_O) are approximately 100 and 12 pc, respectively. Thus, it will be possible to probe the upper end of the SMBH mass function with TMT at these redshifts. Of course, the central surface brightness challenge remains.

As an alternative to measuring M_{BH} using stellar kinematics, consider nuclear disks in AGN. A significant number of these disks exist on the 100 pc scale, which has been shown above to be an interesting spatial size out to redshifts ~ 1. The kinematics of these disks can be used to constrain the central potential and measure the mass of the central SMBH. Relatively high surface brightness emission lines from these disks exist at various rest-frame wavelengths; therefore, measurements of M_{BH} from emission line kinematics are limited by resolution requirements only. Again, this opens window on the upper end of the SMBH mass function at higher redshift.

Parenthetically, dynamical detections of SMBHs out to z = 0.1 will allow a direct calibration of reverberation mapping, a secondary mass estimator with the potential to push SMBH detections to high redshifts. The use of reverberation mapping is at present hindered by the lack of an independent confirmation of the SMBH masses derived to date using this method. A dynamical detection of SMBHs in reverberation-mapped AGNs (of which many examples are available within z < 0.1) would provide such confirmation, as well as offer a direct insight onto the morphology and kinematics of the AGN broad-line region. In this regard, the contribution of TMT would be comparable to that provided by HST in anchoring the distance scale ladder by measuring secure Cepheid distances to local galaxies. With such a calibration, it may be possible to extend SMBH (>10^8 M_O) detection via reverberation mapping out to z ~ 2.5.

6.3 SMBH at very high redshift

The strength of low-redshift SMBH studies is that precise definitions of the relationship between galaxies and their central SMBHs can be achieved across an unprecedented wide range of galaxy types and masses. However, this is the fossil record – the most interesting SMBH evolution occurred long ago and is observable at high redshift. Most of the SMBHs in local galactic nuclei are dormant, or nearly so, because the mass accretion has essentially stopped. However, every galaxy that hosts a SMBH today must have been at one time extremely active – shining brightly as a quasar or some other type of active galactic nucleus (AGN) when the SMBH was still growing and aggressively accreting matter. The duration of the bright (visible) AGN-phase of SMBH growth is believed to be short, just a few 10^7 yrs, but it coincides with an important early stage of galaxy development. High-redshift AGN, in particular, mark the locations (and epochs) where massive galaxies are rapidly being assembled, making stars, and funneling matter into a central SMBH.

There are many open questions. For example:

- At what stage(s) of galaxy evolution do AGN appear? One possibility is that high-redshift AGN are coeval with the first major episode(s) of star formation in very young galaxies, and so the appearance of AGN should be strongly correlated with star formation. On the other hand, if AGN occur before the host galaxies are fully assembled, we might find a very different SMBH-galaxy mass relationship at high redshifts compared to the present.
- What global environmental factors give rise to different types/luminosities/masses of AGN/SMBHs, and are these factors different at different redshifts? Surprisingly little is known about how the most basic AGN properties, such as luminosity and SMBH mass, correlate with global environmental factors, or how the environmental factors that give rise to AGN (might) change with cosmic time.
- To what degree are AGN of a given type, luminosity, or SMBH mass associated with young/old galaxies, rich/poor clusters, and high/low star formation rates? It is often noted that the decline in the quasar number density from $z \sim 3$ to the present is well matched by the declining global star formation rate (Franceschini et al. 1999), but what exactly is the connection?
- Do AGN appear preferentially in galaxies that are young or have enhanced star formation rates? Are AGN at higher redshifts and/or higher luminosities more likely to reside in globally dense environments, i.e. in rich clusters? Models of cosmic structure formation (e.g. Haehnelt & Kauffmann 2000) suggest that AGN "activity," star formation rates, and cluster richness should all be correlated, and each should decline over time (due to the combined effects of gas consumption, smaller galaxy merger/interaction rates, and the general hierarchical agglomeration of mass). But observations so far have been unable to test these ideas.

Using IRIS with its near-IR integral field spectroscopic capability at diffraction-limited spatial resolution, TMT will allow, for the first time, the study of the final (bright) stages of SMBH growth in the context of star formation and galaxy assembly at high redshifts. Type 1 (broad line) AGN that span the widest possible range of luminosities, and thus SMBH masses, at each observed redshift will be selected so that the relationship of AGN mass/luminosity to the galactic surroundings can be explored. SMBH masses, M_{BH}, can be derived from the AGN spectra by exploiting a well-calibrated relationship between M_{BH} and the full width at half maximum (FWHM) of the broad Hβ λ4861 emission line (Peterson et al. 2004). The line width provides a measure of the viral speed in the broad emission line region (BLR) of the AGN, e.g., FWHM ~ vBLR. The radial distance of the BLR from the central SMBH scales with luminosity (because the intense ionizing radiation of more luminous AGN forces the BLR to be farther out, Kaspi et al. 2000, 2005). So with the radius and velocity known, the SMBH masses follow simply from the virial theorem, $M_{BH} \sim r_{BLR} v_{BLR}^2 / G$.

AGN at redshifts $z \sim 2.5$ are one obvious choice for such a study because they probe a major epoch of global AGN activity and galaxy formation. Redshift ~2.4 also places Hβ and [OIII] λ5007 in the H band,

Hα λ6563 and [NII] λ6548/83 in the K band, and [OII] λ3727 in J, thus providing ample diagnostics of the SMBH mass and overall AGN type/properties at observer-frame wavelengths where TMT adaptive optics performance is optimal. These same lines and spectral regions measured in the host and surrounding galaxies will provide measures of their star formation rates, ages of the stellar populations, and accurate redshifts (to confirm the relationship to the AGN). AGN luminosities similar to nearby Seyfert 1 galaxies are will within reach of TMT sensitivities. We can therefore expect to measure SMBH mass across a wide range from a few x 10^6 M_O to >10^9 M_O (see Warner et al. 2004).

The higher redshift universe, at z ~ 4.5 and beyond, is also of great interest because it corresponds to a time less than 1 Gyr after the Big Bang. The luminous quasars most easily detected at these redshifts must be powered by very massive black holes (M_{BH} ≥ 10^9 Mo) and must, therefore, reside in some of the most over-dense regions in the young universe. These environments are also the most likely sites of intense early star formation. TMT can be used to study this redshift range using spectral diagnostics at shorter rest-frame wavelengths. For example, at redshifts near z ~ 5, the broad MgII λ2800 line of AGN (another indicator of SMBH mass, McLure & Jarvis 2002) falls in the H band, and we can estimate star formation rates and population ages in the surrounding galaxies using rest frame UV/blue continuum spectra measured in the red/near-IR. At redshifts z ≥ 6, we will measure quasar emission lines such as Lyα, NV λ1240, CIV λ1550, and HeII λ1640, which can be used not only to measure the SMBH mass but also to estimate the metallicity of the quasar's BLR (Hamann & Ferland 1999, Hamann et al. 2002, Vestergaard 2002, Warner et al. 2004). If the BLR gas was enriched by a surrounding stellar population (as expected according to Hamann & Ferland 1999, Baldwin et al. 2003), then the BLR metallicities are an important indirect tracer of the amount of star formation that occurred at even earlier epochs near these galactic nuclei. If multiple IFUs are available (e.g. with IRMOS), objects in the surrounding region can investigated in parallel to the target AGN.

References

Baldwin, J.A. et al. 2003, ApJ, 582, 590
Ferrarese, L. & Ford, H. 2005, Space Science Reviews, 116, 523
Ferrarese, L. & Merritt, D.A. 2000, ApJ, 539, L9
Franceschini, A. et al. 1999, MNRAS, 310, L5
Gebhardt, K. et al. 2000, ApJ, 539, L13
Haehnelt, M.G, & Kauffmann, G. 2000, MNRAS, 318, L35
Hamann, F., & Ferland, G. 1999, ARAA, 37, 487
Hamann, F. et al. 2002, ApJ, 564, 592
Kaspi, S. et al. 2000, ApJ, 533, 631
Kaspi, S. et al. 2005, ApJ, 629, 61
McLure, R.J. & Jarvis, M.J 2002, MNRAS, 337, 109
Peterson, B.M., et al. 2004, ApJ, 613, 682
Wyithe, J.S.B. 2006, MNRAS, 365, 1082
Tremaine, S. et al. 2002, ApJ, 574, 740
Vestergaard, M. 2002, ApJ, 571, 733
Warner, C., Hamann, F., & Dietrich, M. 2004, ApJ, 596, 72

7 Exploration of nearby galaxies

The stellar content of nearby galaxies (including our home, the Milky Way) make up the fossil record that was produced by the galaxy formation and evolution process that can be observed at high redshift. The spatial, age, and chemical makeup distributions of these stars provide important details about this process, details that are simply unobtainable from observations of high galaxies at high redshift. Hence, the study of nearby stellar populations complements the study of galaxy formation and evolution at high redshift and provides important clues to the underlying astrophysical processes involved.

7.1 Probing the oldest stars in the Milky Way

Big Bang nucleosynthesis in the first 20 minutes of the Universe created deuterium, two isotopes of He (^{3}He and ^{4}He) and a very small amount of lithium as well as ^{1}H. Yet the periodic table of elements includes ~90 stable elements, all of which are found in varying amounts on the Earth. Some of these are common, such as carbon and oxygen, others very rare (europium, neodymium, and the other rare earths); many are essential for life. All these heavier elements were formed in stars, as byproducts of the nuclear fusion near the centers of stars or of supernovae explosions. Each nucleosynthetic path has a different timescale and produces a different, but characteristic, atomic element abundance patterns. By studying these patterns, information about the initial conditions of star formation and subsequent chemical evolution history can be deciphered.

Clearly, the first (so-called Population III) stars must have formed from gas unpolluted by heavy elements, after which all subsequent generations of stars contained increasing fractions of metals. This process has continued during the entire lifetime of the Universe. Hence, the most metal-poor stars in the Milky Way and other galaxies are the oldest stars. These very old stars are hidden amongst a vast number of stars formed later in time. Once found, understanding the chemical composition of the oldest stars provides a direct probe of the initial conditions of star formation as well as the details of chemical evolution and nuclear astrophysics in the early universe.

Recent chemical evolution models of very metal-poor stars in the Milky Way that track hierarchical galaxy formation, stellar populations, and supernovae yields together have suggested that these old, extremely metal-poor stars contain metals that originated in 10 or fewer Population III progenitors. Hence, observed variations in elemental abundances between individual extremely metal-poor stars in the current Milky Way halo probably represent true variations in the masses and supernovae yields that polluted the local gas from which each individual star formed (see Figure 7-1).

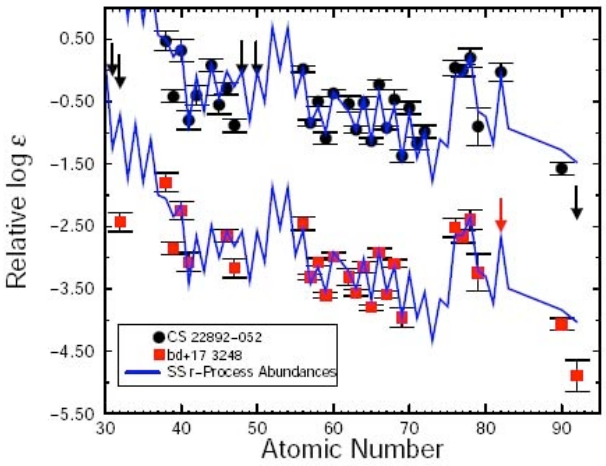

Figure 7-1 – The neutron-capture elemental abundance pattern in the Galactic halo stars CS 22892–052 ([Fe/H] ~-3.1 dex, [Eu/Fe] +1.6 dex) and BD+17 3248 ([Fe/H] ~-2.1 dex, [Eu/Fe] +0.9 dex) (both stars highly enhanced in the r-process elements) compared with the (scaled) solar system r-process abundances (solid blue lines); note that the total solar abundances for these neutron capture elements include contributions from additional production channels. The abundances of the latter star have been vertically shifted to avoid confusion in the figure. (Source: Cowan et al. 2006)

At present, only three stars with [Fe/H] < –4.5 dex (i.e. the relative amount of Fe to H is ~30,000 times smaller than observed in the Sun) are known, all from the Hamburg/ESO Survey (Wisotzki et al. 2000). Each of these stars is very Fe-poor, but C-rich, so that their overall metallicity is close to 1/100 that of the Sun. This has given rise to immense controversy about the relationship of these three stars with the more numerous extremely metal poor stars with [Fe/H] ~ –3 to –3.5 dex. Some of the latter are C-rich, but the majority has low carbon abundances. So, are the three most extremely metal-poor stars in some sense "older", coming from an earlier population? Or has some property of Population II supernovae produced these very large [C/Fe] ratios? Some view these three stars as each inheriting the ejecta from a single SNII for which an unusually large amount of material was not ejected, but instead fell back onto the remnant, so the Fe-rich material formed in the central region of the SN progenitor was never released into the ISM (see, e.g. Tominaga, Umeda & Nomoto 2007). Others suggest that the C-rich material results from a mass transfer binary or includes ejecta from multiple generations of SN. Obviously, a larger sample of extremely metal-poor stars is necessary to clarify this complex and very interesting situation.

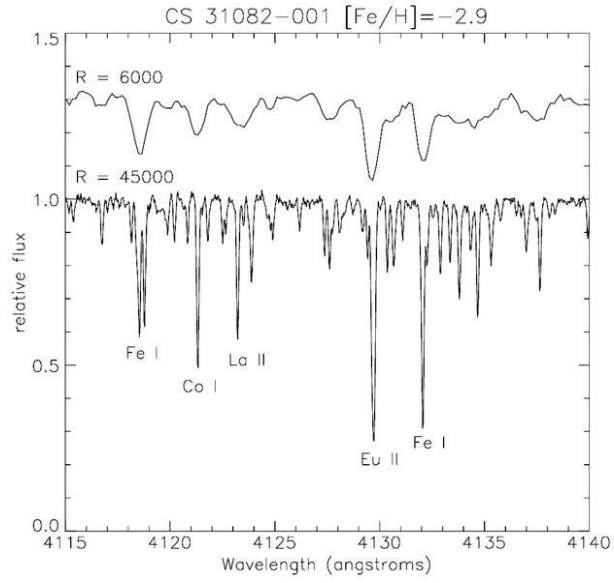

Figure 7-2. Comparison of moderate vs. high-resolution stellar spectrum. Comparison of spectra taken at moderate resolution (upper curve) and high resolution (lower curve) of a metal-poor star. At higher resolution, many important absorption lines become available for study. (R. Guhathakurta, UCSC).

Since the relevant absorption lines are quite weak, the required chemical composition studies require high spectral resolution ($R = \lambda/\Delta\lambda$ ~ 50 000 or greater), high SNR (~ 100 per spectral resolution element) observations (see Figure 7-2). These requirements lead to extremely long integration times on the largest telescopes currently available. For example, an 18-hour integration with UVES on the VLT was required to determine abundances for HE1327-2326, the most extreme metal-poor star ([Fe/H] ~ 5.5 dex) known to data (Frebel et al. 2006). Unfortunately, many potentially interesting stars are too faint for current 8 – 10 m telescopes.

The number of stars accessible to TMT will be much larger, due both to the larger collecting area and more efficient spectrographs. For the seeing-limited high-resolution spectrograph HIRES, the total improvement relative to VLT/UVES or Keck/HIRES is expected to be 15 – 20. For example, a 4-hour integration with HROS will enable $R = \lambda/\Delta\lambda$ ~ 40 000 spectroscopy with SNR = 100 per spectral resolution element for stars as faint as V ~ 21. Candidate objects will come from surveys like SEGUE (Sloan Extension for Galactic Underpinnings and Evolution)[1]. SEGUE itself is expected to yield at least 100 stars with [Fe/H] < – 4 in the next few years – most too faint to be investigated with the current telescope/instrument generation.

[1] http://segue.uchicago.edu/

7.2 Looking deeper: isotope ratios

Nuclear reactions produce specific isotopes. However, because the isotopic shift is generally very small at optical wavelengths, very high spectral resolution is required to measure isotopic ratios in stellar spectra. Measurement of isotopic ratios, however, provides a completely new window into nucleosynthesis, galactic chemical evolution, mixing within stars and stellar evolution. Such data, when available, significantly improves our understanding of nuclear processes in various astrophysical sites.

An example of what can be learned from isotopes is given by considering magnesium (Mg), which has 3 stable isotopes with atomic weights 24, 25 and 26. ^{24}Mg is produced via routine burning of carbon in the interior of massive stars during their normal evolution as a primary element, and is subsequently injected into the ISM by SNII. The two heavier isotopes of Mg, on the other hand, are secondary isotopes believed to be produced primarily in intermediate mass AGB stars. In the young Galaxy, there was not enough time for AGB stars to contribute, while core collapse SN started exploding quickly after massive stars first formed. We can thus use the ratios among the Mg isotopes to explore when the AGB stars began to contribute to the Galactic chemical inventory (see Figure 7-3).

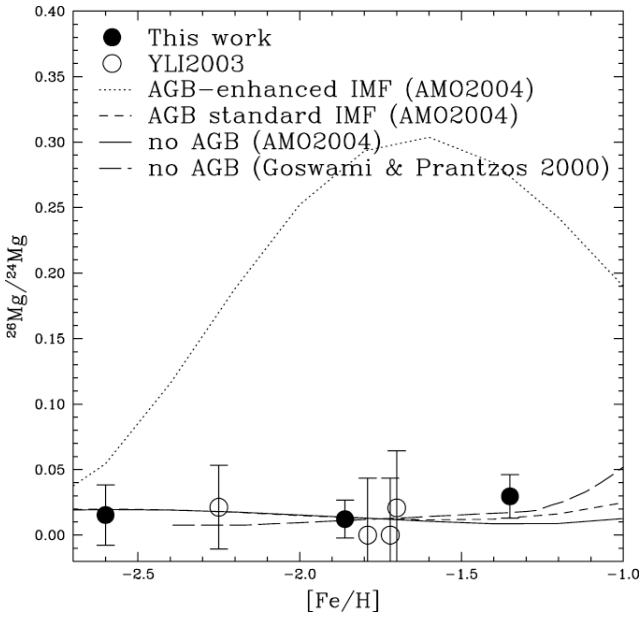

Figure 7-3 – ^{26}Mg/^{24}Mg as a function of [Fe/H] in halo stars. Galactic nucleosynthesis models including yields of massive stars and in some cases intermediate-mass AGB stars are shown. (Source: Melendez & Cohen 2007)

A spectral resolution of at least 90,000 combined with very high signal-to-noise ratios (at least 200 per spectral resolution element) is required to measure Mg isotopic ratios. Similar extremely high precision and high spectral resolution data are required to investigate the ^{6}Li/^{7}Li ratio, a current subject of raging controversy. For example, in apparent contradiction to Big Bang nucleosynthesis theory, Asplund et al. (2007) report the detection of ^{6}Li at a ratio of ~5% of the total Li in extremely metal poor dwarfs.

The distribution among the many stable isotopes of Ba is a key diagnostic of neutron capture nucleosynthesis, as the production mechanism for the odd atomic weight ones is quite different from that of the even ones. But so far this has only been measured in one star other than the Sun (HD 140283; Lambert & Allende Prieto 2002), and that measurement is too uncertain to set useful constraints. Along lines of sight with low interstellar reddening, HROS will enable high-precision measurements of the isotopic ratios of Li, C, Mg, Ba, and Eu throughout the Milky Way, its globular cluster system, and its halo.

7.3 Probing chemical evolution in Local Group dwarf galaxies

In CDM simulations of the growth of structure, dwarf galaxies play an important role as the building blocks of large galaxies. Such simulations suggest that halos of the galaxies like the Milky Way have accreted (and subsequently destroyed) 10s to 100s of small, dwarf galaxies in the past 10 Gyr. However, detailed stellar atmosphere analyses of individual red giant branch (RGB) stars in current day Local Group dwarf galaxies show very little in common with the chemistry of stars in the Milky Way halo, disk, bulge, and moving groups (Venn et al. 2004; Navarro et al. 2004). Furthermore, the number of surviving dwarf galaxies in the immediate neighborhood of the Milky Way is far lower than predicted. There are a variety of possible solutions to these problems. Perhaps dwarf galaxy formation was suppressed during the era of reionization in the early universe. Perhaps star formation within accreted dwarf galaxies was truncated during the accretion events, resulting different chemical evolution histories than unaccreted dwarf galaxies. Or perhaps that the dwarf galaxies that produced the Milky Way halo simply had fundamentally different star formation and chemical evolution histories than the current day dwarf galaxies in the Local Group.

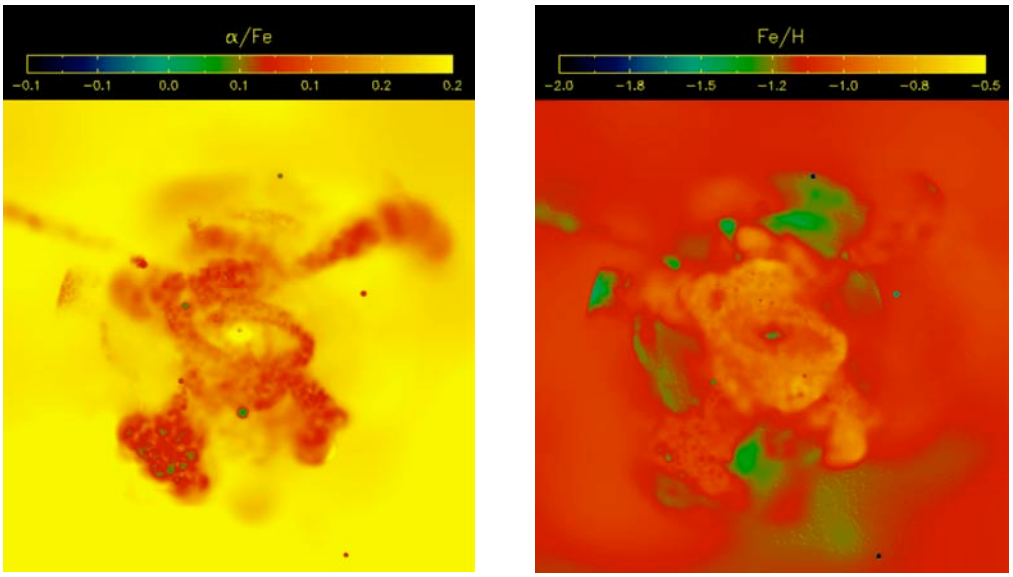

Figure 7-4 – Chemical abundance maps of a hierarchically formed stellar halo from the ΛCDM simulations of Bullock & Johnston (2005) and Johnston et al. (2007). Surviving satellites can be seen as tight knots in the stellar distributions. Alpha-element abundances are shown on the left and Iron is shown on the right. Note that the diffuse stellar halo is alpha enhanced compared to the surviving satellites.

To test these ideas, and to investigate environmental differences between the various dwarf galaxies, detailed examination of the kinematics, metallicities, and abundance ratios of stars in dwarf galaxies beyond the Milky Way halo are necessary. With TMT/HROS, it will be possible to carry out detailed abundance analyses of stars at or just above the tip of the red giant branch throughout the Local Group. For example, current generation high-resolution spectrographs on 8 – 10m telescopes have been able to study tens of stars in Local Group dwarf spheroidal galaxies at V = 17 – 18 with exposure times up to 14 hours. Those systems lie as far away as 250 kpc. TMT/HROS will be able to obtain similar results for stars at V ~ 20 in more distant (~ 400 – 500 kpc) and hence more isolated systems. These optical measurements can be supported by K-band measurements – TMT/NIRES can easily reach below the tip of the red giant branch throughout the Local Group (see Table 7-1). Such K-band measurements will be invaluable for CNO abundance measurements.

Table 7-1: Estimated limiting distances for spectroscopic observations of point sources

	M_V (mag)	WFOS (Mpc)	HROS (Mpc)	NIRES (Mpc)
Blue supergiant	–6.7	10.0	7.0	2.5
Red supergiant	–5.9	7.0	3.5	8.0
RGB Tip	–2.7	1.5	0.5	3.8

Table notes: assumes 4 hour integrations at $\lambda/\Delta\lambda$ = 5000, 50 000, and 25 000 for WFOS, HROS, and NIRES, respectively. The corresponding central wavelengths are 0.5 μm, 0.5 μm, and 1.2 μm. The final SNR per spectral resolution element are 100, 100, and 60, respectively. Courtesy: J. Cohen (CIT).

With such data, the chemistry of the old stellar population in dwarf irregular galaxies (which tend to be more distant and more isolated satellites of the Milky Way) can be compared directly to the old populations of the dwarf spheroidals and Magellanic Clouds. These latter systems are within the dark matter halo of the Milky Way and are thought to have been interacting with the Galaxy over most of their lifetimes, likely affecting star formation histories and chemical evolutions. A comparison with cleaner, more isolated dwarf irregulars will allow us to establish and characterize, for the first time, the effects of environment on chemical evolution through the chemical similarities and differences in old populations. At present, detailed chemistries for dwarf irregular galaxies are only available from young, massive, evolved stars (Venn et al. 2001, 2003) and HII regions (Skillman et al. 1989, Lee et al. 2005). These objects yield the present-day chemistries of these systems, but that includes the integration of the yields from a complex star formation history. To compare dwarf irregular galaxies to the Galactic halo and other Local Group dwarf galaxies, and test their impact on merging hypotheses of galaxy formation, requires detailed chemical analyses of their old RGB stars.

7.4 Chemical evolution histories in the Local Group and beyond

The galaxies of the Local Group are all close enough that they can be resolved into stars by HST imaging and by AO systems on 10 m class telescope. Imaging studies are straightforward, especially with the AO system coupled to TMT. However, for spectroscopy, particularly at the high dispersions necessary to carry out detailed abundance analyses, the extra factor of 6 (on average) in distance of M31 compared to the Milky Way dSph satellites is very limiting.

Analysis of spectra of young giant stars in nearby, actively star forming galaxies nearer galaxies of the Local Group with ongoing star formation (see Figure 7-5), has become possible in the past decade due to a combination of observational data from 8 – 10 m telescopes and advances in model atmosphere techniques. The latter include the development of non-LTE hydrodynamic 3D extended stellar atmospheres, necessary to understand absorption features influenced by supersonic outflowing stellar winds. As shown in Table 7-1, observations with TMT will extend these studies to very large distances allowing the investigation of a variety of start formation environments and galaxy morphologies.

Sophisticated models of galactic chemical evolution are based on nucleosynthetic yields of various elements from each of the possible sources together with the amount of mass ejected from each of these sources, all as a function of stellar initial mass (and to a lesser extent stellar initial metal content). These are folded in with assumptions regarding gas flows within the galaxy and possible accretion of primordial material only recently collapsing into the galaxy. Formation rates and an initial mass function for stars, both as a function of time, must be adopted as well. Prediction of trends of abundance ratios within the galaxy as a function of location require knowledge of any dependencies of all of these inputs on position as well as an assumption regarding migration of stars within the galaxy.

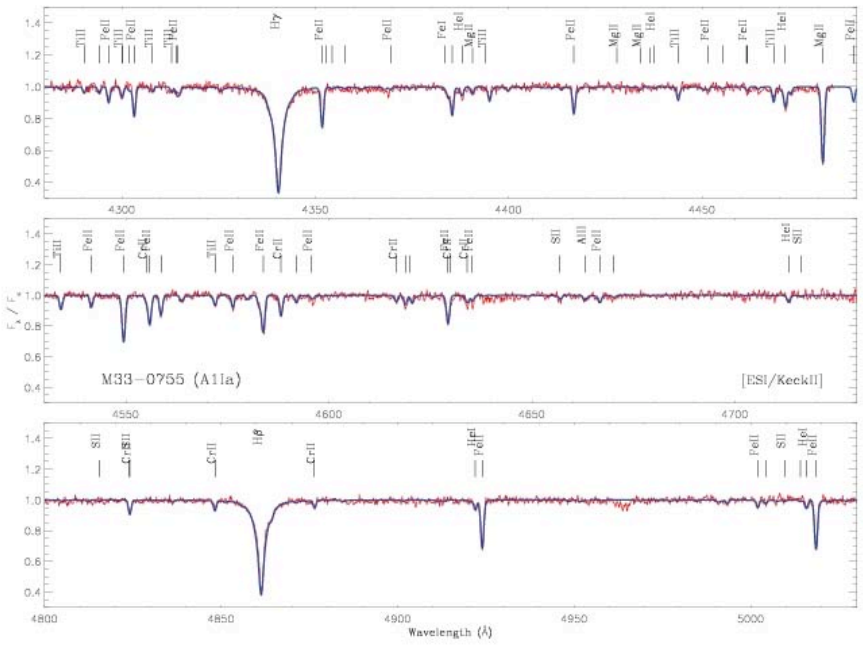

Figure 7-5 – The moderate resolution spectrum of an early A supergiant in the Local Group galaxy M33 (distance ~800 Mpc) and the best fit model. (ESI/Keck spectrum, λ/Δλ=10,000, 2 hour exposure) (Source: Urbaneja et al. 2007)

Figure 7-6 shows the trend based on detailed abundance analyses of large samples of stars in the disk and halo of the Milky Way for the alpha-element Ca. The solid lines are predictions of chemical evolution using two different calculations of nucleosynthesis yields. The gentle rise towards lower Fe-metallicity is generally ascribed to the difference in characteristic timescale for SNII, the major production site for the alpha-elements, as compared to SNIa, where most Fe is produced. The former is much shorter than the latter, which may be as long as ~1 Gyr after the initiation of star formation.

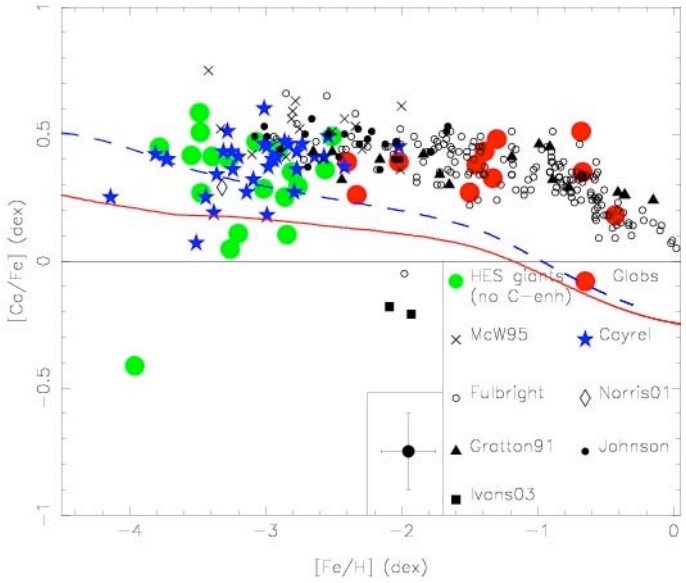

Figure 7-6 – The evolution of Ca in the Milky Way is shown by the ratio of [Ca/Fe] versus Fe-metallicity for C-normal giants compiled from a number of major surveys (sources indicated on the figure) of halo and thick disk stars. The curves indicate the predictions of Prantzos and collaborators using two different prescriptions for the nucleosynthetic yields, those of Chieffi & Limongi (2004) and those of Woosley & Weaver (1995). Note the presence of a single strong outlier, which is extremely-metal-poor with abnormally low [Ca/Fe]. (Source: Cohen et al. 2007 and Prantzos 2007)

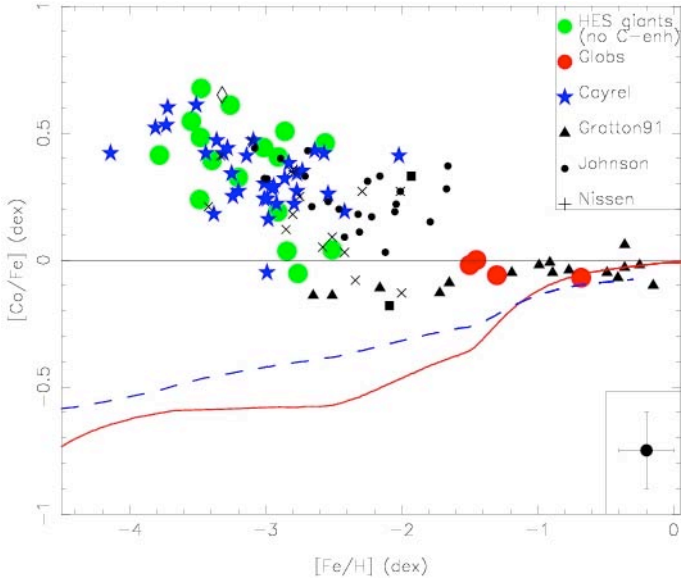

Figure 7-7 – The same as Figure 7-6 for cobalt. For this Fe-peak element, the model of galactic chemical evolution fails to reproduce the observed trends. (Source: Cohen et al. 2007 and Prantzos 2007)

Most of the apparent dispersion in [Ca/Fe] at a fixed [Fe/H] is due to errors in the observations and/or analyses; the intrinsic spread in this relation may be quite small. This is a surprising result given the few SN contributing to their chemical inventory, and the strong dependence of nucleosynthesis yields on stellar initial mass. One strong outlier appears at the lower left of the figure, a very interesting and unusual star described in Cohen et al. (2007). Figure 7-7 shows the same for the Fe-peak element Co.

Although creating a model of galactic chemical evolution requires many assumptions, it does work most of the time. In other words, such models can reproduce in a general way most observed trends of abundance ratios with time since the formation of the Milky Way with what are agreed to be involved reasonable input data. Superposed on Figure 7-6 and Figure 7-7 are the most recent predictions of Prantzos (2007). These illustrate both success (for Ca) and failure (Co) for this approach. Of course, one learns even more from the failures than from the successes.

Such models, with different inputs, justified by observational data, also appear to work for the nearby galaxies, although our knowledge of their stellar populations and their chemical inventory is much more limited than is that for our own galaxy. TMT will make a major contribution to improve our knowledge of the chemical evolution of nearby galaxies. In the TMT era, high dispersion spectroscopy using HROS and NIRES will enable detailed abundance analyses with high accuracy for individual stars in the outer parts of the nearest groups of galaxies, including the M81 group, and for the brightest globular clusters well beyond the Virgo cluster. We will then finally obtain a full picture of the chemical evolution of the nearest galaxy groups out to the Virgo cluster, and be able to compare it to that of the Milky Way.

7.5 Stellar astrophysics

There are still a number of areas important to stellar modeling and evolution that are usually ignored because it is simply unclear how to proceed – there is little observational evidence to guide theoretical models in setting the relevant parameters, hence the resulting uncertainties may be large. Here, two areas are highlighted for which TMT can make major contributions.

The first is diffusion (sinking) of heavy elements in the outer parts of stars. Diffusion is believed to occur whenever the outer parts of a star are quiet without large-scale velocity fields and are then not well mixed. Gravity and temperature will tend to concentrate the heavy elements towards the center of the star

(Salaris, Groenewegen & Weiss 2000). Diffusion acts very slowly with time scales ~ 10^9 yr, so it is most important on the main sequence, and is particularly important for metal-poor stars. Diffusion of He is important in the Sun and affects helioseismology models. Diffusion is also important in precision distance determinations based on main sequence fitting, since the abundances adopted for the model isochrone must agree with those of the stars, while the abundances deduced for the stellar atmosphere may not be those of the interior. Diffusion may also be the solution to a disagreement of a factor of ~2 between the Li abundances derived for halo turn off stars, assumed to be the primordial lithium abundance, and the (lower) value predicted by standard Big Bang nucleosynthesis models that adopt the baryonic density inferred from the current concordance cosmology of WMAP (Melendez & Ramirez 2004; Korn et al. 2006; Bonifacio et al. 2007).

A key project to observe diffusion in action is to compare the elemental abundances for heavy elements near the Fe-peak of main sequence versus red giant and sub-giant stars in metal-poor globular clusters. Stars within a particular globular cluster, assuming its mass is not too high so that gas cannot have been retained beyond the first generation of star formation, are believed to have the same initial chemical inventory, and are sufficiently old that diffusion should have had time to act. The RGB stars have convective envelopes, and thus whatever diffusion might have occurred on the main sequence, the surface helium and heavy elements will have been restored to very close to their initial value, while the main sequence stars will be subject to the predicted larger effects of diffusion for metal-poor stars over their entire lifetime, i.e. that of the Galactic halo, ~13 Gyr. Such observations require high spectral resolution spectroscopy of main sequence stars in globular clusters with SNR difficult or impossible to achieve with existing 8 – 10 m telescopes. The net efficiency gain of HROS on TMT relative to current facilities will enable the required observations of these faint stars.

The second highlighted area is the evolution of massive stars with low metallicity. Massive stars contribute a large fraction of all the heavy elements through SN explosions. They provide the UV ionizing flux for the ISM and their supersonic winds help shape the ISM. They are probably linked to the reionization of the early universe (Bromm, Kudritzki & Loeb 2001) and perhaps to the GRB phenomenon. Massive stars of very low metallicity were, until quite recently, believed not to lose very much mass through radiatively driven winds due to their weaker absorption features. This would mean that such stars might often end up as black holes, locking up their heavy element chemical inventory in perpetuity, while a solar metallicity star of similar mass would lose enough mass to end up as a neutron star. However, Meynet et al. (2007) have suggested that these stars are rapid rotators that lose up to 50% of their initial mass through a rotationally driven wind. The mass loss rates they predict for the main sequence phase of a 60 M_O star are more than 20 times larger than if rotation were ignored. Coupled with rotationally driven instabilities that transport both angular momentum and chemical species (Zahn 1992), this means that massive low metallicity stars can significantly enrich the ISM in H- and He-burning products.

This theoretical development is very attractive as it solves a number of problems, but the observational evidence to support it is essentially non-existent at present. The low metallicity required to produce main sequence rotation rates of ~600 km/sec, close to the breakup rate at which the effective surface gravity becomes zero, is less than that seen any place in the Milky Way where star formation is still underway. The metal depletion of the ISM in the LMC and in the SMC is also not sufficient. A population of young massive stars in a low metallicity galaxy is required, i.e. a very metal-poor star-forming dwarf galaxy. There are none close enough to obtain the required spectroscopy with existing 8 – 10 m telescopes. The most metal-poor dwarf known in the nearby universe, I Zw 18, has a distance of 18 Mpc and an oxygen abundance 1/50 that of the Sun (Skillman & Kennicutt 1993). The galaxy SBS 1415+437 with a distance of 14 Mpc is almost as metal-poor (Aloisi et al. 2005), with oxygen below 1/20 the solar value. With WFOS, it will be possible to observe the brightest supergiants in the nearest very metal-poor dwarf galaxies to determine the mass loss rate as a function of metallicity.

7.6 Reconstructing the star formation histories of nearby galaxies

Reconstructing the star formation history for a given stellar system by analyzing its color-magnitude diagram (CMD) is a fundamental tool for understanding its age and chemical composition that has been calibrated by decades of observational and theoretical work. Starting with Galactic open and globular clusters in the mid-twentieth century, it is now possible to construct CMDs for globular clusters and dwarf galaxies throughout the Local Group, thanks to the exceptional spatial resolution of HST. However, CMD progress within more massive galaxies (or their denser sub-components) has been limited by stellar crowding too severe for the 2.5m Hubble Space Telescope. Recently, higher spatial resolution observations have become possible using near-IR adaptive optics systems on ground-based 8 – 10m class telescopes. By scaling up to 30m and implementing AO systems with improved performance, TMT will enable another giant step forward.

Figure 7-8 shows a crowding limits comparison for Σ_K = 19 mag arcsec^{-2} observed with near-IR AO-corrected 8-m and 30-m telescopes, as well as HST working in the optical at Σ_V = 22 mag arcsec^{-2}. These crowding limits were calculated analytically by comparing the contribution of surface brightness fluctuations on the scale of a telescope resolution element to that of a star of a given magnitude (Olsen, Blum, & Rigaut 2003). The ratio depends on the distance, surface brightness, and luminosity function of the stellar population as well as the photometric accuracy required for a given magnitude of star. The calculations demonstrate that TMT will be able to resolve individual stars in regions with Σ_K = 19 mag arcsec^{-2} in galaxies as far away as 15 Mpc. Of course, as distance increases, the required photometric accuracy becomes more difficult and only feasible for the intrinsically brightest stars.

Figure 7-9 compares actual near-IR AO observations of the nearby dwarf elliptical galaxy M32 with simulated JWST and TMT/IRIS observations. CMD determinations and recovered star formation histories are shown as well. The TMT gain in the recovered star formation is clear. Whereas JWST provides the correct qualitative features, TMT observations provide more precise constraints on the main sequence turnoff, which leads to a more accurate reconstruction of the star formation history. In this (or a similar) situation, *R* ~ 4000 spectroscopy with the IRIS IFU will be possible for many RGB stars, providing additional constraints on the star formation history reconstruction process.

A long sought goal is to construct a deep CMD for a normal elliptical galaxy. Several candidate targets lie within 10 – 15 Mpc, including (e.g.) NGC 3379 (d ~ 11 Mpc). Table 7-2 provides crowding limits at three galactocentric radii for NGC 3379. The crowding limit is defined to be the magnitude at which photometric errors due to crowding reach 20%, corresponding to 50% completeness. At 1 R_e, only the brightest RGB and AGB stars will be accessible before the crowding limit is reached. However, at 3 R_e (perhaps the lowest practical surface brightness given required exposure times) it will be possible to reach the horizontal branch before reaching the crowding limit. This can be compared to actual HST/NICMOS observations at 3 R_e that only reach ~ 1 mag below the TRGB before significant crowding limits photometric accuracy (Gregg et al. 2002).

Table 7-2: Crowding limits for NGC 3379

Name	r (arcsec)	Σ_K (mag arcsec^{-2})	K_{lim}	Time (secs)
R_e	30	17.0	25.7	282
$3R_e$	90	19.3	28.5	47200
R_{tot}	190	22.5	31.6	∞
K (1 hour)	—	—	27.9	3600

Table Notes: the second column (r) is galactocentric distance, the third (Σ_K) is assumed surface brightness at that distance, the fourth (K_{lim}) is the point source magnitude at the crowding limit (as defined in the text), and the last column (t) is the exposure time to reach these limits. For reference, the last row shows the point source limiting magnitude for τ = 3600 secs in the absence of crowding.

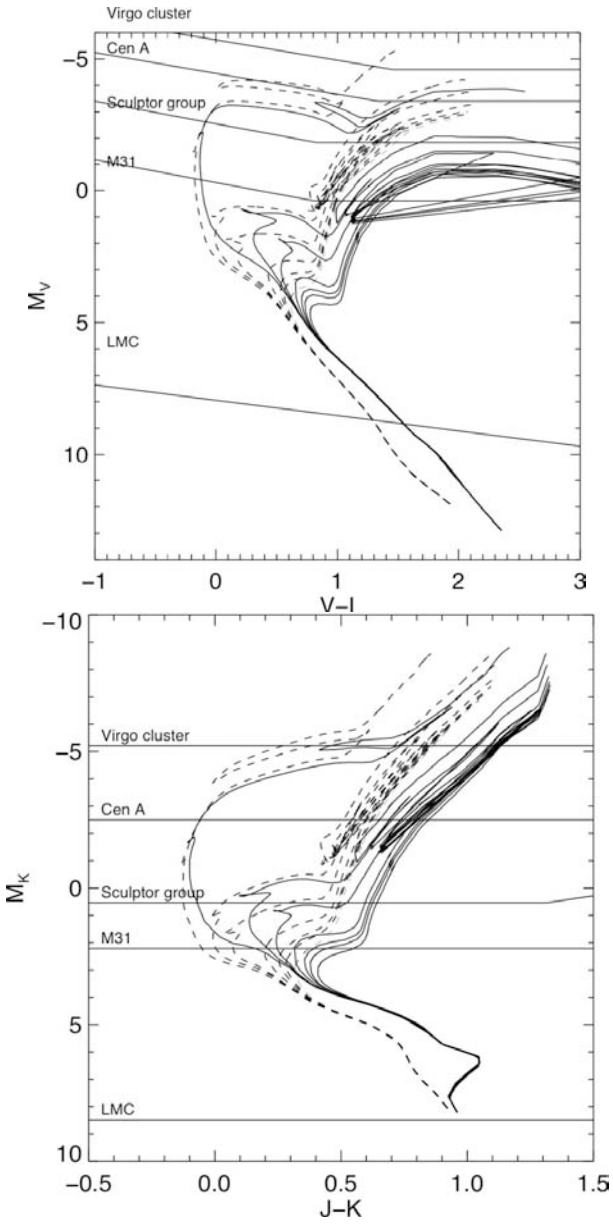

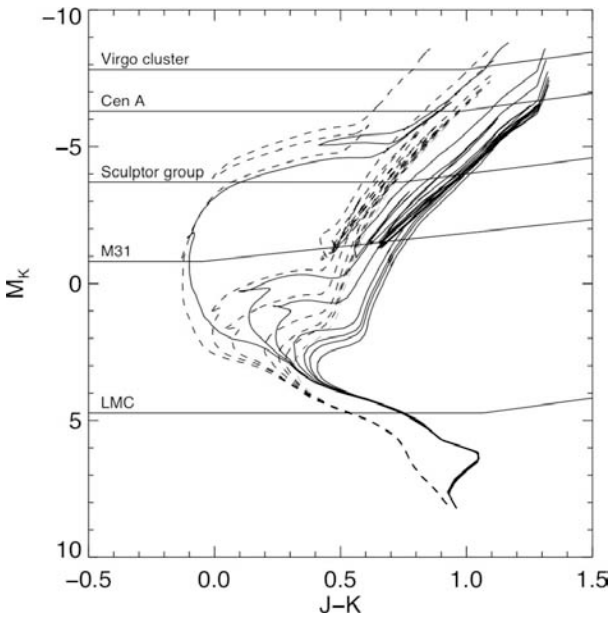

Figure 7-8 – Magnitudes at which crowding limits photometry to 10% accuracy in regions with Σ_K = 19 and Σ_V = 22 mag arcsec^{-2} at the distances indicated are shown as horizontal lines on top of Girardi et al. (2000) isochrones of various ages and metallicities. Top left: HST in the optical. Top right: Gemini North + NIRI/Altair. Bottom: TMT in the near-IR.

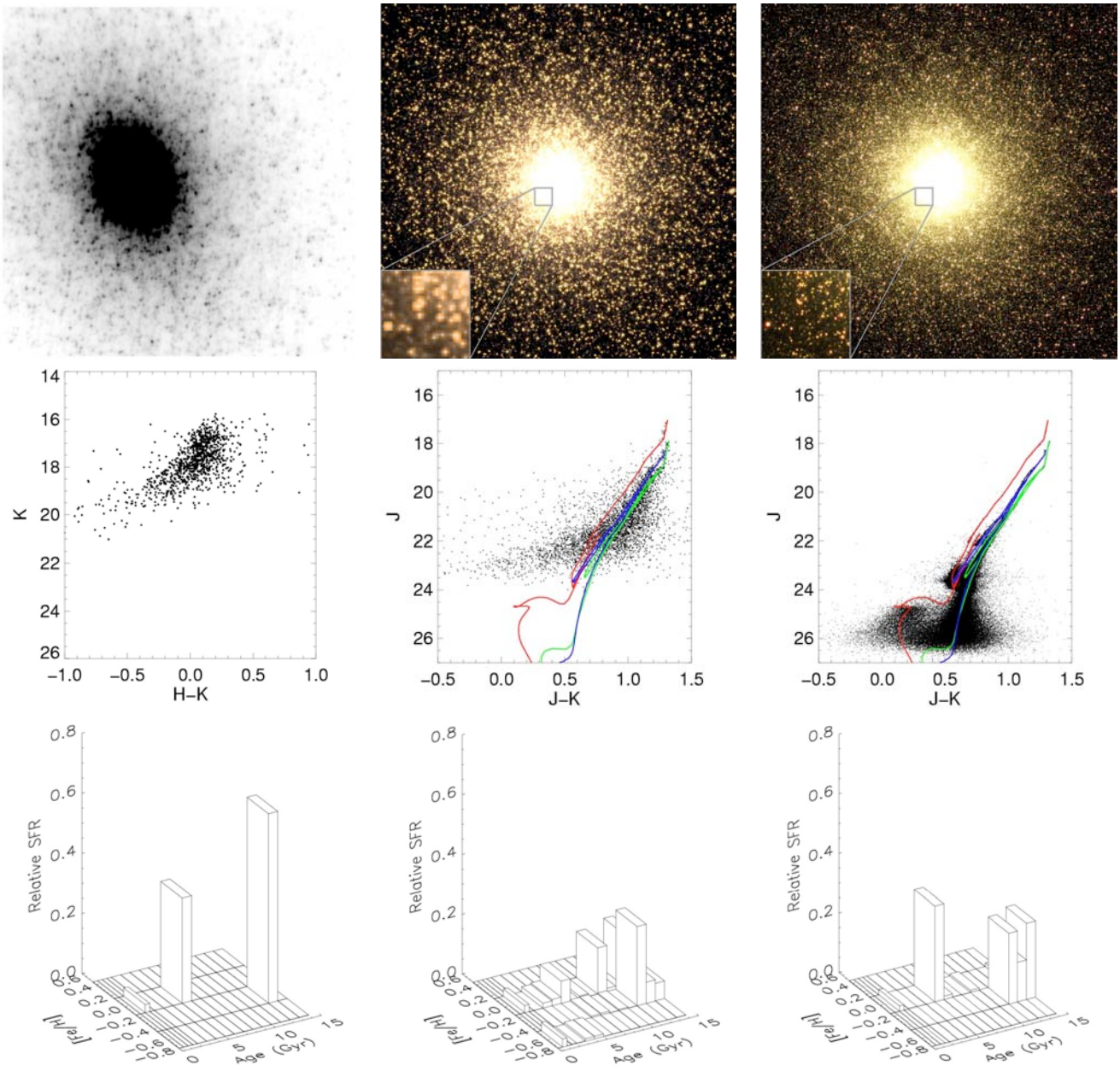

Figure 7-9 – Stellar populations at the center of M32. Top row, left to right: images of the central 30 arcsec of M32 as observed with Gemini N+Hokupa'a (Davidge et al. 2000) and as simulated for JWST and TMT. Middle row, left to right: color-magnitude diagrams of M32 corresponding to the images in the top row. Bottom row: The population box used to create the JWST and TMT simulations is shown at left, while the recovered JWST and TMT population mixes are shown in the middle and right panels.

References

Aloisi, A., van der Marel, R. P., Mack, J., Leitherer, C., Sirianni, M. & Tosi, M., 2005, ApJ, 631, L45
Asplund, Lambert, Nissen, Primas & Smith, 2007, ApJ, 644, 229
Bonifacio, P., et al., 2007, (in press)
Bromm, V., Kudritzki, R. P., & Loeb, A., 2001, ApJ, 552, 464
Bullock, J. & Johnston 2005, ApJ, 635, 931
Chieffi, N. & Limongi, M., 2004, ApJ, 608, 405
Cohen, J. G., Christlieb, N., McWilliam, A., Shectman, S., Thompson, I., Melendez, J., Wisotzki, L. & Reimers, D., 2007, ApJ, in press
Cowan, J. J., et al., 2006, ApJ, 627, 238
Frebel, A., Christlieb, N., Norris, J. E., Aoki, W. & Asplund, M., 2006, ApJ, 638, L17
Goswami, A. & Prantzos, N., 2000, A&A, 359, 191
Johnston, Bullock, et al. 2007, in preparation.
Korn, A., Grundahl, F., Richard, O., Barklem, P. S., Mashonkina, L., Collet, R., Piskunov, N. & Gustafsson, B., 2006, Nature, 442, 657
Lambert, D. L. & Allende Prieto, C., 2002, MNRAS, 335, 325
Melendez, J. & Cohen, J. G., 2007, ApJ, 659, L25
Melendez, J. & Ramirez, I., 2004, ApJ, 615, L33
Meynet, G., Maeder, A., Hirschi, R., Ekström, S. & Chiappini, C., 2007, *Nuclei in the Cosmos*, IX, see astro-ph/0609484
Navarro, J., Helmi, A., & Freeman, K. 2004, ApJ, 601, L43
Olsen, K., Blum, R., & Rigaut, F. 2003, AJ, 126, 452
Pauldrach, A. W. A. et al., 2001, A&A, 375, 161
Prantzos, N., 2007, in *Nuclei in the Cosmos IX*, Proceedings of Science
Przybilla, N., Butler, K., Becker, S. R. & Kudritzki, R. P., 2006, A&A, 445, 1099
Puls, J. et al., 2005, A&A, 435, 609
Salaris, M., Groenewegen, M. A. T. & Weiss, A., 2000, A&A, 355, 299
Skillman, E. D. & Kennicutt, R. C., 1993, ApJ, 411, 655
Skillman, E.D. 1989, ApJ, 347, 875
Steidel, C. C., Shapley, A. E., Pettini, M., Adelberger, K. L., Erb, D. K., Reddy, N. A. & Hunt, M. P., 2004, ApJ, 604, 534
Tominaga, N., Umeda, H. & Nomoto, K., 2007, ApJ, 660, 516
Urbaneja, M. A., Kudritzki, R. P. & Bresolin, F., 2007, in “Galaxies in the Local Volume”, eds. B. S. Koribalski & H. Jerjen
Venn, K. et al. 2001, ApJ, 547, 765
Venn, K. et al. 2003, AJ, 126, 1326
Venn, K. et al. 2004, AJ, 128, 1177
Wisotzki, L., Christlieb, N., Bade, N.,Beckmann, V., Köhler, T., Vanelle, C. & Reimers, D., 2000, A&A, 358, 77
Woosley, S. E., Heger, A. & Weaver, T. A., 2002, Reviews of Modern Physics, 74, 1015
Woosley, S. E. & Weaver, T. A., 1995, ApJS, 101, 181
Zahn, J. P., 1992, A&A, 265, 115

8 The formation of stars and planets

8.1 Overview

Although a general understanding exists of how stars and planets form, many details of this complex process are still elusive. What determines the masses of the stars or the frequency with which planetary systems form is unknown, and the properties of the planets cannot be predicted. Progress in this area requires new observational feedback as input to the development of a more sophisticated theoretical framework.

8.2 The physics of star formation

The spatial resolution and flux sensitivity of TMT will allow individual stars to be resolved, even in crowded fields, within a wide range of stellar environments in our own and nearby galaxies (see Figure 8-1). In the most nearby star formation regions within the Milky Way, mid-IR observations will unveil heavily obscured stars within the densest molecular clouds. These capabilities will open several new windows on one of the most critical astrophysical processes: the formation of stars.

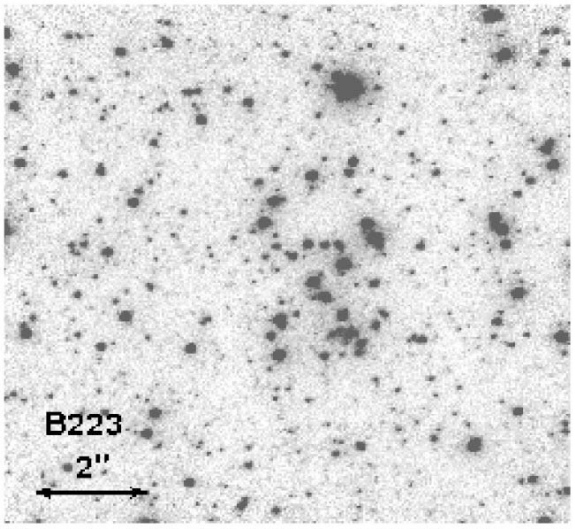

Figure 8-1. Image of a star field in M31 obtained using the Keck 10 meter telescope laser guide star AO system. The area shown is approximately 10 x 10 arcsec with a pixel scale of 10 mas/pixel and FWHM with a core of 60 – 80 mas. TMT will provide 3 times sharper images and 80 times the sensitivity. Hence, TMT will substantially lessen the effects of crowding in such fields, thus improving photometric accuracy and permitting spectroscopy of fainter stars. Image from Cohen, Matthews & Cameron (2005).

8.2.1 Initial mass function in young star clusters

Most stars are believed to form in rich clusters containing between 10^4 and 10^6 stars in volumes of 3 to 30 pc^3. The massive stars in these clusters are the primary source of heavy elements injected into the interstellar medium of their host systems and the nearby intergalactic medium (IGM). Understanding the form of the IMF in these clusters as a function of such physical parameters as metallicity and density is a fundamental step towards a more complete understanding of star formation across all look-back times in the Universe. In turn, a more complete understanding of star formation is fundamental towards understanding such critical issues as galaxy formation and evolution and the chemical enrichment history of the Universe.

Direct observations of rich, dense clusters in the local universe will enable determination of:

- the shape of the IMF over the entire range of masses, from ~100 M_O to well below 1 M_O;
- the time-averaged accretion rates characteristic of protostellar cores through direct observation of the 'stellar birthline' in very young clusters (Figure 8-2); and

- the relationship between emerging stellar masses and local stellar density within a given cluster, which is a potential measure of the importance of collisions between protostellar cores and mergers in forming high mass stars.

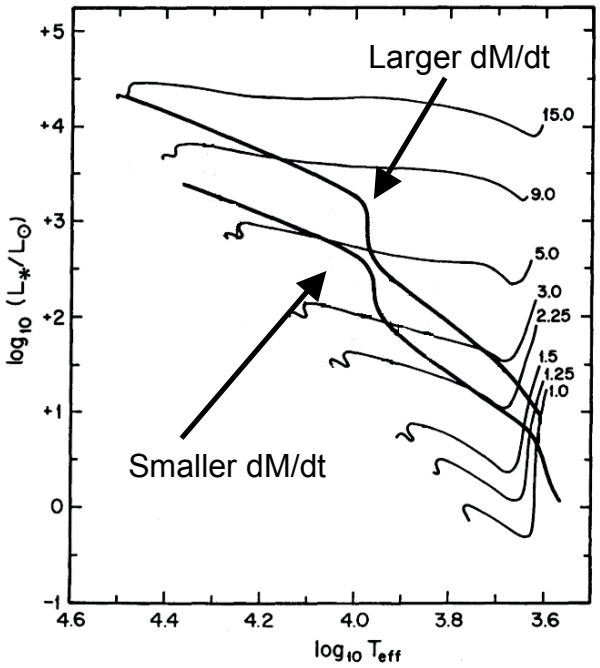

Figure 8-2. Hertzprung-Russell Diagram (HRD) for young star forming clusters. The heavy curves show birth lines corresponding to time-averaged mass accretion rates of 10^{-4} M_O yr^{-1} (upper) and 10^{-5} M_0 yr^{-1} (lower). The thin solid lines are the pre-main sequence evolutionary tracks, labeled in solar units, from Iben (1965). Adopted from Figure 11, Palla & Stahler (1990).

Table 8-1: Limiting K-magnitudes and the corresponding lower mass limits in Arches-like clusters

	Limiting K-magnitude			**Limiting Mass (M_O)**		
Radius (R_e)	**LMC**	**M33**	**M82**	**LMC**	**M33**	**M82**
0.5	>27.5	17	<19.8	~0.01	…	…
1.0	>27.5	18.9	<19.8	~0.01	65	…
2.0	>27.5	22.3	20	~0.01	3	…
5.0	>27.5	27.5	23.9	~0.01	1.1	32

Table notes: for illustrative purposes, photometric crowding and photon statistic limits have been computed for target environments in the LMC, M33, and M82 using the radial profiles of the Arches and R136 clusters, coupled with the crowding limit algorithm given by Olsen et al. (2003). The input luminosity function used for these calculations is a hybrid based on measurements in the Arches cluster (Blum et al. 2001) for the high-mass stars (≥2M_O) and measurements in the Trapezium by Hillenbrand & Carpenter (2000) for the low-mass stars (≤3 M_O). The Arches radial profile is a re-fit to HST data by Blum et al.

TMT will enable the study of the IMF over a range of metallicity, cluster density, and galactic environment as well as the location of the stellar birth line for the low mass stars still descending onto the main sequence. TMT will also enable the exploration of aspects of star formation that are difficult or impossible to investigate with current facilities. For example, what is the spatial distribution of the more massive stars relative to the lower mass stars? If massive stars preferentially form in the densest parts of clusters, this implies collisions or mergers could play a role in their formation. Do the most massive stars form in the

most dense clusters? TMT can provide the imaging and spectroscopic data (with, e.g. IRIS) needed to address these questions.

The limiting K-band magnitude as a function of location in an Arches-like cluster, and the corresponding lower mass limit that can be probed, are shown in Table 8-1. K-band magnitudes are for crowding limited photometry to 10% accuracy. Mass to K magnitude transformation is that given in Blum et al. (2001). At the TMT diffraction limit, only modest exposure times are required to reach the limiting magnitude imposed by crowding in M33 and M82. Because the LMC is closer than the other galaxies, crowding is less of a concern, and deeper photometric measurements can be obtained than in the more distant systems. The expected performance with the IRIS IFU is shown Figure 8-3. It is clear that within the Local Group it will be possible to obtain spectra of stars with masses much smaller than one solar mass.

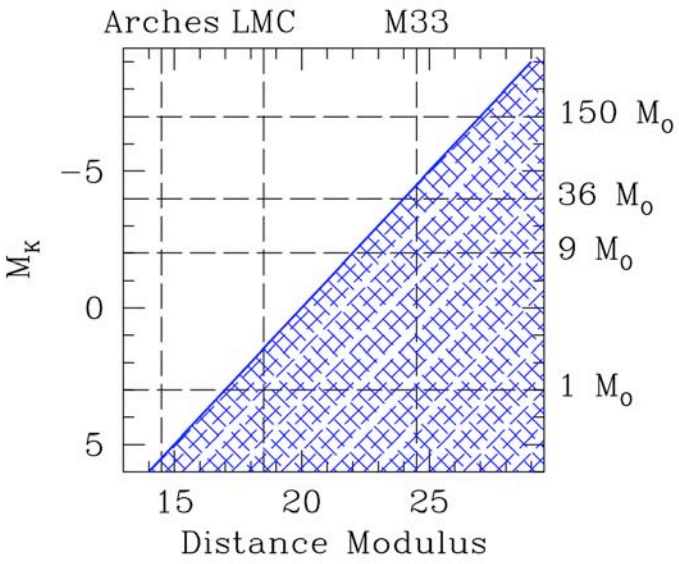

Figure 8-3. M_K limits for SNR = 50 at *R* = 4000 on IRIS in IFU mode during a 3 hour total exposure time. These numbers are valid for the uncrowded outer regions of clusters. At a given distance modulus, stars within the blue area are either not observable or only with lower SNR. For some embedded Milky Way clusters, the limiting M_K will be similar to the LMC owing to the competing effects of extinction vs. distance.

8.2.2 The structure and kinematics of infalling envelopes

In the most nearby clusters, it will be possible to study the physical properties for envelopes surrounding individual protostars. This is critical for understanding the most fundamental physical processes that drive the IMF. Individual stars are believed to form in optically opaque (A_V > 1000 mag) rotating molecular cloud cores of dimension ~0.1pc. To date, these protostellar cores have been studied primarily at mm- and sub-mm wavelengths, and largely in nearby (d < 500 pc) star-forming regions at spatial resolutions typically corresponding to 1000s of AU. Such observations provide a measure of the core mass and large-scale morphology, and kinematic information sufficient to diagnose the onset of gravitational collapse.

Current facilities lack the combination of angular resolution, sensitivity and wavelength coverage critical to enabling more quantitative study of the assembly process. Key questions that must be addressed include:

- How do star-disk systems evolve from protostellar cores?
- What determines the final mass of a star, initial conditions in the protostellar core or feedback from a forming star-disk-wind system?
- When and how are collimated outflows launched? How are their properties related to those of the forming star-disk system? What role do they play in determining the final mass of the star?
- When and how do binary/multiple stars form?

TMT/MIRES will have the sensitivity to allow *R* ~ 100,000 spectroscopic analysis of star-forming cores, and the ability to diagnose the structure and kinematics of infalling envelopes, along with the jets and winds launched from the inner regions of the forming star-disk system. High spectral resolution is required in order to match the velocity widths characteristic of (1) absorption features arising in infalling envelopes (widths ~1 – 3 km/sec); (2) emission features (widths ~10 km/sec) arising in shocks produced as envelope gas infalls supersonically onto the disk; fluxes in shock features (e.g. H_2) can in principle be linked to envelope mass accretion rates; and (3) emission features (widths 10 – 30 km/sec) arising in shocks at the boundary between collimated outflows and infalling material from the protostellar envelope. Such observations will complement lower spatial and spectral resolution observations by JWST. Key information about the composition and densities of the surrounding molecular clouds will come from ALMA.

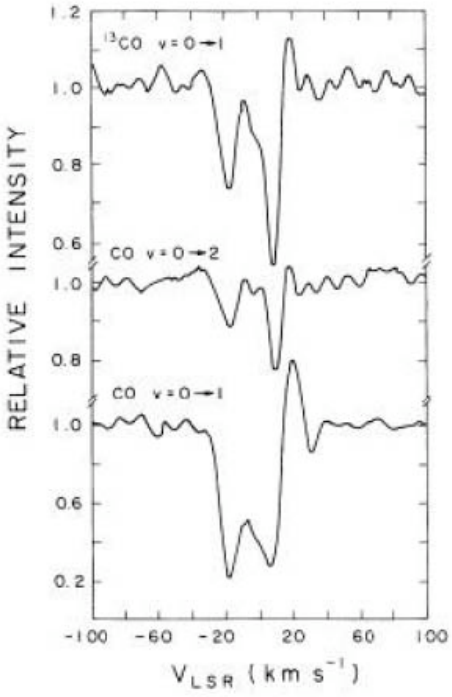

Figure 8-4. Profiles of CO fundamental band absorption features obtained by Scoville et al. (1983) from high spectral resolution (R ~ 50,000) observations of the Becklin-Neugebauer Object – a high mass protostar deeply embedded within an optically opaque core. Observations of several tens of these profiles enabled Scoville et al. to derive temperature, density and velocity structure in the protostellar core and to derive the first quantitative estimate of mass inflow rate from protostellar core to a forming star-disk system.

As an example, high resolution spectra using diagnostics such as molecular hydrogen, water, CO and both permitted and forbidden atomic transitions can be used to map temperature, density and velocity along the line of sight through the protostellar core to the spatially unresolved inner parts (r < 1 AU) of the star-disk system (which serves as the bright 'background' against which these features can be measured). An illustration of the potential of such measurements is provided (see Figure 8-4) by the pioneering study of Scoville, Kleinmann & Hall (1983) for the Becklin-Neugebauer source – a massive (M > 10 M_O) protostar located in the Orion star-forming complex. These authors used *R* ~ 50,000 spectra to obtain profiles for a large number of absorption lines arising in the CO fundamental band. In turn, these profiles mapped both the velocity field and density distribution along the line of sight to BN – leading to the only existing determination of mass inflow rate from a protostellar core to a star-disk system: a critical quantity for assessing the relationship between resulting stellar mass and protostellar conditions.

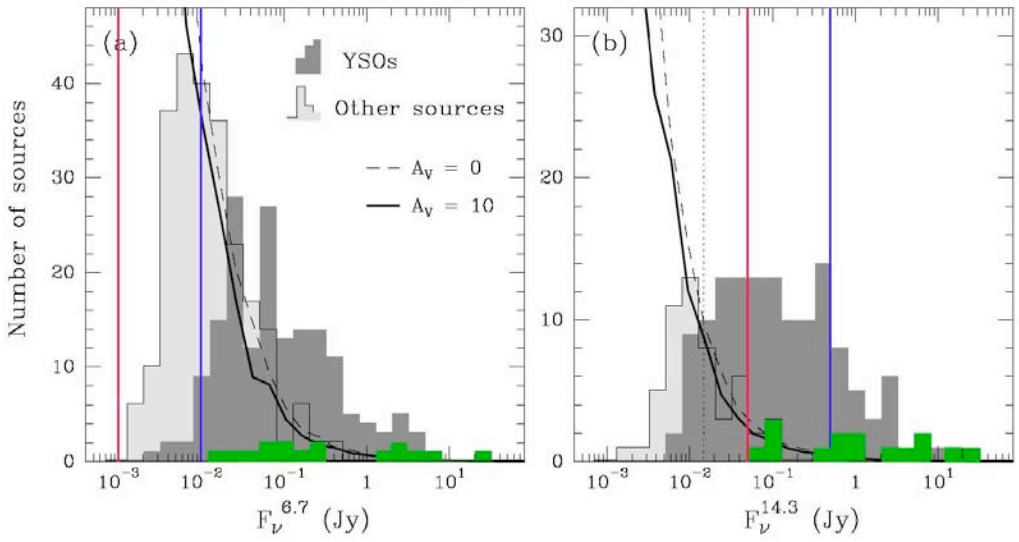

Figure 8-5. Histograms depicting the frequency distribution of source brightness for YSOs surrounded by accretion disks (dark grey) in the Ophiuchus molecular complex (Bontemps et al. 2001). At the earliest evolutionary phases, these cores are sufficiently opaque as to preclude detection of the forming star and its associated circumstellar accretion disk even at mid-infrared wavelengths. The presence of the star-disk system can be inferred from (a) measurement of dust-reprocessed mid- and far-IR emission from which the total luminosity of the forming star and its accretion disk can be inferred; and (b) the kinematic signatures of collimated molecular outflows thought to arise from a magnetically-driven wind originating at or near the boundary between the stellar magnetosphere and a circumstellar accretion disk. At later stages in stellar assembly, the optical depth of the envelope decreases, and emission from the star-disk-outflow system can be observed, first at mid-IR wavelengths, and later at shorter wavelengths.

Figure 8-5 provides an indication of the wide range of sources accessible to TMT. The green-shaded histogram depicts the distribution of observed fluxes among sources in the Ophiuchus molecular cloud complex that are still surrounded by optically-opaque (A_V > 50 mag) protostellar envelopes (so-called 'Class I sources'; see Figure 8-6) – the focus of a possible TMT study. The estimated bolometric luminosities of these sources ranges from 0.1 L_O to 30 L_O; associated forming stars are likely to have masses in the range 0.1 to 2 M_O. As above, the superposed red lines indicate the limiting flux for a 3 hour integration that yields SNR = 100 in the continuum at a resolution *R* = 100,000. The blue lines indicate similar limits for objects located at the distance of the Orion molecular complex. The figure shows that all 15 Class I sources in Ophiuchus are accessible to TMT, while at Orion; most of the sources spanning a similar range of properties would be accessible. Note that Orion will likely contain more than 30 times as many candidate sources; and including a significant number of more luminous Class I sources containing higher-mass forming stars.

Surveys with the Spitzer Space Telescope can be used to construct complete target lists of actively star-forming cores during early collapse phases both in Orion (d ~ 450 pc), and in more distant complexes (d ~ 2kpc) which are expected to harbor large samples of high and intermediate mass protostars (which with few exceptions are absent in more proximate star-forming regions). JWST will carry out targeted studies of core and outflow morphologies via mid-IR imaging, and derive rough estimates of core and jet properties via low-resolution spectroscopy. TMT will provide the sensitivity needed to enable quantitative analysis of a large number of star-forming cores surrounding objects of different mass. Several hundred cores surrounding stars ranging in mass from 0.1 to 3 M_O can be observed out to Orion distances. Cores

surrounding more luminous (and massive) protostars can be observed to distances of several kpc; the number of such targets is at present unknown, but estimated to be 30 – 300 for luminosities L > 1000 L_O. Analysis of cores spanning a range of masses will be crucial to establishing the differences between cores that form low and high mass stars, and to guiding development of a predictive theory of star formation.

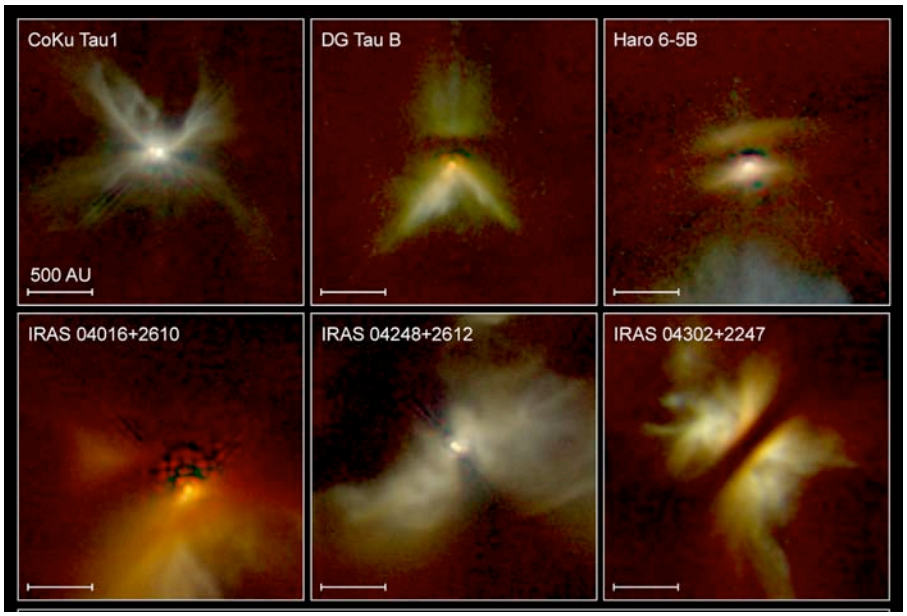

Figure 8-6. HST NICMOS images of solar-mass star-disk systems just emerging from their protostellar cores (so-called Class I objects). The protostellar core material is made visible via near-IR (2 micron) light scattered earthward by dust embedded in the inner regions of the infalling core. The disk is manifest in 'silhouette' against the bright scattered light arising from core material. In all cases, the central forming star is obscured from view by the optically opaque circumstellar disk material. The optical path from star to envelope is believed to be produced by a powerful collimated outflow emanating from the inner disk regions. The solid white lines indicate a scale of 500 AU. At the distance of Orion, TMT will be able to resolve structures of ~5 AU in size. Image credit: NASA/STScI.

TMT will also have the spatial resolution to probe the morphologies of protostellar cores as well as highly collimated jets launched from the inner disk, and broader neutral winds. At 10μm, TMT will be able to provide images of nearby (d ~ 150 pc) cores and jets at a resolution of 1.5 AU; at Orion, the equivalent resolution will be ~4.5 AU. This will enable study of:

- the detailed morphology of protostellar cores, and via comparison of thermal emission and scattered light with models, the temperature and density in the cores.
- the location and number of pre-stellar condensations, thus revealing the origin of stellar multiplicity: formation via instabilities in circumstellar disks or via fragmentation within star-forming cores;
- the morphology of winds and, via reprocessed radiation arising at the shock-heated interface between winds and surrounding molecular material, the mass outflow rate and wind energy input
- the structure of ionized jets, and from this structure, quantitative estimates of the number and cadence of high accretion rate episodes that take place during the stellar assembly phase.

8.3 Protoplanetary disks

Protoplanetary disks are flattened rotating disks of gas and dust surrounding newly formed stars. Planets form within these disks as dust particles collect and grow by accretion. As the planets gain mass they attract surrounding gas, clearing a ring in the protoplanetary disk. Interaction with the disk circularizes planetary orbits, stabilizing the planetary system.

The inner (r < 10 AU) regions of proto-planetary disks are particularly interesting since these are the regions where most planets may form. These regions also intersect the habitable zone of their parent stars. Understanding the chemical composition of these regions as well as the gas viscosity is key to answering the question of why some planetary systems contain hot Jovian planets close to their parent star while at least one (the Solar System) has rocky planets in the same region.

Such inner disks are typically too distant to be spatially resolved by TMT. However, the Keplerian rotation of disks can be used to separate disk regions in velocity (and hence radius) and derive the radial variation of line intensity by fitting resolved line profiles. Making such separations in velocity demands high-resolution spectroscopy. Given the expected temperatures of these disks, atomic and molecular lines of interest will lie between 1 and 25 μm. Since these spectral features will have different sensitivities to density, temperature, and abundance, those quantities can be mapped out along the entire inner disk. Of particular interest to astrobiology are organic molecules, the building blocks for pre-biotic molecules such as amino acids, nucleobases, and sugar-related compounds, which have transitions in this wavelength regime.

High-resolution spectroscopy also provides data on two key parameters: gas dissipation time scale (and how it relates to dust dissipation time scale measured by, e.g. Spitzer) and gas viscosity. Knowledge of both parameters is important to understanding how and when protoplanet and planet orbits are circularized – a key issue in planet formation theory. Yet, both parameters are currently poorly constrained by observation.

Combined with the collecting area of a 30-m telescope, NIRES and MIRES provide the spectral resolution and wavelength coverage necessary to survey proto-planetary disks in the nearest star formation regions to order to address fundamental questions about planetary formation. They provide complementary capabilities to JWST (depending on line-to-continuum contrast, MIRES will be more sensitive than JWST) and ALMA (MIRES and NIRES probe to smaller disk radii and hence warmer gas than ALMA).

8.3.1 Probing gas dissipation timescales

The timescale for dissipation of gas in circumstellar disks governs the viability of plausible giant planet formation mechanisms and consequently, the range of plausible giant and terrestrial planet architectures. Moreover, the persistence of gas in the terrestrial planet region of the disk also affects the masses, eccentricities and consequently the habitability of terrestrial planets.

At present, there appear to be two viable paths for the formation of giant planets: (1) rapid formation (t < 1 Myr) via gravitational instabilities in a massive circumstellar accretion disk; and (2) relatively slow formation (t ~ 10 Myr) via the buildup of a rocky core having a mass of several earth masses, followed by accretion of gas left over following completion of the main disk accretion phase. Understanding the basic underlying physics of giant planet formation and discriminating between these two possible formation mechanisms is central to learning whether systems like our solar system are common in the Galaxy.

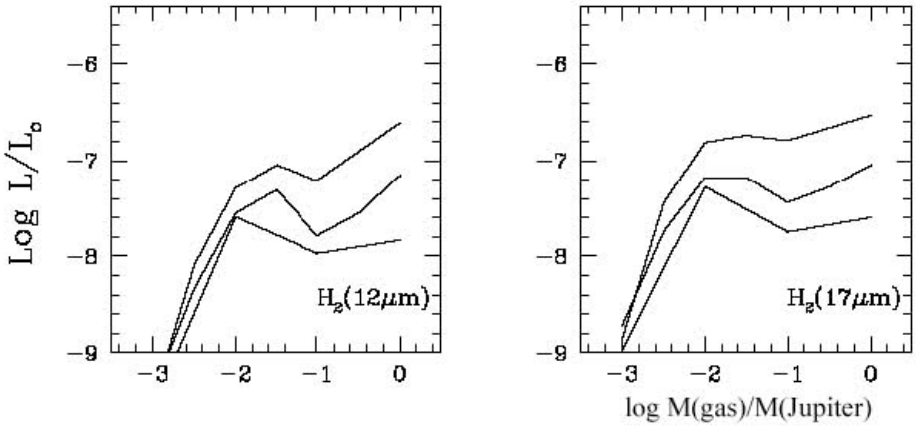

Figure 8-7. Predicted line luminosities (solar units) for potential tracers of gas mass. To determine gas survival timescales requires sensitive measurements of the gas content of disks surrounding stars spanning the relevant timescales. The required sample includes post-accretion phase solar-like stars located (a) in dense star-forming regions (e.g. Orion), where environmental conditions (UV radiation field and stellar density) may best reproduce those in which stars in the Milky Way disk formed; (b) in regions where star-formation is more isolated (and disk lifetimes could be longer) such as Ophiuchus or Taurus; (c) in older associations and clusters (e.g. Sco-Cen; η Cha; NGC 2391; NGC 2602); and (d) in the field, with approximate stellar ages inferred from measures of activity (e.g. Hα; Ca II emission, x-rays) and rotation. Sample sizes of thousands of objects are needed to span the range of ages, environments and outcome diversities expected. The nature of the target list demands the ability to measure disk gas content for stars as distant as 450 pc (Orion). Figure credit: MIRES study team

Central to addressing this problem is constraining the timescale over which significant amounts of gas survive following the accretion phase. If the timescale for gas survival is short (t << 10 Myr) at distances beyond several AU in most systems, gas giant formation via accretion onto a rocky core is unlikely. Moreover, if the residual gas in the terrestrial zone is << 10^{-3} that of a minimum mass solar nebula, it becomes difficult to understand how the Earth and its sister planets in the inner solar system ended up in low-eccentricity orbits.

TMT/MIRES will have the flux sensitivity and spatial resolution needed to constrain this timescale across a wide variety of environments using both molecular (e.g. H_2) and atomic tracers. Figure 8-7 depicts the line luminosities as a function of disk gas mass for two tracers, H_2 S(2) 12.4 μm and H_2 S(1) 17.0 μm, predicted from recent thermochemical models produced by Gorti & Hollenbach (2004).

In Table 8-2, predicted luminosities for these tracers are listed for a range of disk gas masses. Note that 10^{-7} L_O = 1.4 x 10^{-17} ergs cm^{-2} sec^{-1}. In Table 8-3, estimates are shown for limiting distance to which disks of a given mass can be detected using each of these tracers. These correspond to a limiting flux, estimated by assuming *R* = 100,000 spectra, SNR =10 for robust detection and an integration time of 10^4 sec. These estimated limiting distances encompass a large enough range of nearby star formation regions that at least 1000 targets in the mass range 0.3 to 1.5 M_O will be observable in the magnitude range K = 3 to 13 (V = 5 to 15).

Of course, observatory altitude above sea-level (and hence temperature and preciptitable water vapor) will play a role in the productivity of such mid-IR observations. Using monochromatic sensitivity calculations provided by J. Graham (UCB, private communication), estimated exposure times were calculated to achieve a 'typical' line flux sensitivity of ~2 x 10^{-17} erg/s/cm^2, 10σ for the H_2 0-0 S(1) 17.035 μm and 0-0 S(2) 12.278 μm lines assuming a spectral resolution of 100,000. The exposure times were calculated for a grid of site conditions including five elevations from 8000 to 16,000 ft (2440 – 4880 m)

and six values of the water vapor burden (0.25 – 8 mm). The atmospheric temperature was assumed to follow the international standard atmosphere (15 C at sea level and a mean lapse rate of 6.5 C per km). The ground ambient temperature was assumed to be 10 K warmer than the free atmosphere. The results are summarized in Figure 8-8. As these (and similar) simulations suggest, locating TMT on a site where PWV < 1 mm occurs at least 10% of the time is highly desirable.

Table 8-2: Predicted feature strength vs. gas mass for selected gas diagnostics

Feature	Wavelength (μm)	$M_{gas} = 10^{-3}\ M_O$	$M_{gas} = 10^{-4}\ M_O$	$M_{gas} = 10^{-5}\ M_O$
H_2 S(2)	12.4	$5.3 \times 10^{-8}\ L_O$	$1.8 \times 10^{-8}\ L_O$	$2.7 \times 10^{-8}\ L_O$
H_2 S(1)	17.0	$7.2 \times 10^{-8}\ L_O$	$4.2 \times 10^{-8}\ L_O$	$6.1 \times 10^{-8}\ L_O$

Table 8-3: Limiting distances for detecting emission for disks with a given mass

Feature	Limiting Flux ergs cm^{-2} sec^{-1}	$M_{gas} = 10^{-3}\ M_O$	$M_{gas} = 10^{-4}\ M_O$	$M_{gas} = 10^{-5}\ M_O$
H_2 S(2)	0.3×10^{-17}	790 pc	460 pc	560 pc
H_2 S(1)	1.0×10^{-17}	500 pc	390 pc	460 pc

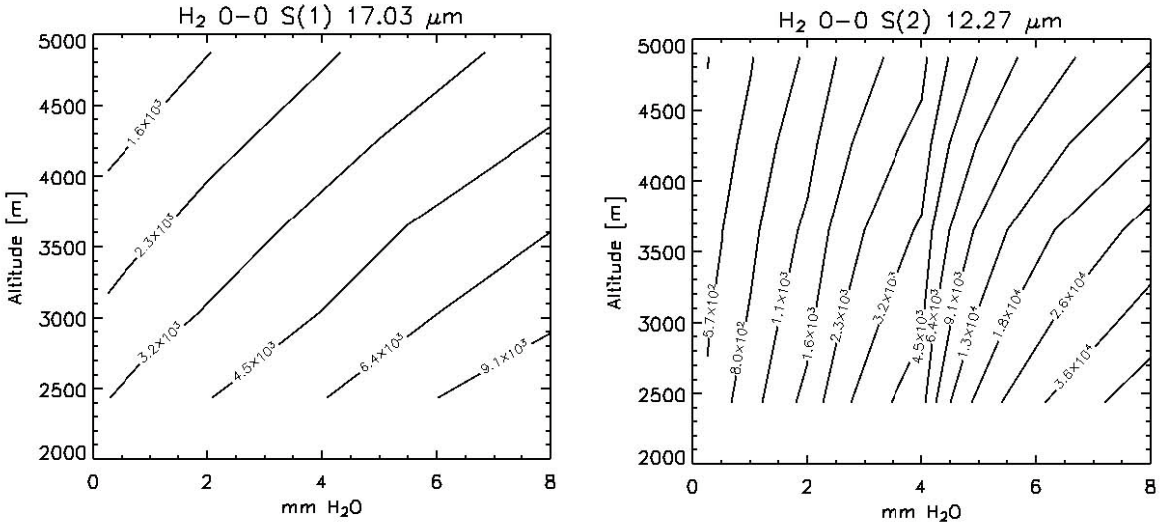

Figure 8-8. Contours of exposure time in seconds for achieving line flux sensitivity of 2×10^{-17} erg/s/cm^2 (10σ) for elevations between 2440 - 4880 m. Contours give the exposure time per target for a typical T Tauri star in Orion for each of the three gas mass diagnostics discussed above. The contour intervals are at $\sqrt{2}$ for H_2. The telescope temperature runs from 9 C at 2440 m to -6.6 C at 4880 m. The dependence exhibits different behavior depending on the strength of the adjacent atmospheric absorption lines. For the S(2) lines, the principal factor determining the exposure time is water vapor. Both elevation/temperature and water vapor factor into the exposure time for the S(1) line. Credit: MIRES study team.

8.3.2 Probing protoplanetary disk gaps

As noted above, extrasolar giant planets (EGPs) may form rapidly, as a result of instabilities that arise in massive (~ 0.1 M_O) accretion disks surrounding young stellar objects. Forming EGPs should produce tidal 'gaps' in the accretion disk. Optically thin emitting gas in these gaps can be used to diagnose the presence of forming protoplanets and quantify their orbital distances and masses. Making such measurements can provide insight into the formation mechanism for EGPs, and via comparison with the architectures of mature planetary systems, their dynamical evolution.

Determining the Keplerian velocity of emitting gas within the gap provides a measure of the EGP semi-major axis, while the mass of the EGP can in principle be assessed from the gap width as inferred from the shape of the emission line arising from the gas diagnostic. The targets are young stellar objects still surrounded by circumstellar accretion disks – diagnosed via their infrared spectral energy distributions (large excess emission from dust embedded within the disk) and from optical photometry (UV excess) and spectroscopy (line profiles indicative of accretion along magnetospheric columns). A variety of gas diagnostics sensitive to emission arising at different temperatures (300 K at 1 AU; 150 K at 5 AU) will be used; they include CO fundamental (4.6μm), H_2 (12μm; 17μm).

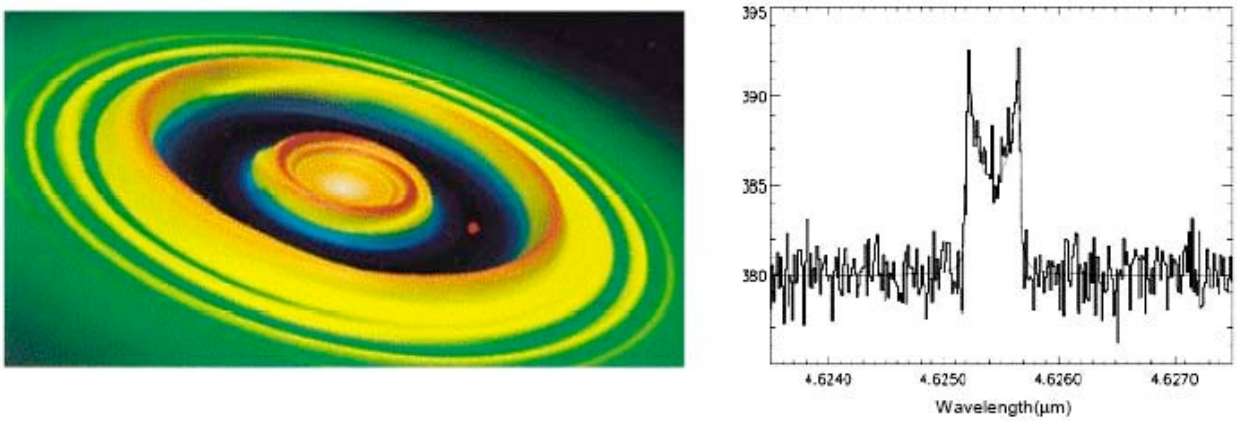

Figure 8-9. A simulation (left) depicting the dynamical effects of a newly-formed gas giant planet (the red dot embedded within a dark elliptical ring) on a disk of circumstellar gas and dust surrounding a young star. The gravitational effect of the planet on surrounding disk material opens up a gap, or ring, within which the amount of residual gas and dust is miniscule compared to the regions inward and outward of the gap. The residual gas produces a spectral signature (right panel, a simulated profile produced by a Jupiter mass planet orbiting a solar mass star at a distance of 1 AU), in this case a double-horned profile manifest in emission from carbon monoxide. The wavelength separation of the horns diagnoses the distance of the planet from its parent sun, while the width of each horn measures the width of the gap, which in turn reveals the mass of the planet. The simulated spectrum is representative of the expected performance of an *R* =100,000 mid-IR spectrograph on TMT for an 8-hour exposure. Courtesy G. Bryden, CIT (left) and J. Najita, NOAO (right).

The number of candidate targets accessible at TMT sensitivity can be assessed from Figure 8-5, which depicts the frequency distributions of 6.7μm and 14.8μm flux values measured by ISO for a sample of young stellar objects with masses from 0.1 to 3 M_O, surrounded by accretion disks, and located in the nearby Ophiuchus molecular cloud complex (dark grey-shaded histograms). Superposed on these histograms are the detection limits estimated for TMT at wavelengths corresponding to the CO fundamental band (4.6 μm) and the H_2 S(2) line (12) for (1) resolution *R* = 100,000; (2) SNR = 100 in the continuum (enabling robust detection of lines 5% above the continuum), and (3) integration time of 3 hours. In short, more than 100 sources in the Ophiuchus complex would be available for high resolution,

high SNR spectroscopic study with TMT. Comparable numbers would be available in other complexes (Taurus; Chamaeleon; Lupus) located at similar distances.

8.3.3 Pre-biotic molecules in disks

A large number of extra-terrestrial organic and pre-biotic molecules are known to exist both in the Solar system and the interstellar medium, and a better understanding of the inventory and formation of these molecules in star-forming molecular clouds and circumstellar disks is a key goal of astrobiology. The extent to which interstellar organic material is destroyed or modified as it is accreted into and processed within protoplanetary disks is an open question. While the similar compositions of cometary volatiles and interstellar molecules strongly suggest a direct connection, numerous differences indicate processing within the presolar nebula. In addition, complex organic compounds could be synthesized in regions of protoplanetary disks by the similar processes that operate in the interstellar medium.

Determining whether pre-biotic compounds can have an extra-terrestrial origin will require two parallel investigations. One is to measure the presence and quantity of pre-biotic material. In the Solar system, this is currently reflected in the inventory of organics found in comets and meteorites. An essential complement to these 'in situ' measurements will be a directed search for pre-biotic molecules and their precursors in planet-forming circumstellar disks surrounding young stellar objects. Together, such studies will provide the insight critical to determining whether the ingredients necessary for the origin of life are commonly available within forming planetary systems.

To determine whether such pre-biotic molecules can successfully be delivered to Earth via bombardment by minor bodies, and if so, at what rate, represents the next stage in learning whether the ingredients for life on Earth are delivered from external sources. Both Solar system studies and theory provide major clues, but a more general answer to this question depends on deepening our understanding of the range of planetary architectures and the resultant dynamical history of the system. A combined understanding of (1) whether and in what quantity pre-biotic molecules are produced in molecular clouds and circumstellar disks, and (2) how and in what quantity such molecules are transported to exo-Earths, would allow one to predict the importance of the delivery of pre-biotic compounds on the origin of life.

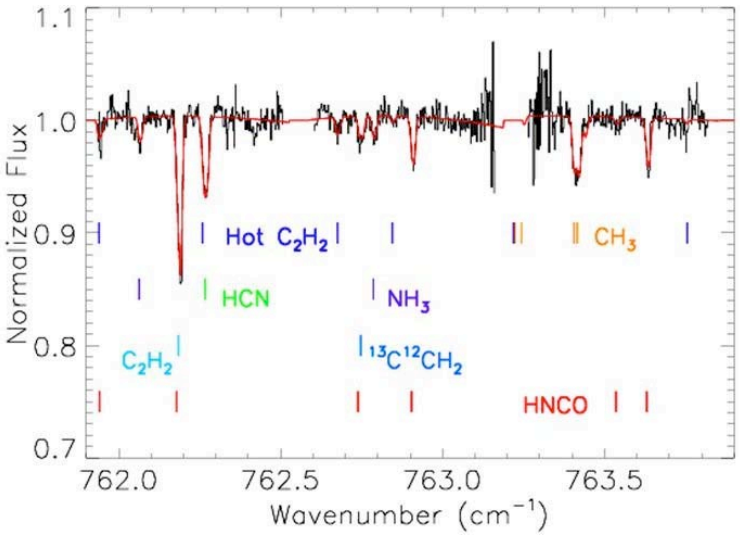

Figure 8-10. Pre-biotic molecules. Mid-infrared spectrum of the massive protostar NGC 7538 IRS 1 with the IRTF telescope showing absorption lines of organic molecules. (Knez et al. 2005)

Mid-infrared spectroscopy with MIRES will be an essential tool for investigating the inventory and content of organic molecules in protoplanetary disks. Most simple and complex hydrocarbon compounds have strong mid-infrared transitions and a majority of these are accessible to ground-based observations. High-spectral resolution is essential, particularly in searching for more rare molecular species. A given spectral

region may be crowded with molecular lines, and lines of more complex molecules will be weak due to lower abundances and the typically larger number of transitions. Thus, the very high signal-to-noise observations obtainable only with TMT are required. Broad wavelength coverage, providing access to large numbers of transitions, will also increase the detectability of rare molecules.

References

Bontemps, S. et al. 2001, A&A, 372, 173
Blum, R.D. et al. 2001, AJ, 122, 1875
Cohen, J., Matthews, K., and Cameron, P.B. 2005, ApJ, 634, L45
Gorti, U. & Hollenbach, D. 2004, ApJ, 613, 424
Hillenbrand, L.A. & Carpenter, J.M. 2000, ApJ, 540, 236
Iben, I. 1965, ApJ, 141, 993
Knez, C. et al. 2005, ApJ, 635, 145
Olsen, K.A.G., Blum, R.D. & Rigaut, F. 2003, AJ, 126, 452
Palla, F. & Stahler, S.W. 1990, ApJ, 360, 47
Scoville, Kleinmann & Hall 1983, ApJ, 275, 201

9 Exoplanets

We now know of more than 200 planetary systems beyond the solar system. The great majority of these have been found by detecting the small periodic motion of the host star due to the gravitational perturbation of its planets. Since the perturbation is proportional to planetary mass, most of the planets that have so far been detected are massive gas-giants like Jupiter.

9.1 Doppler detection of planetary systems

TMT with HROS will expand the number of host stars accessible to Doppler spectroscopy by a factor of 30 by allowing a greater volume of space to be explored. In addition, the higher sensitivity will allow lower-mass stars, such as M stars – the most common stars in the galaxy, to be observed. These stars are more strongly affected by gravitational perturbations so lower-mass planets can be detected. In fact, TMT will be able to detect Earth-mass planets orbiting in the habitable zone of M stars (the habitable zone is the region surrounding the star where a planet would have a temperature conducive to the formation of life).

Almost all known exoplanets were discovered indirectly by measuring the reflex motions of their parent stars using radial velocity (RV) measurements. Most of these planets are Jovians orbiting G and K dwarf stars where the planet/star mass ratio was large enough to produce measurable reflex motions.

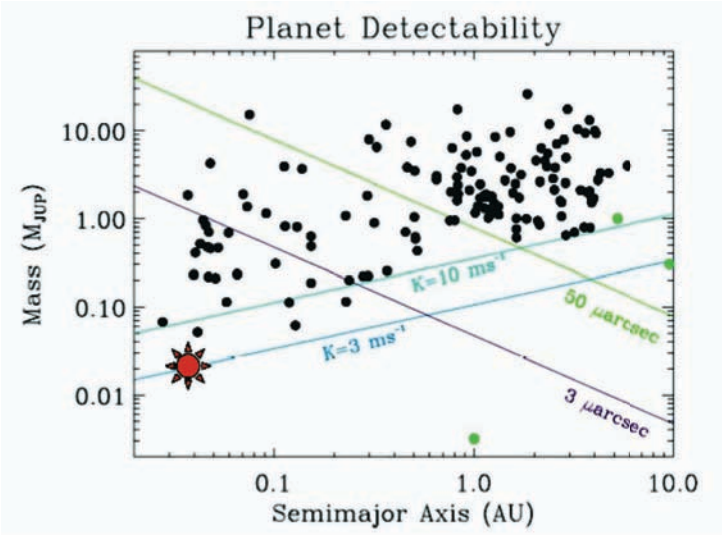

Figure 9-1. Masses of known exoplanets. Masses of known exoplanets plotted vs. the semi-major axis of their orbits. The lines show detection limits for Doppler and astrometric surveys as a function of velocity and astrometric semi-amplitudes. For required measurement precision, divide by 3. The red star is the 7.5 Earth-mass planet around dM4 star GJ 876 at 4.7 pc (Rivera et al. 2005). (Figure credit: Butler, California-Carnegie Planet Finder Team)

Over the next 15 years, a major goal will be to extend these RV surveys to M and L dwarf stars for several reasons. First, many more M and L stars exist than G and K stars – it is likely that the majority of planets in the local solar neighborhood revolve around such stars. Second, since M and L stars have lower mass, rocky, Earth-like planets can produce measurable reflex motions. Third, planets revolving in M and L dwarf habitable zones will have periods of 30 – 100 days or less, making it straightforward to characterize such orbits in less than a year.

Detecting rocky, Earth-like planets in the habitable zones of cool dwarf stars requires radial velocity measurements with 1 m/s precision (see Figure 9-1). The California-Carnegie Planet Finder team (PIs: Butler, Fisher, Marcy, Vogt) has demonstrated that such precision is possible on Keck/HIRES using an

iodine cell near 0.5 μm. However, to reach interesting apparent flux limits for M stars would require 1 – 3 hours per RV measurement with Keck, severely constraining the number of stars that can be surveyed. Given the diversity of planetary systems discovered so far, it is clearly necessary to survey tens or hundreds of stars, not just a handful, to truly characterize the potential population of nearby rocky planets.

The intrinsically more efficient HROS design coupled with the 10-fold increase in TMT collecting area relative to Keck will enable the required RV precision at V = 11, 12, and 13 in approximately 1.5, 3.5, and 8.5 minutes, respectively. These shorter exposure times allow for the characterization of an entire orbital period (30 – 100 days) for tens to hundreds of candidate planets around early M dwarf stars in one year. Only the vagaries of time allocation limit the potential sample size.

It will be difficult for TMT/HROS to survey dwarf stars cooler than M5 – few if any such stars are close enough to Earth to produce the apparent flux at 0.5 μm needed for TMT/HROS studies. Beyond 1 μm, however, such stars are bright enough for RV surveys with TMT/NIRES. Although the required 1 m/s precision has not yet been demonstrated at near-IR wavelengths, the Gemini Observatory is currently developing the near-IR Precision Radial Velocity Spectrometer (PRVS) to blaze this trail. TMT/NIRES will build on PRVS lessons learned about precision near-IR RV measurements. The larger TMT aperture will enable reaching stars 2 mag fainter than PRVS. Based on available catalogs, it can be shown that ~ 400 late M and early dwarf stars could be surveyed with NIRES over five years using 40 nights per year. As with HROS, the sample size is not limited by available stars but by available telescope time.

Of course, RV survey results alone contain ambiguities about inclination angles and hence planetary masses. It may be possible to remove such ambiguity in systems with multiple stars using high spatial resolution, precision astrometric observations with TMT/IRIS (see, e.g. Neuhäuser et al. 2006).

Transit surveys like Kepler and Corot have a different challenge. They may detect dozens to hundreds of nearby rocky planet candidates with known inclinations. But follow up RV measurements will be necessary to constrain the masses of these candidates and separate “false positive” icy planets on long orbits from rocky planets on short orbits. At V = 14, TMT/HROS can reach 1 m/s in less than 30 minutes per point. Hence, HROS (and perhaps NIRES) will be ideal instruments for Kepler and Corot follow up investigations.

9.2 Direct detection and characterization of exoplanets

It is now possible, using adaptive optics, to directly image giant planets. New instruments being built for 8 meter telescopes will be able to study young planets that are still glowing from internal heat produced by their formation. The higher resolution provided by TMT/PFI will extend the reach of these observations to the nearest star-forming regions, making it possible to relate the properties of the planetary systems to the environment, and to observe directly large planets forming within circumstellar disks. TMT will also be able to detect planets that are close to their host star, probing for the first time scales that are comparable to the size of the inner Solar System. Since planets in this region intercept and reflect more light from the host star, it will be possible to image even cold Jovian planets directly by reflected starlight and study the atmospheric composition of these planets.

In general, RV surveys are tuned to a specific range of parent star mass, planetary mass, star-planet separation, and stellar activity. For example, RV surveys are insensitive to planets around young stars (too much stellar activity) and Jovian planets beyond 5 AU (reflex motion too small and orbital periods too long). Via direct imaging, TMT will be able to explore a regime not addressed by RV surveys.

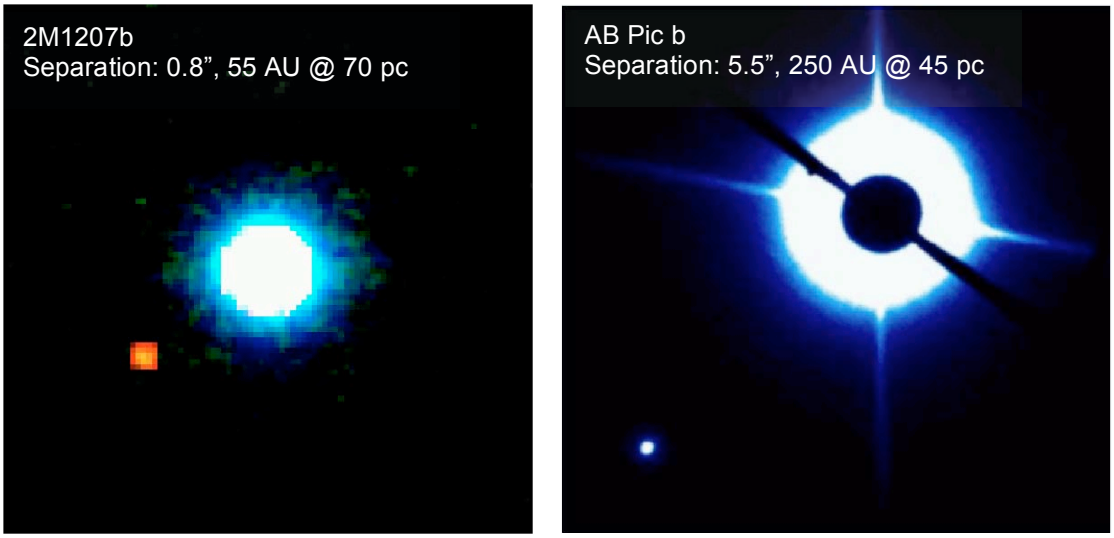

Figure 9-2. Two giant planets imaged with adaptive optics. The red object on the left is a planet with four times the mass of Jupiter, orbiting a brown dwarf (Chauvin et al. 2004). On the right is an 80-Jupiter-mass planet orbiting a solar-type star (The black disk is an artifact of the observing technique) (Chauvin et al. 2005)

T**able 9-1**: TMT angular resolution and equivalent spatial resolutions

		Physical Separation (AU)			
λ (μm)	**5 λ/D (arcsec)**	**150 pc**	**50 pc**	**10 pc**	**5 pc**
1.20	0.04	6.2	2.1	0.4	0.2
1.65	0.06	8.5	2.8	0.6	0.3
2.20	0.08	11.3	3.8	0.8	0.4
3.50	0.12	18.0	6.0	1.2	0.6

Table 9-1 shows TMT angular resolution at various wavelengths and corresponding physical resolutions at various distances. Recall that the Taurus-Auriga star formation region and the TW Hya association are 150 and 60 pc distant, respectively. Equivalent (or better) angular resolution is possible using interferometric techniques but the larger TMT collecting area enables either equivalent signal-to-noise ratios (SNR) at fainter flux limits or larger SNR at equivalent flux limit.

Using a combination of coronographic imaging and precision astrometry, TMT/IRIS can explore the moderate-contrast (10^3 – 10^5) wide-separation (> 50 AU) regime that may be occupied by young (< 1 Gyr), self-luminous Jovian planets. If such planets are detected, moderate-resolution spectroscopic follow up will also be possible with IRIS. Recent reports (e.g. Neuhäuser et al. 2005; Chauvin et al. 2005) about planets detected in this regime remain controversial.

To study more evolved planets closer to their parent stars, higher contrast imaging is necessary. TMT/PFI is designed to enable 3 λ/D spatial resolution, high-contrast (10^8) imaging with low spectral resolution (R ~ 70) follow up at 1.65 μm (see Figure 9-3). A moderate-resolution spectroscopic mode (R ~ 700) will also be available. This will allow systematic surveys in the mass range $0.5 < M_J < 12$ over 0.5 – 50 AU out to

100 pc or more. If present, both self-luminous young Jovians at large separations and cool, reflecting Jovians at smaller separations should be observable.

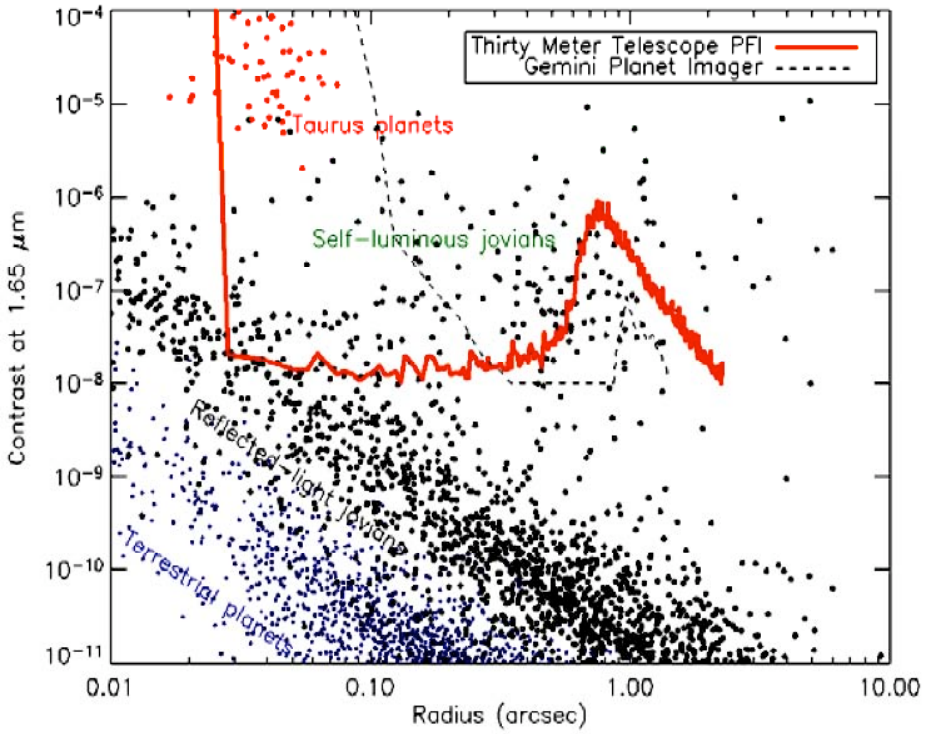

Figure 9-3. High-contrast imaging of exoplanets. The ratio of brightness between the planet and the host star is plotted as a function of the angular separation between the planet and star for a large number of hypothetical planets. The detection limit of TMT/PFI is shown by the red curve. TMT will be able to detect directly giant planets forming in star forming regions such as Taurus, and older planets orbiting close to their host stars. (TMT PFI team).

9.3 Planetary atmospheres

The light received from distant planetary systems is a combination of light from the planets and that from the host star. At optical wavelengths, the star is typically about a billion time brighter than the planets, so the light from the planets cannot be distinguished. However, at mid-infrared wavelengths, the brightness contrast between a planet and its host star is much smaller, making it possible to distinguish spectral features in the radiation emitted by the planet, superimposed up on the spectrum of the star. These features have a small wavelength shift due to the motion of the planet around the star, which makes it possible to separate them from features produced by the star itself by a process of spectral deconvolution.

For planets that pass in front of their host star, as seen from the Earth, another technique is possible. During the transit, a small portion of the light emitted by the star passes through the atmosphere of the planet. As a result, absorption features due to molecules in the planetary atmosphere are superimposed on the spectrum of the star. These features are extremely weak since only a very small portion of the light is affected by the atmosphere. However, they can be detected with a thirty-meter telescope and high-resolution spectrometer. Simulations indicate that it should be possible to detect oxygen in the atmosphere of an Earth-like planet orbiting in the habitable zone of an M star, in about three hours with TMT/HROS. Detection of oxygen would be highly significant since it is indicative of photosynthesis, and thus the presence of life.

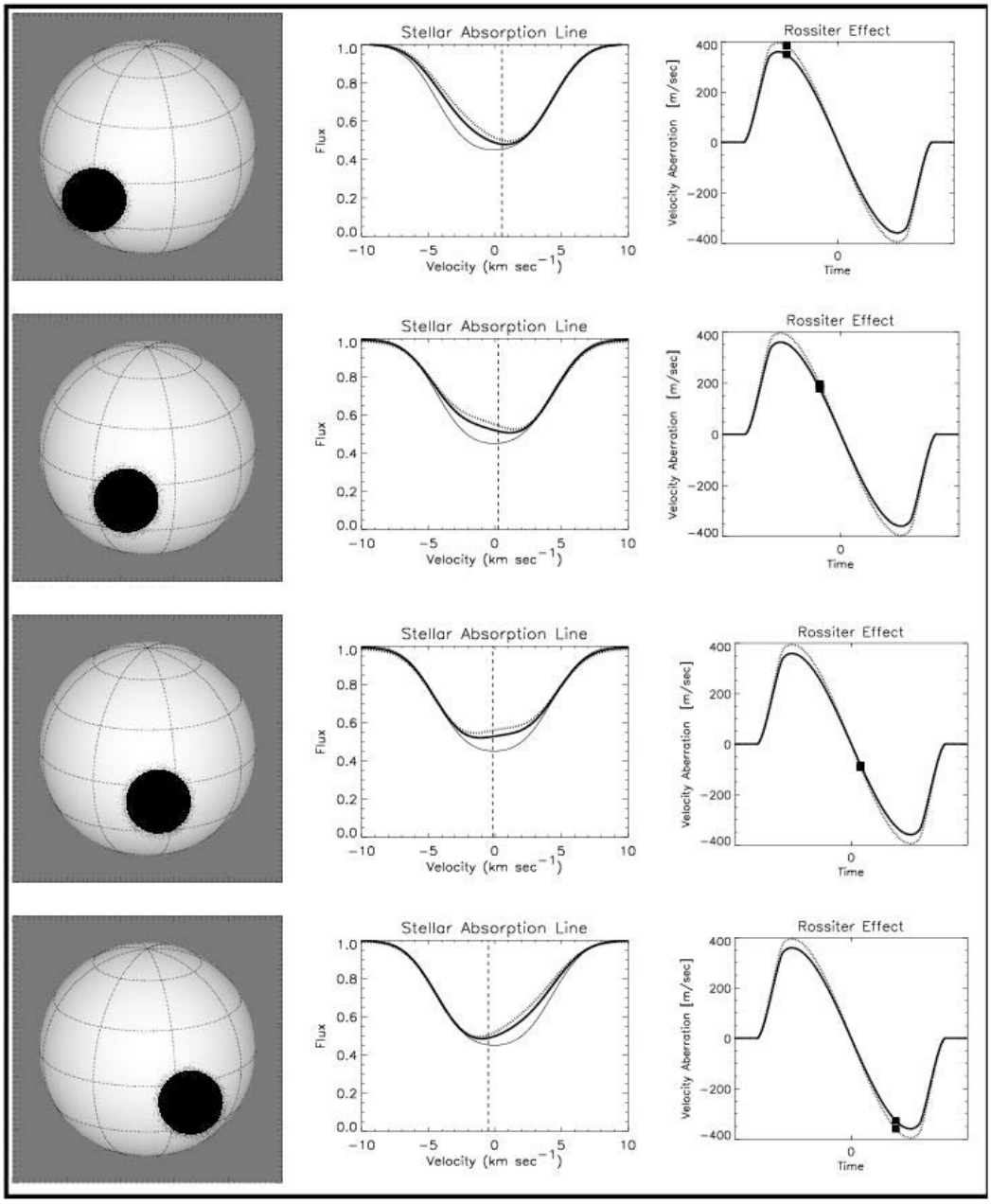

Figure 9-4: Rossiter-McLaughlin effect. As a dark object transits a rotating star, it subsequently blocks the approaching and receding parts of the stellar surface, causing a change in the profile of the rotationally broadened stellar absorption line. This results in an effective red and blue shifting of the line. The perturbed and unperturbed absorption line profiles are shown in the middle panels by the thick and thin solid lines respectively. The resulting RM effect is shown in the panels to the right. The effect of extra absorption caused by a possible atmosphere is indicated by the dotted lines. In fast- rotating M dwarfs, the transit of a Jupiter-size planet will produce a RM effect with an amplitude of 1–2 km s^{-1}. (Figure from Snellen, 2005).

As pointed out above, TMT/PFI will allow direct spectroscopic observations of Jovian atmospheres. However, planetary transits enable a different approach: transmission spectroscopy – the comparison of high SNR, high-resolution spectra taken before and during a transit to seek spectra changes related to the atmosphere of the transiting planet. Although the success of this approach has been demonstrated using HST observations (e.g. Charbonneau et al. 2002; Vidal-Madjar et al. 2003, 2004), ground-based attempts have been less successful, mostly due to instrument and weather instabilities between the necessary in-transit and off-transit observations. Recently, Snellen (2004; see also Snellen, 2005) has demonstrated that the possibility of using the Rossiter-McLaughlin (RM) effect to make ground-based observations more tractable (see Figure 9-4) (see also Narita et al. 2007). RM measurements also provide constraints on planetary orbit axis relative to stellar spin axis (see Gaudi & Winn, 2007; Giménez, 2006; Ohta et al. 2005).

With or without the RM effect, the key is high-resolution spectroscopy and many photons. Furthermore, to take advantage of the RM effect, many short (~ 5 min) observations are needed during the transit. Integrating during an entire 3 hour transit, TMT/HROS can achieve SNR = 31,000 at *R* = 50,000 at V = 11 – the shorter exposures will result in SNR ~ 3000, good enough for this purpose. Sodium and potassium are predicted to be strong at optical wavelengths in hot Jupiters, making them prime spectral features to attack.

Between 1 and 2.5 μm, strong water, carbon monoxide and methane features exist and should be observable by TMT/NIRES. Since these features contain 10s to 100s of individual lines, the effective SNR increases by an order of magnitude relative to the measurement of a single line like Na D in the optical. Fast rotating, late M dwarfs are particularly interesting targets in this regard since the amplitude of the RM effect is directly proportional to the stellar rotational velocity.

In the mid-IR (5 – 20 μm), such observations become easier for Jovian planets because the contrast between the planetary and stellar spectral features is higher (10^3 – 10^4 ; see, e.g., Sudarsky et al. 2003; Burrows et al. 2004) and the molecular features found in the planetary atmospheres are more distinctive. Richardson et al. (2007) have published the first such mid-IR measurement based on Spitzer observations.

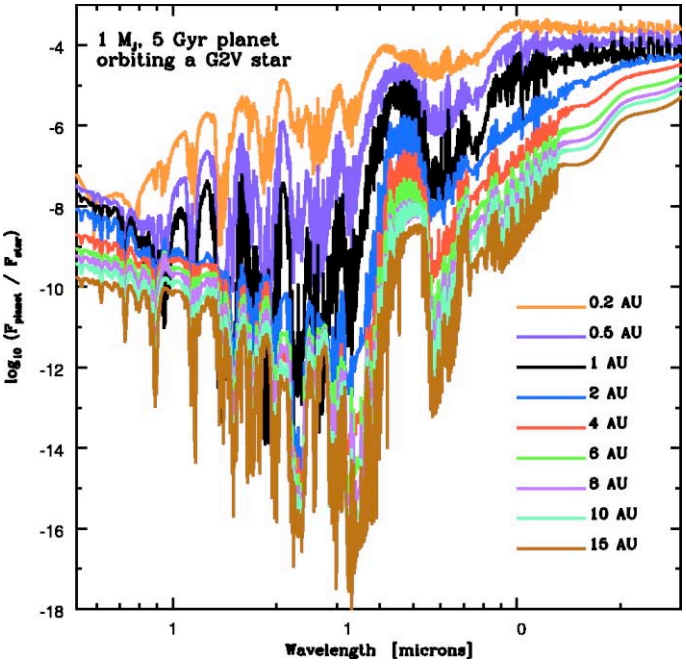

Figure 9-5. Mid-IR imaging of exoplanet atmospheres. Contrast ratio as a function of wavelength for a Jupiter-like planet orbiting a solar-type star, for a range of orbital radii. Molecular bands can be distinguished in the 5 – 20 μm region (From Burrows et al. 2004).

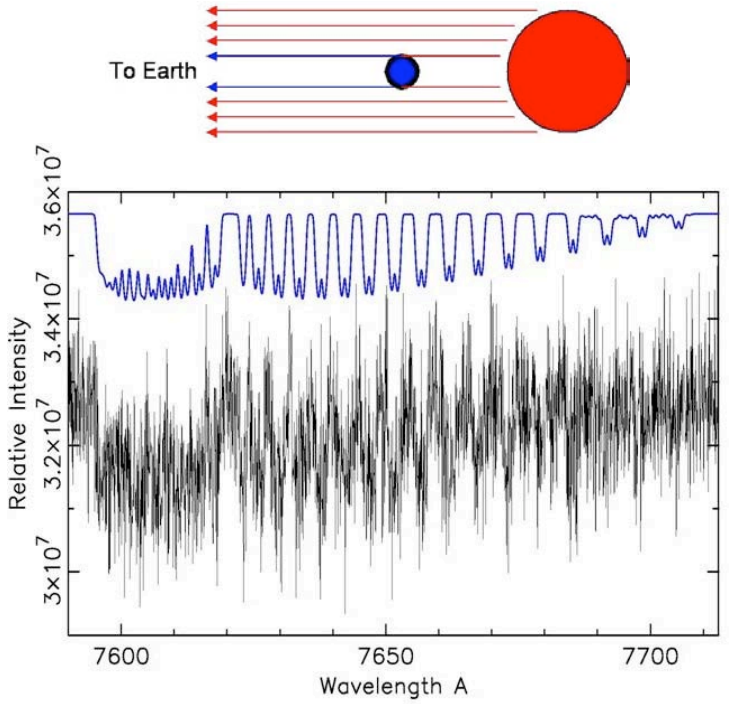

Figure 9-6. Detecting oxygen in exoplanet atmosphere. Simulated high-resolution spectrum of the oxygen A-band absorption feature in the atmosphere of a transiting planet. The feature can be detected in a 3 hr integration by TMT/HROS (adapted from Web & Wormleaton 2001)

The most exciting but perhaps more speculative high-resolution spectroscopic project is the search for oxygen (a key bio-marker) in the atmospheres of rocky planets transiting M dwarf stars. Simulations by Webb & Wormleaton (2001) suggest such measurements are possible if *R* ~ 40, 000 spectra with SNR ~ 30,000 can be achieved for V = 13 M dwarf stars – well within the grasp of TMT/HROS. More than 2500 candidate stars are visible from any given location on Earth. The obvious approach is to narrow down this list using an RV survey and then focus on the most suitable candidates. Of course, before investing this effort, the simulations of Webb and Wormleaton must be confirmed and extended.

In a similar vein, Ehrenreich et al. (2006) recently suggested that the atmospheres of transiting terrestrial planets could also be probed with lower (R ~ 200) resolution spectroscopy. According to their simulations, spectral signatures of water, carbon dioxide, and ozone are detectable in transiting Earth-like planets with 30-m class telescopes. While these are not direct bio-makers, they are certainly indicative of planets that could support life. TMT/IRIS is capable of such observations.

References

Burrows, A., Surdarsky, D. & Hubeny, I. 2004, ApJ, 609, 407
Charbonneau, D et al. 2002, ApJ, 568, 377
Chauvin, G. et al. 2005, A&A, 425, L29
Chauvin, G. et al. 2005, A&A, 438, L25
Ehrenreich, D. et al. 2006, A&A, 448, 379
Gaudi, B.S. & Winn, J.N. 2007, ApJ, 655, 550
Giménez, A. 2006, ApJ, 650, 408
Narita, N. et al. 2007, astro-ph/0702707
Neuhäuser, R. et al. 2005, A&A, 330, L29
Neuhäuser, R. et al. 2006, astro-ph/0610547
Ohta, Y., Taruya, A. & Suto, Y. 2005, ApJ, 622, 1118

Richardson, L.J. et al. 2007, Nature, 445, 892
Rivera, E.J. et al. 2005, ApJ, 634, 625
Snellen, I.A.G. 2004, MNRAS, 353, L1
Snellen, I.A.G. 2005, IAU Coll. 196, 220
Sudarsky, D., Burrows, A. & Hubeny, I. 2003, ApJ, 588, 1121
Vidal-Madjar, A. 2003, Nature, 422, 143
Vidal-Madjar, A. et al. 2004, ApJ, 604, 69
Webb, J.K. & Wormleaton, I. 2001, PASA, 18, 252

10 Our Solar System

Our own Solar System is the planetary system that we can study in the most detail, and provides a reference for studies of exoplanets. TMT will contribute greatly to our knowledge, particularly of the planets, satellites, and small bodies of the outer Solar system.

10.1 The outer Solar System

Most of the original material in the disk of gas, dust, and ice that formed the sun and planets of our Solar System has been heated, stirred, compressed beyond recognition, and chemically modified leaving little information about the initial conditions that led to the current Solar System. However, at the outer edge of the Solar System there exists a vast swarm of small icy bodies within the Kuiper Belt. These so-called Kuiper Belt Objects (KBOs) have been preserved in deep freeze since the time of the formation of the Solar System. Study of the composition of these objects therefore provides direct access to the make-up of the material out of which the planets formed.

With current generation 4m class telescopes, astronomers have been studying the broadband colors of KBOs from the blue to the infrared. While colors alone cannot provide compositional information, they can at least indicate which objects might be compositionally similar and which different. Indeed, from studies of dozens of objects, it is apparent that KBOs come in a wide range of compositions with colors varying from essentially neutral to the reddest objects ever observed in the Solar System.

The composition of icy bodies such as these is best determined through moderate resolution (R ~ 1000) spectroscopy in the near-infrared (1 – 2.5 μm) where most important ices have strong absorption features. Because of their vast distances and small sizes, these objects are extremely faint, so such infrared spectroscopy has only been possible for a small number of the largest objects, where 8 – 10m telescopes have been used at low spectral resolution to search for the signatures of a few extremely abundant ices with broad spectral bands. Unfortunately, these large objects are the least effective at preserving the early chemical signatures, so the promise of studying primordial material remains unfulfilled.

With TMT/IRIS, we expect that hundreds (if not thousands) of moderately faint KBOs will be well within the range of moderate resolution spectroscopy. Many objects in the 1 km diameter range will be observable in 15 minutes. Because of the relative youth of this field, it is difficult to speculate on the discoveries that will be enabled by these advances. However, it is clear that this type of basic exploration of the Solar System will yield important insights into the formation of our and other planetary systems for many years to come.

10.2 Surface physics of Jovian satellites

With adaptive optics, TMT will have a resolution of 7 mas at a wavelength of 1 μm. This corresponds to 25 km at the distance of Jupiter, sufficient to resolve features on the surfaces of the moons of the outer planets. With TMT/IRIS it will be possible to obtain spatially-resolved spectra to study the atmospheric and surface chemistry, and monitor these objects regularly and detect changes due to weather, vulcanism and tectonic activity. This is highly attractive given the large cost and infrequency of space missions to the outer Solar System.

Figure 10-1. Image of Europa at the resolution of TMT/IRIS. Cracks in the icy crust, craters and surface features are clearly visible (M. Brown, CIT).

As an example, consider the case of the Galilean satellite Europa, which has a surface covered with water ice. Evidence suggests that underneath this ice layer, a global liquid water ocean may exist. The water from this ocean may sporadically reach the surface of Europa in the many cracks penetrating the icy surface of the satellite. One piece of supporting evidence for this ocean is that low-resolution spectroscopy from the Galileo spacecraft has suggested that the dark regions around the cracks are composed of hydrated salts, possibly evaporated from the seawater below.

If this were true, the composition of the salts would hold important answers to questions of composition of the proto-solar nebula, the degree of aqueous processing of the satellites, and the potential for supporting life or pre-organic chemistry. Unfortunately, at the spectral resolution of Galileo (R ~ 200), the identification of the dark materials on Europa is not certain. A resolution ≥10 times higher, however, would allow the many different salt species or other possible components to be readily discerned. While such spectral resolutions are routinely available from the ground today, at the low spatial resolution of typical ground-based observations the spectra of the large icy regions hide the spectra of the unresolved dark areas. At TMT resolution, however, the dark regions on Europa will be resolved. High spatial and spectral resolution imaging of the satellite will allow definitive compositional identification that will help to solve many of the questions of this satellite and its possible oceanic interior. Similar problems will be solvable on the other Galilean satellites and on many other bodies of the Solar System.

10.3 Atmospheric physics of the outer planets and satellites

High-resolution mid-infrared spectroscopy can reveal the composition of the atmospheres of the outer planets and their satellites in great detail. By combining this with physical modeling, one can study the complex chemical and photochemical reactions that produce the diversity of inorganic and organic molecules. TMT will be able to study the atmospheres of all planets and satellites in the Solar System with much high spectral resolution than any space probe that has visited these objects.

Understanding the hydrocarbon chemistry of planetary atmospheres in the outer solar system is the a key to understanding the chemistry of early Earth's atmosphere that eventually led to life. While there is no place in the present day solar system where conditions match those of early Earth, atmospheric conditions in the outer solar system (Titan, Uranus, Neptune) are similar enough to provide a suite of test cases for our understanding of atmospheric physics and chemistry that allow us to then extrapolate to the conditions of early Earth. Only through testing our understanding of atmospheric physics and chemistry against many disparate test cases will we be sure that our understanding of atmospheric processes is as complete as possible and that we can properly extrapolate our understanding to the conditions found in atmospheres of extrasolar planets. Aside from in situ sampling, which is not practical beyond the occasional probe sampling an atmospheric profile at one specific location and one specific time, the best

way to observe the chemistry of these atmospheres is with high-resolution spectroscopy in the mid-IR where many of the molecules of interest have their fundamental vibration-rotation bands. Many of these emission bands overlap and high-resolution (R ~ 100,000) is required to disentangle the different emission components. At lower spectral resolution the emission lines of less abundant species are simply lost amongst the strong emission lines of the most abundant species.

The atmospheres of primary interest are those of Titan, Uranus, and Neptune, each of which has extreme differences in physical conditions that lead to differences in the pathways of the chemical processes. Titan is a solid body with a cold Earth-like atmosphere (P_{surf} = 1.5 bar, T_{surf} = 93 K, 90% N_2) where the carbon of atmospheric methane is consumed by a large network of photochemical reactions and eventually ends up on the surface as part of much larger molecules (from propane up to enormous poly-aromatic hydrocarbons or long polymer chains) that will remain on Titan's surface for the age of the solar system. Neptune and Uranus are both gas giants where the carbon of atmospheric methane, lost to photochemistry and the building of larger molecules, is recycled back into methane deep in the interior. Neptune and Uranus differ greatly, at least in their current seasons, in that Neptune has a far greater abundance of methane and heavier hydrocarbons in its stratosphere than Uranus. This difference may be due to the extreme obliquity of Uranus, but observations during different Uranian seasons are required to understand why the two outer gas giant planets appear so different.

The key questions are:

- What are the chemical pathways by which larger organic molecules are formed in planetary atmospheres?
- Do we understand conditions and processes in the atmospheres of our own solar system to predict conditions and processes on extra-solar planets or on the early Earth?
- Why do the stratospheric compositions of Neptune and Uranus appear so very different, in spite of having similar overall composition and low levels of sunlight? What role does the extreme obliquity of Uranus play in driving the processes of the atmosphere?

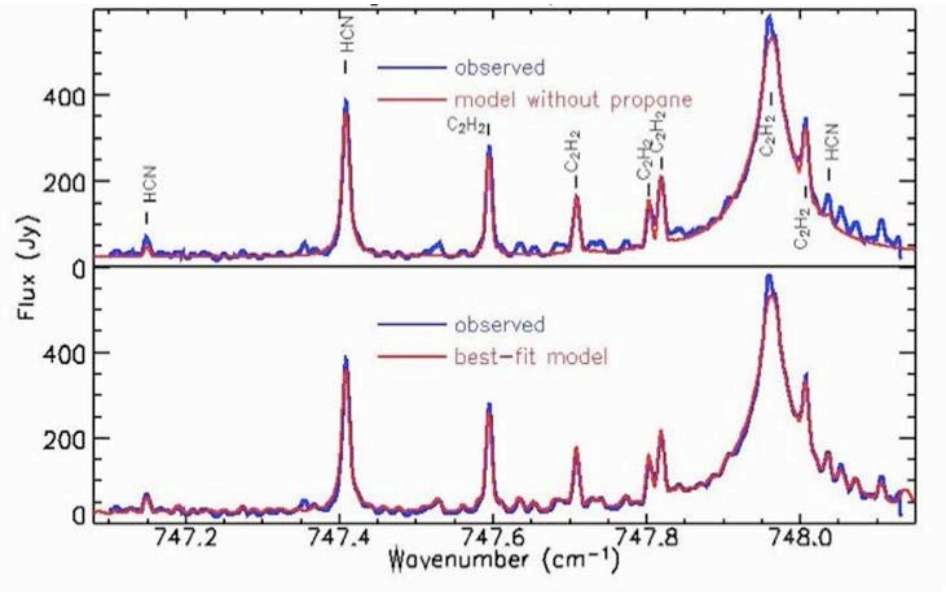

Figure 10-2. High-resolution spectrum of Titan obtained with the TEXES mid-infrared spectrometer, illustrating how high-resolution observations can give detailed information about the abundances of molecular species. (Roe et al. 2003)

TMT/MIRES will be the equivalent of an extended space mission to each of these planets. Although probes have flown by all of these planets (and Cassini continues to regularly fly by Titan for the next few years), no probe has ever flown a mid-infrared spectrometer with a resolution greater than $R \sim 2000$. The spectral resolution of MIRES, some 50 times better than the spectroscopic resolving power of Cassini, is the key to disentangling the incredible number of emission lines from these atmospheres. Many of the less abundant species that are critically important to our understanding show only weaker emission lines on the wings of strong emission lines from more abundant species. The only way to separate the flux of the different lines and detect and measure the rarer species is with high spectral resolution.

The angular resolution of TMT will be sufficient to map these bodies spatially, giving the seasonal evolution of the stratospheric chemistry. The size of each of these objects and the resolution of TMT with adaptive optics at 10 μm is: Titan 5150 km diameter at a resolution of 425 km, Uranus 25600 km diameter at a resolution of 900 km, Neptune 24800 km diameter at a resolution of 1450 km.

References

Roe et al. 2003

This page was intentionally left blank.